Effects of natural aerosols on climate

Douglas Stephen Hamilton

Submitted in accordance with the requirements for the degree of
Doctor of Philosophy

The University of Leeds
School of Earth and Environment

September 2016

The work submitted in this thesis is my own, except where work that formed part of jointly–authored publications has been included. All contributions are explicitly indicated below and appropriate credit is given within the thesis where reference has been made to the work of others.

Chapter 3 is from two published articles: Hamilton, D.S. et al., 2014. Occurrence of pristine aerosol environments on a polluted planet. Proceedings of the National Academy of Sciences of the United States of America, 111(52), pp.18466–71 and Hamilton, D.S., 2015. Natural aerosols and climate : Understanding the unpolluted atmosphere to better understand the impacts of pollution. Weather, 70(9), pp.264–268. Both manuscripts were written by me with advice from K.S. Carslaw and D.V. Spracklen during the preparation phase. Analysis of results was performed by me based on model emulation and sensitivity analysis results carried out by L.A. Lee and K.S. Pringle and radiative forcing calculations carried out by C.L. Reddington.

Chapter 4 in its entirety is based on a draft ACPD paper. The manuscript will be jointly authored with contributions from K.S. Carslaw, D.V. Spracklen, G.A. Folberth, L.A. Lee, K.S. Pringle and J.S. Johnson. Manuscript text is written by me with advice from K.S. Carslaw, D.V. Spracklen, G.A. Folberth and J.S. Johnson during the preparation phase. Analysis of results was performed by me based on the same Chapter 3 data set of model emulation and sensitivity analysis results carried out by L.A. Lee and K.S. Pringle.

Chapter 5 in its entirety is based on a draft Nature Letters paper. The manuscript will be jointly authored with contributions from S. Hantson, J.O. Kaplan, C.E. Scott, K.S. Carslaw, D.V. Spracklen, G.A. Folberth and K.S. Pringle. Manuscript text was written by me with advice from S. Hantson, K.S. Carslaw, D.V. Spracklen and C.E. Scott during the preparation phase. Creation of fire emission datasets was performed by me for the LMfire model based on a simulation performed by J.O. Kaplan and by S. Hantson for the SIMFIRE–BLAZE model. Analysis of results was performed by me based on aerosol modelling simulations performed by me and radiative forcing calculations performed by C.E. Scott.

Acknowledgements

First and foremost I would like to thank my supervisors Ken Carslaw, Dominick Spracklen and Gerd Folberth. They have each supported, guided and taught me numerous skills throughout my Ph.D for which I am very grateful. Furthermore, I appreciated the manner in which the supervision was given, it allowed me to freely explore my own ideas and be creative within my Ph.D while also being direct and forthright when I needed it. I would also like to thank the research support I received from Kirsty Pringle, Lindsay Lee, Jill Johnson and Graham Mann, again for which I am very grateful.

Many thanks are due to the aerosol modeller group, both past and present, for the many great science discussions and helping with modelling and learning to write computer code. Likewise, many thanks are also due to the modelling statistics group. In particular, my desk neighbours Steve, Anja, Erin, Cat and Carly as well as Leighton and Jill deserve large thanks for all their help and the tea/coffee/cake breaks which made the days brighter.

I would like to acknowledge the funding I received from the Natural Environment Research Council and The Met Office in funding my Ph.D. I would also like to acknowledge the data provided by Jed Kaplan and Stijn Hantson, as well as thank them for the invaluable discussions about fire behaviour.

A big thanks goes out to the board games group for helping keep mid-week evenings fun, particularly to Leighton and Joey. Thanks to all my family and friends for supporting me throughout the Ph.D (as well distracting me from it when necessary). I would particularly like to thank Steven Woods for his help and moral support during the final months of writing this thesis. Finally, I would like to thank my parents for believing in me and encouraging me throughout the past four years.

Abstract

Natural aerosols are a key component of many biogeochemical cycles, they define the baseline from which the pre–industrial to present–day anthropogenic aerosol radiative forcing is calculated, and they dominate the net effect of all aerosols on the incoming solar radiation. However, their impacts on climate are complex, often nonlinear, and poorly understood; leading to large uncertainties.

Global model simulations are used in this thesis to define aerosol regions unperturbed by anthropogenic pollution. On a global annual mean, unperturbed aerosol regions cover 12% of the Earth (16% of the ocean surface and 2% of the land surface) with about 90% of unperturbed regions occurring in the Southern Hemisphere. In cloudy regions with a radiative forcing relative to 1750, results suggest that unperturbed aerosol conditions could still occur on a small number of days per month. However, these environments are mostly in the Southern Hemisphere, potentially limiting the usefulness in reducing Northern Hemisphere forcing uncertainty.

Clustering techniques were used to identify natural emissions regimes in the pre-industrial and present-day where biomass burning, biogenic volatile organic compounds, dimethyl sulphide, volcanic sulphur dioxide and sea spray emissions dominate the variance in cloud condensation nuclei concentrations. Regimes are generally located in regions close to each emission source, before significant mixing occurs within the atmosphere with other emission types. These regimes are ideal “natural laboratory” locations for field study of the impacts of each natural emission on aerosol behaviour.

When pre-industrial fire emissions from two global fire models are implemented in a global aerosol model, pre-industrial global mean cloud condensation nuclei concentrations increase by a factor 1.6-2.7 relative to the widely used AeroCom dataset. Higher pre-industrial aerosol concentrations cause a substantial reduction in the calculated global mean cloud albedo forcing of between 40 and 88 percent and a reduction in the direct radiative forcing of between 5 and 10 percent. When compared to twenty-eight other sources of uncertainty in our model, pre-industrial fire emissions are by far the single largest source of uncertainty in pre-industrial cloud condensation nuclei concentrations, and hence in our understanding of the magnitude of the historical radiative forcing due to anthropogenic aerosol emissions.

Table of Contents

List of Tables

List of Figures

*Chapter 1
Motivation and background

The most exciting phrase to hear in science, the one that heralds new discoveries, is not 'Eureka!' but 'That's funny...'

Isaac Asimov

1.1 Motivation

Natural aerosols are a key component of many biogeochemical cycles (Carslaw et al., 2010; Mahowald et al., 2011), they define the baseline from which the pre–industrial (PI) to present–day (PD) anthropogenic aerosol radiative forcing is calculated (Andreae, 2007; Andreae and Rosenfeld, 2008; Carslaw et al., 2013; Hamilton et al., 2014; Penner et al., 2011; Schmidt et al., 2012), and they dominate the net effect of all aerosols on the incoming solar radiation (Satheesh and Krishnamoorthy, 2005). However, their impacts on climate are complex, often nonlinear, and poorly understood; leading to large uncertainties (Carslaw et al., 2010, 2013; Mahowald, 2011; Regayre et al., 2014; Wilcox et al., 2015).

Field campaigns over the last three decades, such as the Aerosol Characterization Experiments (ACE 1, ACE 2, ACE–Asia), those within The integrated Land Ecosystem–Atmosphere Processes Study (iLEAPS), the Global Tropospheric Experiment (GTE), the Amazon Aerosol Characterization Experiment (AMAZE–08), and the biogenic aerosol formation in the boreal forest (BIOFOR) project in Finland have improved our understanding of natural aerosol and related precursor gas emissions, processes, and their interactions with both climate and the Earth system (e.g., Bates, 1999; Johnson et al., 2000; Kulmala et al., 2001; Martin et al., 2010a; McNeal et al., 1983; Suni et al., 2015). However, large uncertainties in the magnitude of natural emissions and processes still exist (Carslaw et al., 2010).

Two main factors affect our ability to study natural aerosol processes. First, natural emissions are highly variable across seasonal, interannual and decadal timescales (e.g., Dunne et al., 2014; Lana et al., 2011; Mahowald et al., 2013; Tsigaridis et al., 2005; van der Werf et al., 2010) due to variability in factors such as temperatures, wind speeds, light availability and biological activity (Andreae and Crutzen, 1997; Andreae and Rosenfeld, 2008; Fitzgerald, 1991; Fowler et al., 2009). Second, ageing of the aerosol through coagulation and condensation of low volatility gases

means that at any location in the atmosphere the particles will contain a mixture of both natural and anthropogenic components (Andreae and Rosenfeld, 2008).

Natural emissions are also sensitive to anthropogenic perturbations of the Earth system and climate (Arneth et al., 2010; Carslaw et al., 2010; Kloster et al., 2007). For example, increases in temperature can increase emissions from terrestrial vegetation (Guenther, 2002), but also reduce emissions from marine phytoplankton (Kloster et al., 2007). Furthermore, natural emissions from vegetation and wildfires are susceptible to alterations in the underlying vegetation distribution driven by anthropogenic land use and land cover change (Archibald et al., 2009; Ellis, 2011; Ellis et al., 2013; Ward et al., 2014). The overall global impact of anthropogenic activity could also be supressing the magnitude of Earth system–natural emission–climate feedbacks (Spracklen and Rap, 2013), but this remains highly uncertain especially on the regional scale.

Uncertainty in the magnitude of aerosol radiative forcing of climate over the industrial period hampers efforts to quantify the sensitivity of global temperature to the radiative perturbations caused by human activity (Stocker et al., 2013). Because forcings are referenced to PI conditions, a large part of the uncertainty will be reduced only by accurately defining pristine aerosol conditions before air pollution (Carslaw et al., 2013; Hamilton et al., 2014). Furthermore, to understand the processes involved in how different natural emissions impact aerosol number concentrations it is important to define those regions where each natural emission can be studied in as close to isolation as possible.

This thesis aims to define those regions best suited as “natural laboratories” for further study of natural aerosols, the processes they undergo and their climate impacts. First in terms of those PD environments which are still close to PI conditions and then in a detailed analysis of where the impact of each natural emission on cloud condensation nuclei (CCN) number concentrations could be studied in as close to isolation as possible. Finally fire modelling results show that PI fire emissions are currently the largest uncertainty in our understanding of the PI aerosol state within our model, and hence the magnitude of anthropogenic radiative forcing over the industrial period.

1.2 Introduction to natural aerosol systems

Natural aerosol and precursor gas emissions originate from both terrestrial and marine environments (Carslaw et al., 2010). They are emitted directly to the atmosphere, termed primary aerosol, or formed by gas–to–particle conversion from natural precursor gas emissions, termed secondary aerosol. Satheesh and Krishnamoorthy (2005) estimated that the natural environment accounts for 89% of the mass from all emissions, contributes 81% of the total atmospheric aerosol mass and 52% of the total aerosol optical depth. Natural emissions are highly diverse and include sea salt, dust, secondary organic aerosol (SOA) from biogenic volatile organic compound (BVOC) emissions, carbonaceous particles from wildfires, and sulphate from volcanic sulphur dioxide, wildfire, and marine phytoplankton dimethyl sulphide (DMS) emissions (Figure 1.1).

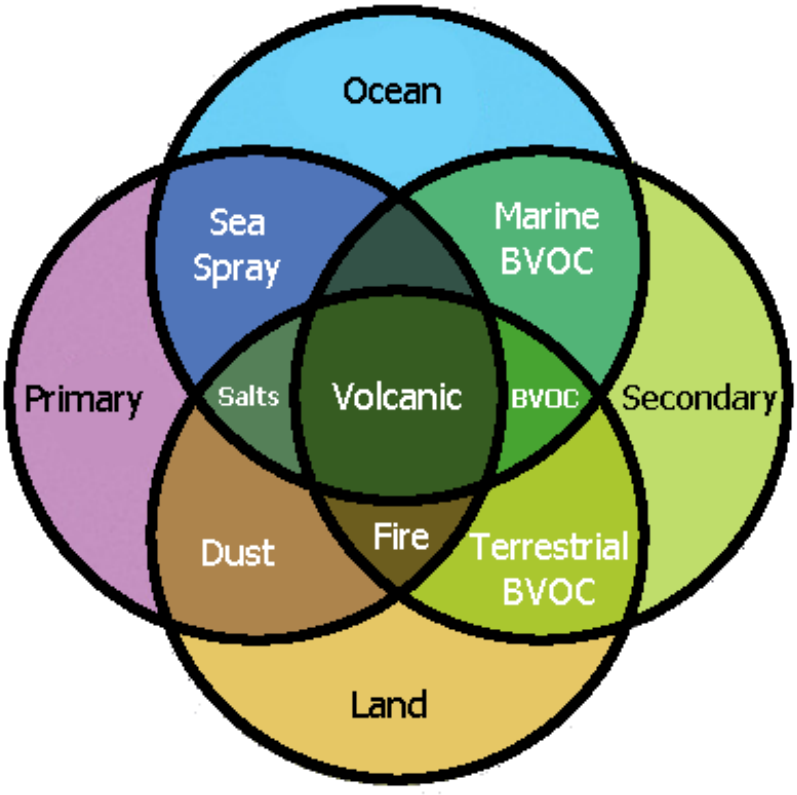

Figure 1.1. Venn diagram of major natural aerosol types (white text) characterised by source environment and production method (black text).

Aerosols are an important part of the Earth's radiation budget. Aerosol particles of a sufficient size directly alter the energy balance of the atmosphere through absorbing and scattering incoming solar radiation, termed aerosol radiation interactions (ARI). The effect of this interaction can be seen through changes to visibility (haze) on polluted days and increases linearly with increasing aerosol concentrations, except at very low aerosol optical depths (Boucher et al., 1998). Additional to this direct effect on solar radiation, aerosol-cloud interactions (ACI) indirectly alter the energy balance of the atmosphere by changing cloud brightness (albedo), termed the cloud albedo effect (CAE). Aerosols above a certain size, with the ability to attract and retain water (hygroscopic), play a critical role in the atmosphere at supersaturations below a few percent by acting as the seed, termed cloud condensation nucleus (CCN), upon which cloud drops can grow. For a fixed amount of cloud liquid water, an increase in aerosol concentrations leads to brighter clouds by increasing the number and reducing the average size of the cloud drops (Boucher et al., 2013). Clouds are considerably more sensitive to changes in cloud droplet concentration in those regions where initial cloud drop concentrations are low (Twomey, 1991), such as remote regions where natural emissions can dominate, because the sensitivity of cloud albedo *R* to changes in cloud drop concentrations *N,* at fixed liquid content, is approximately:

$$\left(\frac{dR}{dN}\right)_w = \frac{R(1-R)}{3N} \qquad (1.1)$$

Figure 1.2 illustrates the non–linear relationship between aerosol concentrations and cloud radiative properties in results from four global climate models. Changes to emissions from the natural environments alter CCN number concentrations, and hence cloud droplet number concentrations, cloud albedo and the energy balance of the atmosphere (Rap et al., 2013; Schmidt et al., 2012; Scott et al., 2014). Natural aerosols are also a major component of the baseline from which the magnitude of the PI-to-PD aerosol radiative forcing (RF) is determined; uncertainties in the magnitude of PI natural emissions contribute substantially to the overall uncertainty in the magnitude of the aerosol-cloud radiative forcing (Carslaw et al., 2013; Regayre et al., 2014; Schmidt et al., 2012; Wilcox et al., 2015).

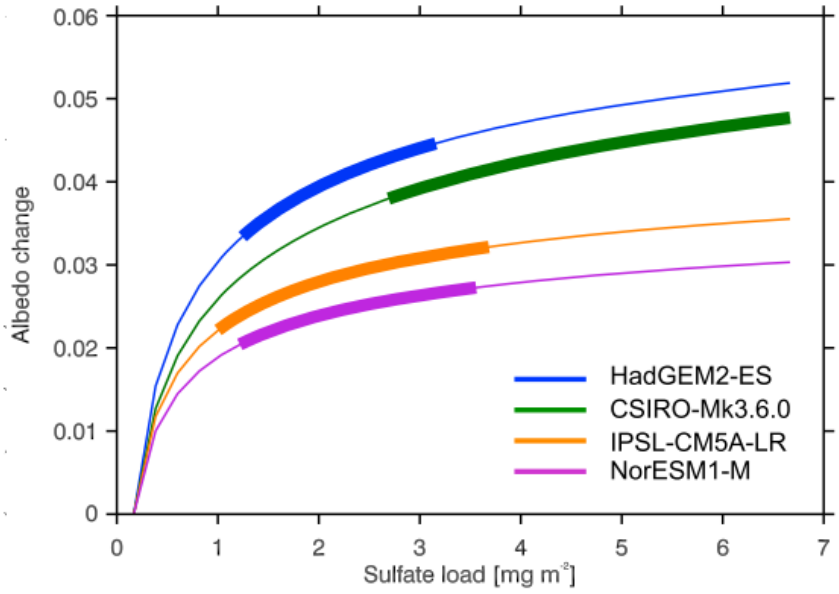

Figure 1.2. Sensitivity of cloud albedo to changes in the global sulphate burden (load) in four global climate models. Figure from Wilcox et al. (2015).

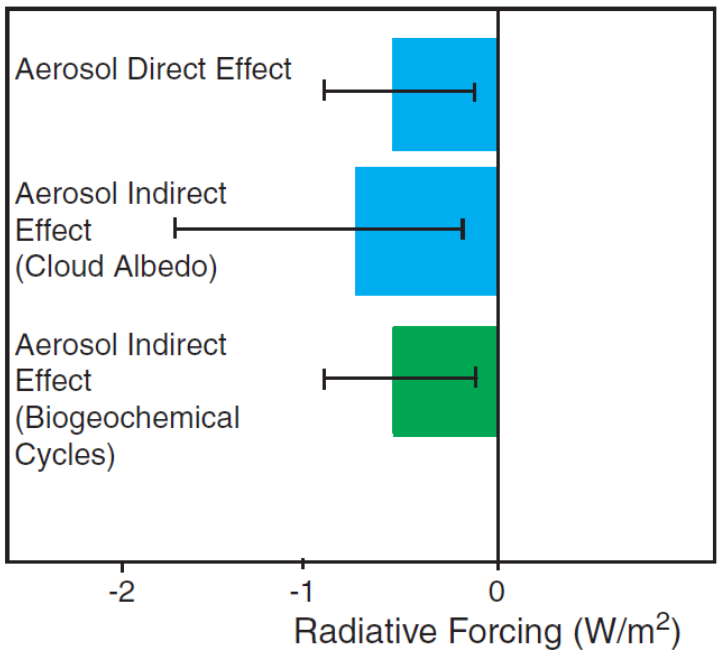

Figure 1.3. Intergovernmental Panel on Climate Change (AR4, Forster et al. 2007) aerosol radiative forcing estimates compared to radiative forcing estimates from the indirect effect of aerosols within biogeochemical cycles. Figure from Mahowald (2011).

Aerosols can also indirectly alter climate by providing essential nutrients to ecosystems (Mahowald et al., 2011), often in remote locations far from the aerosol emission source. The effective forcing of climate through aerosol impacts on biogeochemical cycles has been estimated by Mahowald (2011) to be equal to the direct radiative forcing of anthropogenic aerosols (Figure 1.3). Any future changes to the transport of nutrients can potentially alter the land or ocean primary productivity which depends upon it.

Unlike long–lived greenhouse gases, aerosols are short lived in the atmosphere with typical atmospheric lifetimes of up to a few weeks (Figure 1.4). Pure natural aerosols can often be observed close to strong local emission sources, like wildfires. Nevertheless, we are often interested in how the emissions affect aerosol and cloud properties in remote locations (Koren et al., 2014). In these environments, far from well-defined aerosol sources, it is much more difficult to unambiguously separate purely natural aerosol environments from those that are subject to anthropogenic influences because particles become mixed over long time scales.

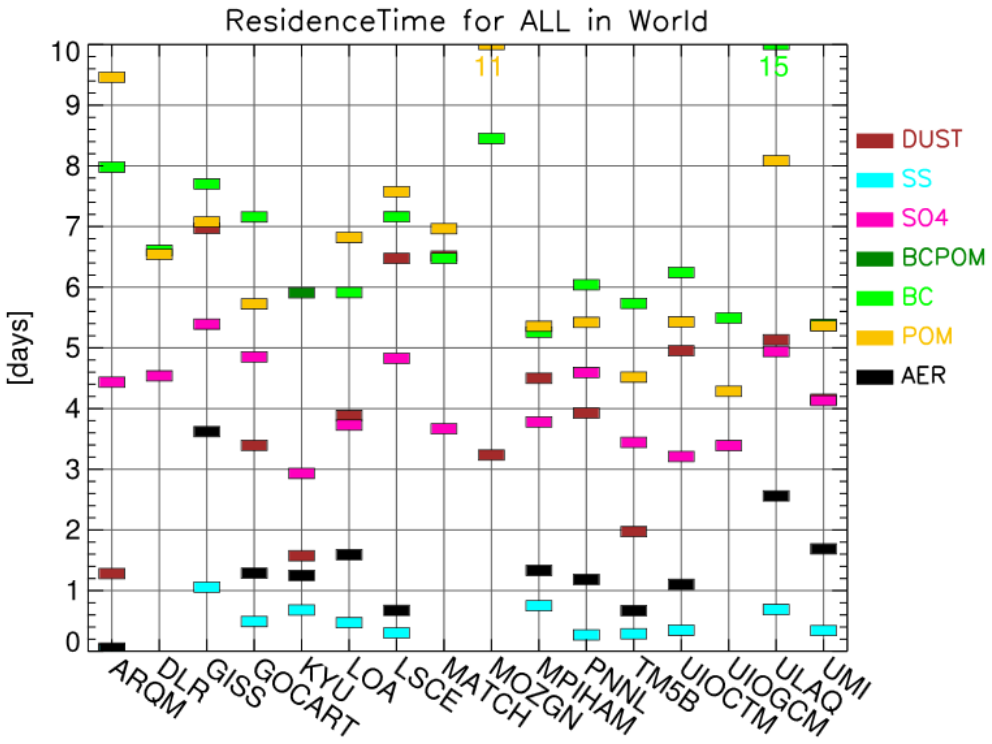

Figure 1.4. Tropospheric residence times in [days] from 16 AeroCom models for the species: dust (DU), sea salt (SS), sulphate (SO_4), black carbon (BC), particulate organic matter (POM), and the total aerosol (AER). Figure from Textor et al. (2006).

Various chemical tracers can be used to stratify aerosol measurements, such as carbon monoxide (Clarke and Kapustin, 2010), black carbon (O'Dowd et al., 2014) or even particle concentrations (Fiebig et al., 2014; Koren et al., 2014), but none of these tracers are uniquely natural or anthropogenic. For example, wildfires produce natural precursor gases that can contribute to particle formation through nucleation, perhaps even more effectively than anthropogenic vapours (Kirkby et al., 2016). Assuming that remote locations containing low aerosol concentrations are pristine is not always appropriate either due to the long range transport of pollutants. For example, Antarctica can become polluted by anthropogenic aerosols originating from South America during the biomass burning season (Fiebig et al., 2014).

Detection of purely natural environments with respect to aerosols becomes even more challenging because many natural emissions lead to formation of low volatility gases like sulphuric acid or low volatility organic compounds that can condense onto pre-existing anthropogenic and natural particles (Keskinen et al., 2013) or nucleate to form new ones (Riccobono et al., 2014; Spracklen et al., 2006). The microphysical evolution of such an aerosol system implies that, observationally, there is no means of detecting the boundaries of a purely or predominantly natural aerosol environment.

1.3 Natural emissions

The following sub-sections are a background summary for each natural aerosol and precursor gas emission discussed within this thesis.

1.3.1 Dimethyl sulphide

The vast majority of DMS is oceanic in origin (Gondwe, 2003) and is produced within the ocean mixed layer. It is the dominant biogenic sulphur emission to the atmosphere (Bates et al., 1992; Lin et al., 2012). DMS accounts for approximately half of the total natural sulphur sources (Kettle and Andreae, 2000) and between 18 to 42% of the total mass of all atmospheric sulphate aerosol (Woodhouse et al., 2010).

Figure 1.5 shows the basic formation and transformation processes in the DMS cycle. Oceanic DMS is one of the products of dimethyl sulfoniopropionate (DMSP) which is released by many species of phytoplankton, and to a lesser extent some diatoms (Spielmeyer et al., 2011), during zooplankton grazing, senescence or viral lysis (Curson et al., 2011).

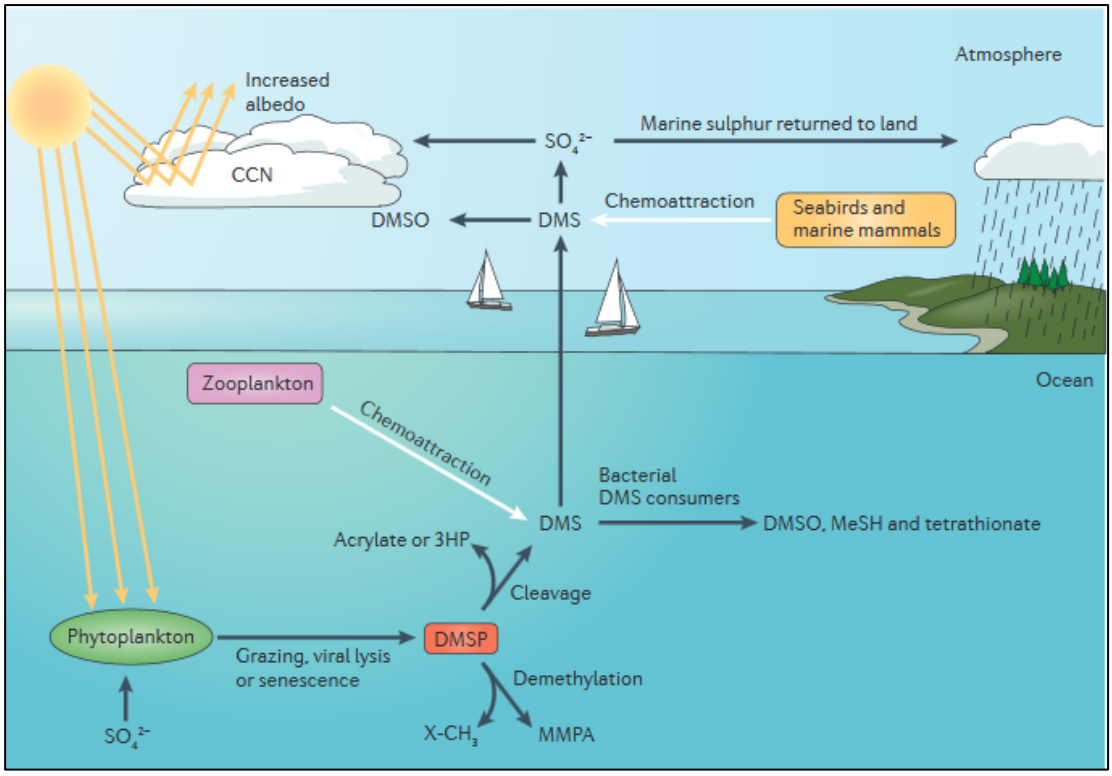

Figure 1.5. The formation and fate of dimethyl sulphide. Figure from Curson et al. (2011)

Once in the atmosphere DMS is readily oxidised by hydroxyl radicals during the day (Pham et al., 1995) and by nitrate radicals at night (Stark et al., 2007) to form sulfuric (see section 1.2.8) and methane–sulfonic acids (Andreae and Crutzen, 1997). DMS therefore plays an important role in both the formation and growth of sulphate containing aerosol particles. Once formed, sulphate aerosol impacts climate through scattering solar radiation and altering cloud properties (section 1.5).

The Charlson, Lovelock, Andreae and Warren (CLAW) hypothesis (Charlson et al., 1987) is a well–known natural aerosol–climate feedback hypothesis. It proposed that increasing DMS emissions concurrently increases CCN number concentrations, hence altering aerosol–cloud interactions and ultimately increasing cloud albedo. This increase in the albedo was then suggested to form a negative feedback by cooling the underlying ocean surface and reducing net primary productivity. However, later work showed that if sulphate grows existing particles instead of creating new ones it can have the opposite effect on cloud albedo (von Glasow, 2007; von Glasow and Crutzen, 2004). Furthermore, recent studies (Brévière et al., 2015; Woodhouse et al., 2010, 2013) have shown that DMS emissions alter aerosol concentrations via particle nucleation in the free

troposphere more than within the marine boundary layer. After formation new particles can then be transported long distances downwind of their original DMS source locations, with any resulting climate impacts therefore not spatially co–located with the emissions. The sensitivity and location of CCN formation to any changes in the DMS flux is therefore a limiting factor in any feedback cycle. Even though supporting evidence of a DMS emission–climate feedback is still limited (Quinn and Bates, 2011) DMS emissions are highly important in climate studies due to the high sulphate formation rates from DMS emissions. DMS emissions could also be a possible unaccounted source of sulphur to the stratosphere (Marandino et al., 2013). Furthermore, while CCN number concentrations may not be as sensitive as previously thought to changes in the flux of DMS from current emission locations, any future changes to the spatial distribution of DMS emissions (e.g., due to sea ice loss) could still be important (Woodhouse et al., 2010).

The modelled flux of ocean DMS to the atmosphere in this thesis is parametrised based on ocean DMS concentrations from the Kettle and Andreae (2000) climatology and the Nightingale (2000) sea-air transfer velocity.

1.3.2 Biogenic volatile organic compounds

Plants and marine biota release biogenic volatile organic compounds (BVOCs) into the atmosphere which, once oxidised, are able to partition into the atmospheric particle phase, forming secondary organic aerosol (SOA) (e.g., Kavouras et al., 1999; Tsigaridis et al., 2005; Tsigaridis and Kanakidou, 2003; Went, 1960).

It is estimated that there are over 10,000 reactive carbon species, which are produced in terrestrial ecosystems at varying rates depending on the vegetation type (Guenther, 2002). Many plants produce BVOCs in response to environmental stressors such as excessive heat (Peñuelas and Llusià, 2003), damage to photosynthesis pathways from high ozone levels (Pacifico et al., 2015), or herbivory (Blande et al., 2009; Peñuelas et al., 2005). It is hypothesised that by producing BVOCs the potential damage to the plant from external stressors can be reduced. Therefore, those plants lacking this mechanism are at a selective disadvantage over those that do (Lerdau, 2007).

Vegetation is sensitive to the local climate, with temperature, light availability and precipitation all controlling photosynthetic BVOC production rates (Laothawornkitkul et al., 2009). Temperature effects can be direct (e.g., altering metabolic reaction pathways) or indirect (e.g., modifying the growing season or latitudinal/altitudinal

migration) (Peñuelas and Staudt, 2010). Specifically, rates of BVOC emission are linked to enzyme synthase (Silver and Fall, 1995) with an optimum around 40°C (Guenther et al., 1993). Modelling suggests that an increase of 2°C from PD levels can increase BVOC emissions up to 25% (Guenther, 2002). The role of light in photosynthesis leads to summer emission maxima with equivalent peaks in particle nucleation (Kulmala et al., 2004b). Precipitation effects on BVOC emissions depend upon the severity of the event. For example, a mild drought can increase BVOC emission whereas a severe drought can decrease them (Peñuelas and Staudt, 2010).

The diurnal cycle of BVOC concentrations can vary depending on location and compound type. For example high daytime concentrations of monoterpenes (C-10 compounds) are observed over tropical forests, while the larger sesquiterpenes (C-15 compounds) peak at night and closer to the ground (Jardine et al., 2011). Conversely, over boreal forests high night time monoterpene concentrations are observed (Hakola et al., 2012). Figure 1.6 shows the seasonal variation in monoterpene emissions, which are linked to the ambient temperature. Tropical emissions contribute around half of all global BVOC emissions due to being persistent throughout the year, while boreal emissions are prevalent only in the summer (Guenther et al., 1995). Once in the atmosphere BVOCs are readily oxidised to form lower volatility products, by hydroxyl radicals and ozone during the day and by nitrate radicals at night.

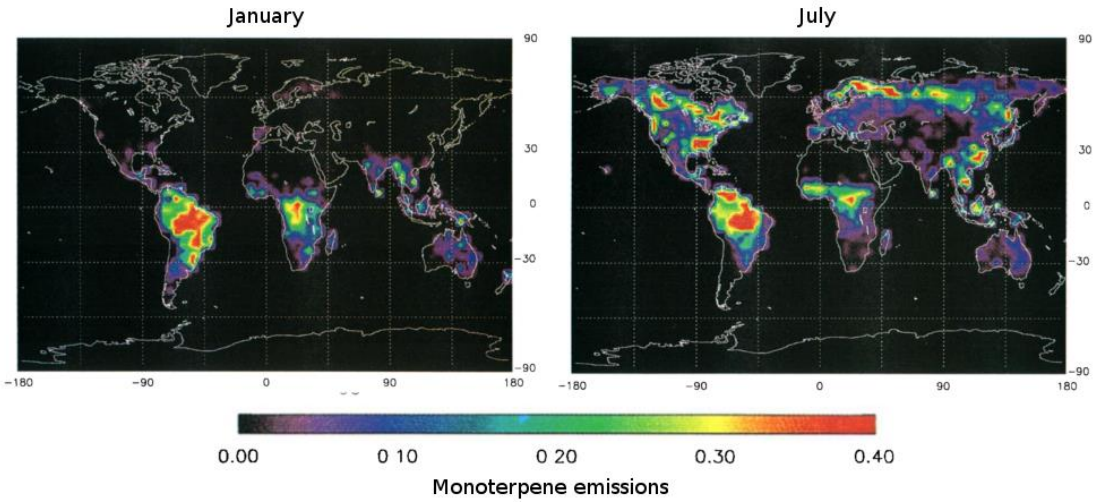

Figure 1.6. Global monoterpene emission rate estimates (g C m^{-2} $month^{-1}$) for January and July. Figure from Guenther et al. (1995).

Vegetation is also sensitive to anthropogenic emissions, with anthropogenic aerosols and gases impacting the net primary productivity of plants both directly and indirectly. Directly, high ozone levels cause stomatal closure, reducing net primary productivity (Sitch et al., 2007). Increasing CO_2 levels increases net primary productivity (Kulmala et al., 2004b) through a fertilization effect, but can also lead to reductions in photosynthetic productivity which supresses BVOC formation (Arneth et al., 2007; Heald et al., 2009; Young et al., 2009). Indirectly, anthropogenic aerosol increase the amount of diffuse radiation reaching vegetation, leading to higher net primary productivity (Mercado et al., 2009).

Many not readily modelled factors exist when considering the impact of BVOC emissions on SOA concentrations, such as marine BVOC emissions (Bonsang et al., 1992), chirality (Yassaa et al., 2008) and herbivory (Blande et al., 2009; Peñuelas et al., 2005). Different oxidation pathways from BVOC species to SOA also exist (Atkinson and Arey, 2003). Estimates of SOA production from BVOCs therefore vary considerably from 12–1820 Tg (SOA) a^{-1} (Goldstein and Galbally, 2007; Hallquist et al., 2009; Spracklen et al., 2011b; Tsigaridis et al., 2005). There is also a secondary contribution to the total SOA burden from anthropogenic precursor gases (Weber et al., 2007). When combined the best global estimate of total SOA (biogenic and anthropogenic) is between 50–380 Tg (SOA) a^{-1} (Spracklen et al., 2011b). The monoterpene emissions used in this thesis come from Guenther et al. (1995) and produce 50 Tg SOA a^{-1} (Lee et al., 2013). Vegetation also contributes to the atmospheric mass of particulate organic matter (POM) via spores, pollen and leaf materials (Spracklen et al., 2008b), but this primary source of POM is not currently modelled.

1.3.3 Fire

Global fire activity is linked to both human activity and climate (Bowman et al., 2009; Pechony and Shindell, 2010) and fire has long been employed as a tool by humans to manage their habitat (Bowman et al., 2011). Fire contributes large quantities of trace gases and aerosol to the atmosphere (Andreae and Merlet, 2001; van der Werf et al., 2010). For example, the late–18^{th} to mid–19^{th} Century peat burning in Germany and the Netherlands caused haze clouds that encompassed Paris, Warsaw and the Alps (Prestel, 1861). This can lead to assumptions that fire emissions are a predominantly anthropogenic phenomenon. However, historical records of West African natural wildfires date back to the

explorer Hanno in ~470 BC (von Danckelman, 2009) and natural fire occurrences are prevalent throughout geological history (Bowman et al., 2009).

Fire ignition is strongly linked to human activity but recent evidence points to an overall negative relationship between population density and total burnt area (Bistinas et al., 2013; Knorr et al., 2014). Total burnt area is also linked to climate (Pechony and Shindell, 2010; van der Werf et al., 2008b). Low precipitation reduces net vegetation primary productivity and so fuel levels become insufficient, whereas high precipitation causes the fuel to become non-flammable (van der Werf et al., 2008b). Strong climate cycles, such as the El Niño Southern Oscillation (ENSO) or the Indian Ocean Dipole, are therefore important considerations in many fire studies (Field et al., 2009; Fuller and Murphy, 2006; Giglio et al., 2010; van der Werf et al., 2008a). For example during drought years, usually in response to ENSO, a third or more of the Amazon is susceptible to fire (Nepstad et al., 2004) and observations suggest that drought can increase fire emissions by more than a factor of two compared to non-drought years (Reddington et al., 2015).

The PD pattern of fire is relatively well understood based on global satellite measurements of burnt area (Figure 1.7), with an estimated 3.3 to 4.3 Mm^2 of vegetation burnt from 1997–2008 (Giglio et al., 2010). Over 70% of fire occurrence is in Africa (Giglio et al., 2010), where wildfires help savannahs keep the balance between grassland and trees (Bond, 2008). The northern hemisphere (NH) African Savannah dry season depends on the inter–tropical convergence zone (ITCZ) position and burning lasts for up to 4 months, centred on January. The southern hemisphere (SH) African savannah dry season depends on the interoceanic confluence, which peaks in July, with the burning season slightly longer than in the NH at 4–5 months (Cachier and Ducret, 1991).

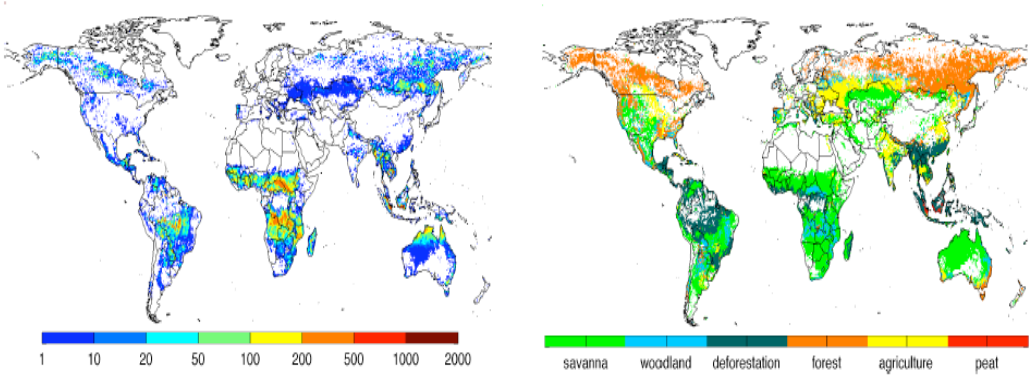

Figure 1.7. Left map: Annual mean (1997–2009) carbon emissions (g C m^{-2} a^{-1}) calculated as a product of the fuel consumption and burned area. **Right map:** dominant fire type. Figures from van der Werf (2010).

The impacts of fire emissions are observed throughout the Earth system, including: changes to cloud microphysics (Kaufman et al., 1998; Rosenfeld, 1999), altering of the Hadley circulation (Tosca et al., 2013), black carbon deposition on ice and snow which alters its albedo and melting rates (Quinn et al., 2008; Skeie et al., 2011), warming the atmosphere through the solar radiation absorbing properties of both black (Bond et al., 2013) and brown (Feng et al., 2013) carbon emissions, or conversely, cooling the atmosphere through creation of sulphate (SO_4) particles from sulphur dioxide (SO_2) emissions (see section 1.4) which reflect solar radiation. Human land use change and deforestation change the land surface albedo, and hence the regional energy budget, in a way that persists all year round, not just during the burning season (Sena et al., 2013). Poor air quality and haze occurs frequently in periods of intense biomass burning (Reddington et al., 2014, 2015), with detrimental effects on human health. However, despite the prominent role of fire in past and present climate (Ward et al., 2012), current understanding of PI fire emissions is limited (van der Werf et al., 2013).

Fire emissions used throughout this thesis come from the AeroCom inventory (Dentener et al., 2006), and in Chapter 5 the PI emissions are compared to recent modelling estimates of emissions in the same period.

1.3.4 Sea salt

The marine boundary layer contains two major aerosol components, those that are sea salt derived and those that are non–sea salt derived (Keene et al., 1986). Around 90% of the ocean salt composition is sodium chloride (NaCl), and therefore also constitutes the highest mass fraction to sea spray aerosol (Grythe et al., 2014). Sea salt constitutes the largest component of aerosol mass to the marine boundary layer (Textor et al., 2006), except during very high dust events (Fitzgerald, 1991). Sea spray aerosol is produced by bubble bursting and mechanical disruption of wave crests (de Leeuw et al., 2011), with significantly higher amounts produced when wind speeds are above 10 ms^{-1} (Fitzgerald, 1991; Ovadnevaite et al., 2014).

Sea salt is highly hygroscopic and therefore acts as an efficient CCN particle upon which a cloud drop can form. While wind speeds are a major factor in the contribution sea spray makes to the total marine aerosol mass, the relationship may not extend between wind speed and marine CCN number concentrations except over the Southern Ocean (Dunne et al., 2014).

Sea salt composition can contain significant marine biological elements. While marine biological particles are efficient ice nucleating particles (Burrows et al., 2013; Wilson et al., 2015) they act to reduce the overall hygroscopicity of sea salt and therefore can reduce (up to 32%) the efficiency of smaller sized (< 180 nm) sea spray aerosol to activate into cloud drops (Prather et al., 2013).

Modelled fluxes of sea salt in this thesis are calculated using the Gong (2003) parametrisation, and based on 10 m above sea level (termed U_{10}) wind speeds. A wind speed only parametrisation does not capture all of the variability in emissions (Ovadnevaite et al., 2014), because the impact of variables such as the sea surface temperature or wave height on emissions is neglected, but the overall relationship is well captured (Figure 1.8).

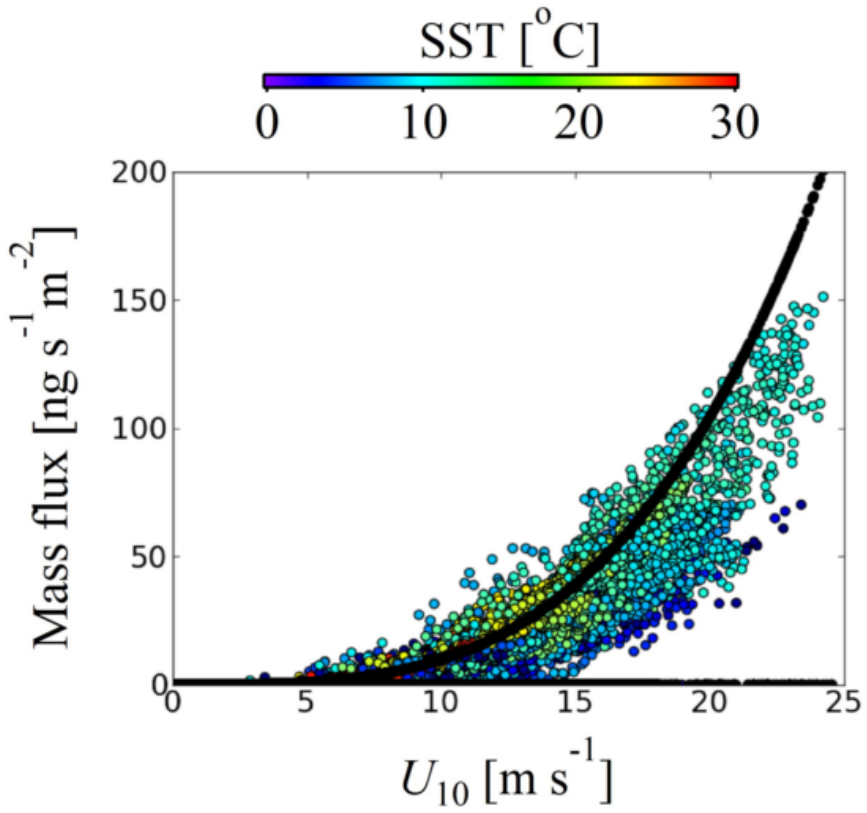

Figure 1.8. Modelled mass flux of sea spray aerosol using two schemes. The Gong (2003) scheme which is based on wind speed only (black dots) and the Ovadnevaite et al. (2014) scheme which also includes the Reynolds number representing the wave height and water viscosity (coloured dots). Figure from Ovadnevaite et al. (2014).

1.3.5 Volcanic emissions

The climate impacts of volcanic eruptions have received much attention in the literature (Robock, 2000) due to the substantial cooling effect that the large quantities of sulphur ejected with the tephra has on the climate. As the residence time of stratospheric sulphate is around a year (Robock, 2000), compared to around five days in the troposphere (Penner et al. 2001), the magnitude of the cooling is mainly determined by how much sulphur reaches the Junge (lower stratosphere from ~15-25 km) layer (Junge et al., 1961). For example, the St. Helens eruption was a highly explosive eruption but limited in its cooling effect as insufficient altitude was attained (Robock, 1981). In contrast, the El Chichon eruption was only a few km higher (Pollack et al., 1983), but the end result was that the El Chichon eruption reached the stratosphere and bolstered the Junge layer, thus providing a cooling to the climate.

As well as eruptive events, volcanoes also change aerosol concentrations and cloud properties from continuous passive degassing of SO_2 (von Glasow et al., 2009; Schmidt et al., 2012). Due to volcanic emissions being injected at higher altitudes than many other natural sulphur emission sources they are more likely to be oxidised to SO_4 and less likely to be deposited to the surface as SO_2 (Stevenson et al., 2003). This results in volcanic emissions being estimated to be almost twice as efficient than DMS emissions at producing CCN (Schmidt et al., 2012). As baseline volcanic emissions produce large amounts of SO_2 in many regions far from anthropogenic SO_2 sources (e.g., White Island volcano: Rose et al., 1986; Wardell et al., 2001), volcanoes can have a large impact on their surrounding climate.

Volcanic eruptions can also act as a natural fertiliser due to the high levels of nutrients contained within the tephra, such as nitrogen, iron and phosphorus compounds (Duggen et al., 2007; Huebert et al., 1999; Olgun et al., 2011; Uematsu et al., 2004). This is especially important in marine regimes where access to limiting nutrients is the limiting factor in net primary productivity (Achterberg et al., 2013; Hamme et al., 2010), which are often in high latitude regions where CO_2 drawdown to the deep ocean is also linked to the biological productivity (Frogner et al., 2001).

Emissions from volcanoes differ substantially between sites as well as over the evolution of an eruption's lifetime. The spatial, temporal and type of volcanic activity therefore determines any resulting impact on climate. In this thesis volcanic emissions of SO_2 are based upon the continuously and sporadically erupting

volcanic emission inventory from Andres and Kasgnoc (1998) which could underestimate emissions (Andres and Kasgnoc, 1998).

1.3.6 Dust

As dust has been shown to have only a small effect on CCN number concentrations (Manktelow et al., 2010) it is not explicitly investigated in this thesis. However, dust is an important natural aerosol in terms of its role in biogeochemical cycles and the cryosphere (Okin et al., 2011). Changes in dust levels could therefore have an indirect effect upon CCN concentrations and climate through changing biogeochemical cycles, particularly iron fertilization in iron depleted ocean regions (Jickells et al., 2005).

1.4 Sulphur cycle

In the natural environment DMS and volcanic activity are major sources of SO_2, with a secondary minor contribution from wild fires (Dentener et al., 2006). Once in the atmosphere SO_2 can be removed via dry deposition or oxidised to form sulphate; with a residence time in the troposphere of a few hours to days, increasing up to a few weeks in the stratosphere (Bluth et al., 1992). Oxidation can occur in both the gas (homogeneous) and aqueous (heterogeneous) phases.

Homogenous reactions are dominated by the hydroxyl radical (OH) during the day (Pham et al., 1995), which reacts with SO_2 to form sulphur trioxide (Stockwell and Calvert, 1983)

$$SO_{2\,(g)} + OH_{\,(g)} + M \rightarrow HOSO_{2\,(g)} + M \qquad (1.2)$$

$$HOSO_{2\,(g)} + O_{2\,(g)} \rightarrow HO_{2\,(g)} + SO_{3\,(g)} \qquad (1.3)$$

This reaction may also proceed with per-oxy radicals (Berndt et al., 2008) and at night by nitrate radicals (Stark et al., 2007). Sulphur trioxide can then react with water in either the gas or liquid phase (after uptake into the aqueous medium) to form sulphuric acid (H_2SO_4)

$$SO_{3\,(g)} + H_2O_{\,(g/l)} \rightarrow H_2SO_{4\,(aq)} \qquad (1.4)$$

Due to the high relative concentrations of water and the high sticking coefficient of SO_3, no other significant reaction pathways for SO_3 are expected to occur in the

atmosphere (Lovejoy et al., 1996). H_2SO_4 is a low volatility gas, and so it rapidly nucleates to form new aerosol particles or condenses onto existing ones.

Heterogeneous reactions are dominated by hydrogen peroxide and proceed via the sulphite ion under the proposed following mechanism

$$SO_{2\,(aq)} + H_2O_{\,(l)} \rightarrow H^+_{\,(aq)} + HSO_3^-{}_{(aq)} \quad (1.5)$$

$$HSO_3^-{}_{(aq)} + H_2O_2 \rightarrow A^-_{\,(aq)} + H_2O_{\,(l)} \quad (1.6)$$

$$A^- + H^+_{\,(aq)} \rightarrow H_2SO_{4\,(aq)} \quad (1.7)$$

Where A^- could possibly be the peroxymonosulphurous acid ion (Hoffman and Jacob, 1984). The reaction can also proceed with ozone

$$SO_{2\,(aq)} + H_2O_{\,(l)} \rightarrow H^+_{\,(aq)} + HSO_3^-{}_{(aq)} \quad (1.5)$$

$$HSO_3^-{}_{(aq)} + O_3 \rightarrow H_2SO_{4\,(aq)} \quad (1.8)$$

Sulphate (SO_4^{2-}) is then formed by the double dissociation of the diprotic H_2SO_4 molecule

$$H_2SO_4 \rightarrow H^+ + HSO_4^- \quad (1.9)$$

$$HSO_4^- \rightarrow SO_4^{\,2} \quad (1.10)$$

For example, the chemistry of ammonium (NH_4^+) is closely related to that of SO_4^{2-}

$$2NH_3 + H_2SO_4 \rightarrow (NH_4)_2SO_4 \quad (1.11)$$

With additional significant analogues of hydrochloric acid (HCl) and nitric acid (HNO_3). The main loss of sulphate is then via wet deposition.

1.5 Radiative forcing

Aerosols can alter the energy balance of the atmosphere in various ways, including through aerosol-radiation interactions (ARI) and aerosol-cloud interactions (ACI). The most recent IPCC (AR5) definition for radiative forcing (RF) is,

"*RF is defined, as it was in AR4, as the change in net downward radiative flux at the tropopause after allowing for stratospheric temperatures to readjust to radiative equilibrium, while holding surface and tropospheric temperatures and state variables such as water vapour and cloud cover fixed at the unperturbed values.*" (Myhre et al., 2013)

The effect that the PI–to–PD increase in anthropogenic aerosol concentrations has had on climate is measured by the difference in RF over the same period, measured in W m^{-2}. A positive forcing indicates an increase of surface temperatures (warming) in that region, while a negative forcing represents a decrease of surface temperatures (cooling). Due to the wide array of natural emissions, natural aerosols have varied compositions and, thus, different interactions with solar radiation (Figure 1.9).

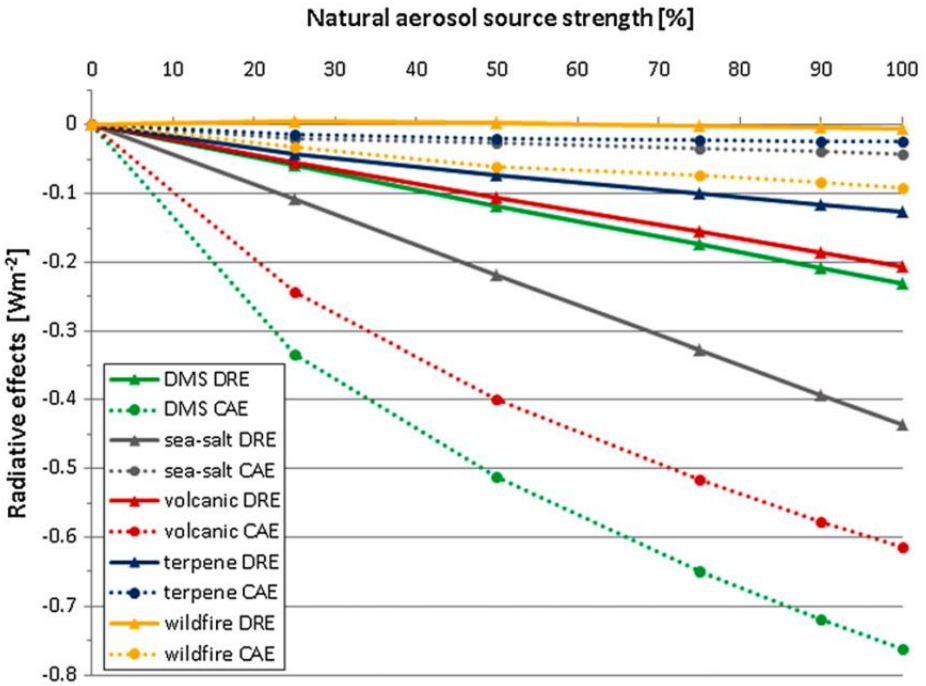

Figure 1.9. The direct and indirect radiative effects of natural aerosols. Figure from Rap et el. (2013).

1.5.1 Aerosol-radiation interactions

Aerosols of a sufficient size directly alter the energy balance of the atmosphere through absorbing and scattering incoming solar radiation (Figure 1.10). An example of the effect of this interaction can be seen through changes to visibility on polluted days. The amount of radiation absorbed or scattered is determined by the aerosol number concentration and optical properties (particle size, shape and chemical composition). Particle size is a key factor in determining the light scattering properties of aerosol (e.g., Schwartz 1996) with accumulation mode (0.1–1 μm) aerosol highly efficient in the shortwave part of the spectrum.

The direct interactions of natural emissions with solar radiation range from light absorbing black carbon particles from fires and volcanoes to light scattering sea salt particles. However, although the extensive Bond et al. (2013) study of BC showed it has a large positive PI–to–PD aerosol DRF at +0.71 W m^{-2} (90% confidence of +0.08 to +1.27 W m^{-2}), they also note it is generally co-emitted with light reflective sulphate, and so the net industrial–era climate forcing from all BC–containing sources reduces to a slightly negative value of –0.06 Wm^{-2} (90% confidence of -1.45 to +1.29 Wm^{-2}). In general, the amount of radiation scattered scales linearly with increasing emissions (Figure 1.9). The exception occurs at low aerosol optical depths (Boucher et al., 1998).

1.5.2 Aerosol-cloud interactions

Additional to the direct effect of aerosols on solar radiation, aerosols also alter the energy balance of the atmosphere by perturbing cloud properties (e.g., Andreae & Rosenfeld 2008; Boucher et al. 2013). Both the particle composition (Roesler and Penner, 2010) and size (McFiggans et al., 2006) affect its capacity to act as a CCN, with size being more significant (Dusek et al., 2006). Cloud drop number concentrations (CDNC) are related to the amount of liquid water contained within the cloud and how it is dispersed over the amount of particles present acting as CCN (Figure 1.11). For a fixed volume of cloud liquid water content, an increase in CCN number concentrations results in more numerous smaller sized cloud droplets being formed. As cloud albedo is related to the total reflective surface area of cloud drops contained within, more solar radiation is reflected with increasing CCN concentrations; this is known as the Twomey or “first aerosol indirect effect” (Twomey, 1974, 1977). Figure 1.9 shows that the change in cloud albedo with changing natural emission strength is largest when emission sizes are smallest (i.e. DMS and volcanic sulphur emissions).

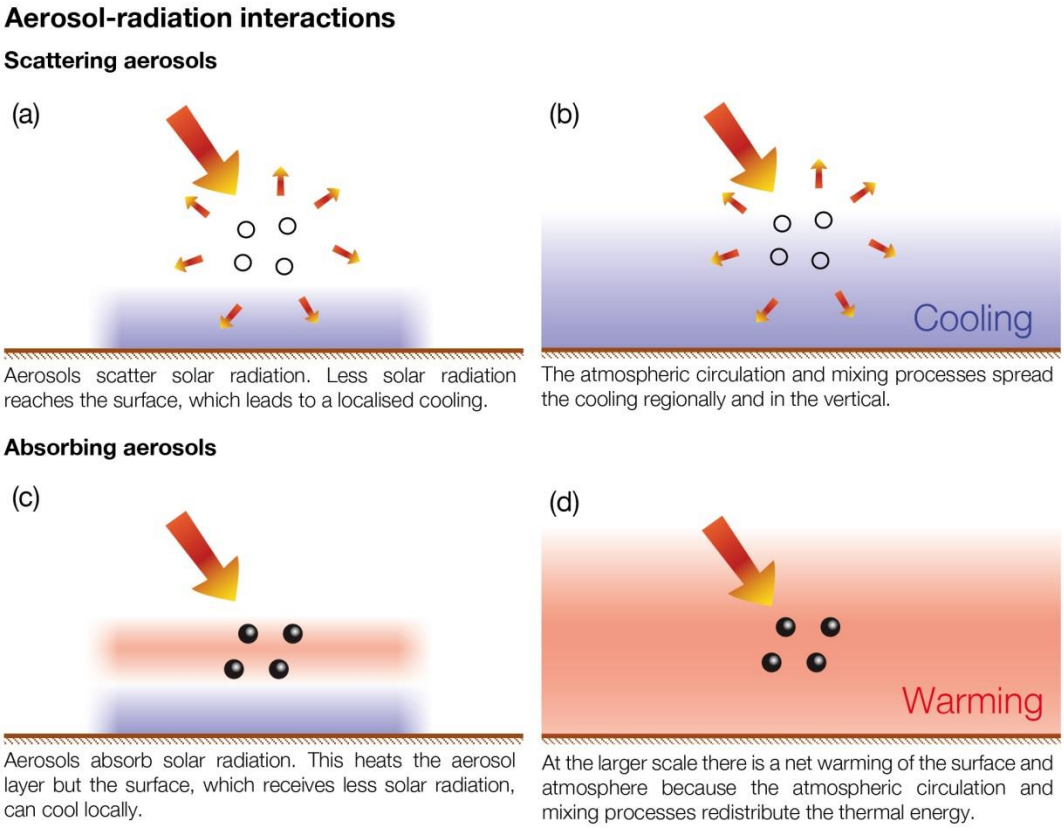

Figure 1.10. Aerosol-radiation interactions. Figure 7.23 from Chapter 7 of the IPCC AR5 report (Boucher et al., 2013).

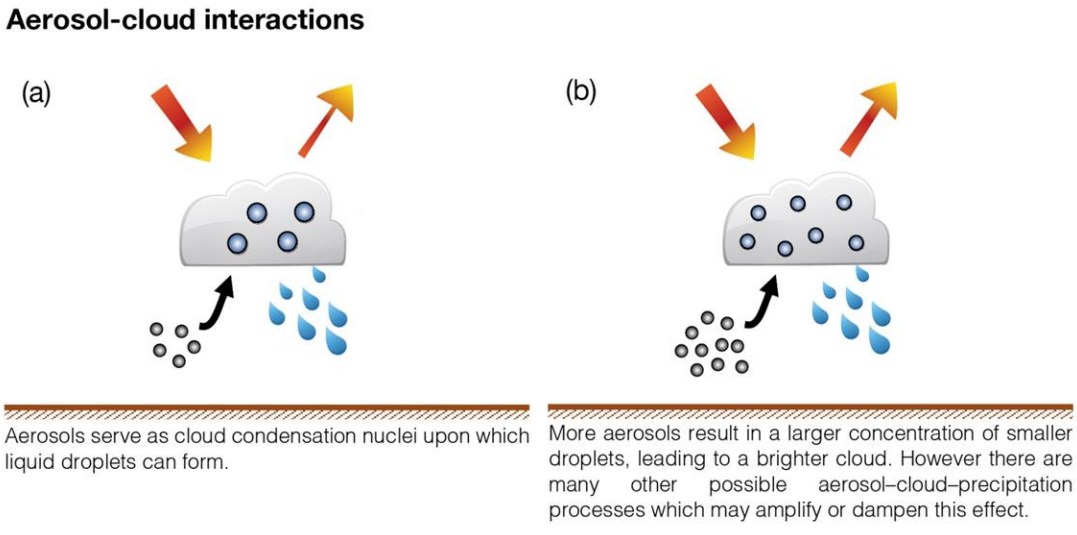

Figure 1.11. Aerosol-cloud interactions. Figure 7.24 from Chapter 7 of the IPCC AR5 report (Boucher et al., 2013).

A secondary effect is that smaller cloud drops increase the cloud life–time via reduced precipitation rates; known as the Albrecht or “second aerosol indirect effect” (Albrecht, 1989). Other more complex cloud adjustments are also likely to respond sensitively to small changes in aerosol under clean conditions (Koren et al., 2014; Rosenfeld et al., 2014). However, none of these rapid adjustments are calculated in this thesis, as the effective radiative forcing (Myhre et al., 2013) is not assessed, and stated for completeness only.

1.5.3 Uncertainty in aerosol-cloud radiative forcing

Figure 1.12 shows the percentage contribution to the global mean PI-to-PD uncertainty (variance) in radiative forcing due to 28 perturbed model parameters including natural emissions (green), anthropogenic emissions (red) and aerosol processes (blue). Natural emissions are a major component of the PI baseline state from which the magnitude of anthropogenic aerosol effects on climate are calculated, and are the largest component in the variance throughout the year (Carslaw et al., 2013). Even under the assumption that natural emissions do not change over time, the magnitude of PI-to-PD aerosol-cloud forcing is very sensitive to emissions in the PI because of the non-linear relation (Figures 1.2 and 1.9) between aerosol concentrations, cloud drop concentrations and cloud albedo (Carslaw et al., 2013; Pringle et al., 2009; Schmidt et al., 2012). The major contributing factor to the overall uncertainty in PI-to-PD anthropogenic radiative forcing of climate in the global aerosol microphysics model used throughout this thesis (see Chapter 2) stems from a lack of understanding of how natural emissions affect aerosol concentrations in the PI atmosphere.

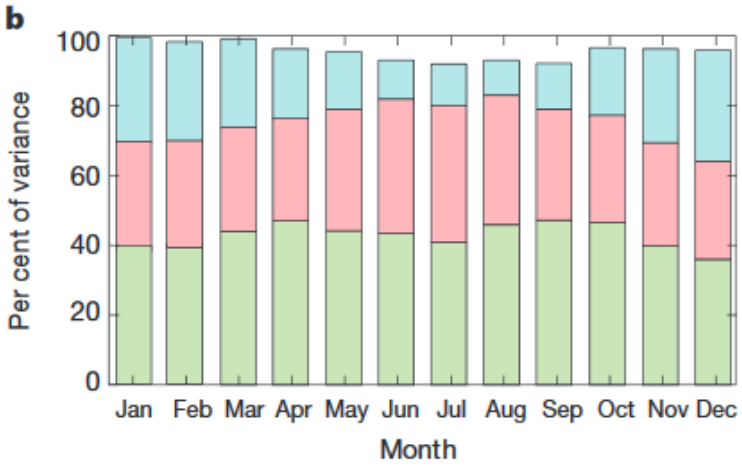

Figure 1.12. Contribution of different groups of parameters to global monthly mean forcing variance (green, natural emissions; pink, anthropogenic emissions; blue, aerosol processes). Figure from Carslaw et al. (2013).

1.6 Thesis aims

This thesis is centred on the uncertainty in the impact of natural emissions on aerosol concentrations and climate. The tools used are a global aerosol microphysics model, a suite of radiation models and two state–of–the–science fire models. All models used throughout this thesis are described at a level of complexity commensurate with my interaction with their respective running. In all chapters, the wider set of pre-industrial (1750) and present–day (2000) aerosol and precursor gas emissions are mainly based upon the recommendations set out by Dentener et al. (2006) in the AeroCom inventory. In Chapter 5, an additional two sets of pre-industrial fire emissions were generated from two fire models: LPJ–LMfire (LMfire herein) and LPJ–GUESS–SIMFIRE–BLAZE (SIMFIRE–BLAZE herein). Fire modelling is described further in Chapter 5. In all chapters, aerosol and precursor gas emissions are run within the GLObal Model of Aerosol Processes (GLOMAP). The impact of changing aerosol number concentrations on climate, via changes to the radiation balance of the atmosphere, is explored using the suite of radiation models (SOCRATES; incorporating the Edwards and Slingo and RADAER models). Results from the Edwards and Slingo model are discussed in Chapters 3 and 5, while results from the RADAER model are discussed in Chapter 5 only. The focus of the analysis throughout the thesis is on CCN because of the high sensitivity of cloud radiative forcing to the aerosol load (Andreae and Rosenfeld, 2008). In particular this thesis addresses the following three issues,

In Chapter 3 this thesis aims to define where on Earth can we observe and learn about the behaviour of pristine aerosol environments. In this study pristine aerosol environments are defined as where the PD aerosol environment looks and behaves similarly to the PI. Specifically:

1. What are the CCN number concentrations for the PI and PD and by how much have they changed?
2. On how many days are PD CCN concentrations similar to those in the PI?
3. How similar is the CCN response (or sensitivity) to perturbations in natural and anthropogenic emissions and microphysical processes in the PI and PD?
4. How does the location of pristine regions compare with both regions of significant anthropogenic RF and regions of significant low cloud cover?
5. Which current aerosol baseline observational stations are best situated to observe pristine aerosol environments?

Chapter 3 identified PD regions where the aerosol environment is close to a PI state. However, it didn't investigate which, if any, natural emissions are controlling CCN number concentrations in different regions and where and at what time of year the effects of each natural emission can be studied in the present atmosphere under conditions unperturbed by anthropogenic emissions.

In Chapter 4 this thesis aims to define where on Earth can we observe and learn about the behaviour of natural emission regimes. In this study natural emission regimes are defined in terms of the dominant natural emission (or combination of two natural emissions) that control CCN number concentrations, with very–little–to–no influence from other emission types. Specifically:

1. Where are CCN number concentrations sensitive to natural emissions (natural regimes) in the PI and PD?
2. How does seasonality in the surrounding environment affect the duration of natural emission regimes in the PI and PD?
3. How have anthropogenic emissions altered the extent and duration of natural emission regimes from the PI to the PD?

In Chapter 5 this thesis aims to understand how recent developments in fire modelling impact the PI aerosol state and the magnitude of the PI–to–PD radiative forcing. Specifically:

1) How do estimates of PI fire emissions from two fire models compare with the widely–used AeroCom 1750 dataset?
2) How sensitive are PI aerosol concentrations to changes in fire emissions?
3) How does modelled atmospheric PD/PI changes in black carbon concentrations compare with observed PD/PI changes in black carbon concentrations derived from northern hemisphere ice core records?
4) How does the magnitude of the historical radiative forcing alter with fire modelling emissions?

Chapter 2
Global aerosol microphysics model description

2.1 Introduction

The GLObal Model of Aerosol Processes (GLOMAP) was run by Dr. K. Pringle (University of Leeds) for Chapters 3 and by myself for Chapter 5.

The modal configuration version of GLOMAP is used throughout this thesis (Mann et al., 2010). GLOMAP–mode (GLOMAP herein) is a two–moment (number and mass of particles) global 3D aerosol microphysics model (Mann et al., 2010; Spracklen et al., 2005a, 2005b) incorporated within the Toulouse Off–line Model of Chemistry and Transport (TOMCAT, Chipperfield 2006). The version of GLOMAP used in this thesis simulates the aerosol microphysical processes of binary homogeneous nucleation, condensation, hygroscopic growth, coagulation, wet and dry deposition of aerosols and cloud processing (cloud droplet oxidation of sulphur dioxide to sulphate). GLOMAP can be configured to run using any number of modes. The configuration used throughout this thesis generates aerosol size and number distributions over seven log–normal modes (one soluble nucleation mode, plus one insoluble and one soluble for each of the Aitken, accumulation, and coarse modes, Table 2.1). The geometric standard deviation (σ) in each mode is assumed to remain constant while GLOMAP tracks the geometric mean radius of each mode. This configuration has been slightly updated from the standard configuration in Mann et al. (2010) to include smaller σ values for the Aitken and Accumulation mode width (Lee et al., 2013). When the mean radius exceeds the upper boundary size limit the particle number and mass, in the fraction that is exceeding the limit, is conveyed to the neighbouring mode – so-called mode merging.

The horizontal grid resolution is 2.8° × 2.8° with 31 vertical levels between the surface and 10 hPa. Using hybrid σ–pressure levels vertical levels results in a model level below ~100 hPa being terrain following, while model levels above are pure pressure levels. All simulations used meteorology for the year 2008 from the European Centre for Medium-range Weather Forecasts (ECMWF) reanalyses.

Table 2.1 GLOMAP–mode aerosol configuration. Table updated from Mann et al. (2010).

Mode	Soluble	Particle dry diameter size range	Composition	Sigma (σ)
Nucleation	Yes	<10 nm	SU, POM	1.59
Aitken	Yes	10–100 nm	SU, BC, POM	1.50
Accumulation	Yes	0.1–1 μm	SU, BC, POM, SS, DU	1.50
Coarse	Yes	>1 μm	SU, BC, POM, SS, DU	2.00
Aitken	No	10–100 nm	BC, POM	1.50
Accumulation	No	0.1–1 μm	DU	1.50
Coarse	No	>1 μm	DU	2.00

Where: SU=sulphate; POM=Particulate organic matter (=1.4*organic carbon); BC=Black carbo; SS=sea salt; DU=dust and σ is the geometric standard deviation of the respective mode.

2.2 Gas–phase species and chemistry

Gas–phase oxidant fields are generated from a single global chemistry simulation of TOMCAT with detailed tropospheric chemistry (Arnold et al., 2005). Other gas–phase emissions used throughout this thesis are mainly based upon AeroCom recommendations for year 1750 and 2000 (Dentener et al., 2006). The main exception is in Chapter 5 where the AeroCom 1750 fire emissions are compared to two recent fire modelling estimates of fire emissions in the PI period.

2.2.1 Oxidant species

Gas–phase oxidants fields from TOMCAT provide monthly mean oxidant concentrations of ozone (O_3), hydrogen peroxide (H_2O_2), and the hydroxyl (OH), hydroperoxyl (HO_2), and nitrate radicals (NO_3) at six–hourly intervals. Oxidants are subsequently interpolated onto the 3–D GLOMAP grid in order to calculate the oxidation of aerosol precursor gases (sections 2.2.2 and 2.2.3). GLOMAP treats H_2O_2 semi–prognostically by depletion via aqueous reaction with SO_2 and replenished by HO_2 self–reaction up to the upper limit determined from the background H_2O_2 concentration from the offline oxidant field.

Table 2.2 Emissions of aerosols and gases (Carslaw et al., 2013; Hamilton et al., 2014; Lee et al., 2013). C = carbon, S = sulphur, POM = Particulate organic matter (POM = 1.4*organic carbon).

Source	Emitted species	PD (2000) flux	PI (1750) flux	Refs.
Fossil fuel	BC	3.0 Tg a^{-1} C	Zero	(1)
	POM	3.2 Tg a^{-1} POM	Zero	(1)
Power stations	SO_2	24.2 Tg a^{-1} S	Zero	(1,2)
Industrial	SO_2	19.6 Tg a^{-1} S	Zero	(1,2)
Transportation	SO_2	4.8 Tg a^{-1} S	Zero	(1,2)
Off-road	SO_2	0.8 Tg a^{-1} S	Zero	(1,2)
Biofuel	BC	1.6 Tg a^{-1} C	0.4 Tg a^{-1} C	(1,3)
	POM	9.1 Tg a^{-1} POM	1.6 Tg a^{-1} POM	(1,3)
Domestic	SO_2	4.8 Tg a^{-1} S	0.12 Tg a^{-1} S	(1,3)
AeroCom	BC	3.10 Tg a^{-1} C	1.03 Tg a^{-1} C	(1,4)
Wildfires	POM	34.7 Tg a^{-1} POM	12.8 Tg a^{-1} POM	(1,4)
	SO_2	2.10 Tg a^{-1} S	1.46 Tg a^{-1} S	(1,4)
LMfire	BC	3.10 Tg a^{-1} C	5.19 Tg a^{-1} C	-
Wildfires	POM	34.7 Tg a^{-1} POM	90.3 Tg a^{-1} POM	-
	SO_2	2.10 Tg a^{-1} S	2.64 Tg a^{-1} S	-
SIMFIRE–BLAZE	BC	3.1 Tg a^{-1} C	3.30 Tg a^{-1} C	-
Wildfires	POM	34.7 Tg a^{-1} POM	46.4 Tg a^{-1} POM	-
	SO_2	2.1 Tg a^{-1} S	2.13 Tg a^{-1} S	-
Volcanoes	SO_2	12.6 Tg a^{-1} S	12.6 Tg a^{-1} S	(5)
Marine dimethyl sulphide	DMS	17.1 Tg a^{-1} S	17.1 Tg a^{-1} S	(6,7)
Sea spray	Sea salt	Wind–dependent flux	Same as PD	(8)
Biogenic volatile organic carbon	Mono-terpenes (α-pinene)	50 Tg a^{-1} POM produced	50 Tg a^{-1} POM produced	(9,10)
Anthropogenic volatile organic carbon	VOC	80 Tg a^{-1} POM produced	Zero	(9)

References:

1(Dentener et al., 2006); **2**(Cofala et al., 2005); **3**(Bond et al., 2013); **4**(van Der Werf et al., 2003); **5**(Andres and Kasgnoc, 1998) ; **6**(Kettle and Andreae, 2000); **7**(Nightingale et al., 2000) ; **8**(Ayash et al., 2008); **9**(Spracklen et al., 2011b) ; **10**(Guenther et al., 1995).

2.2.2 Sulphur species

Table 2.3 Gas phase sulphur chemistry used in GLOMAP–mode. Table modified from Mann et al. (2010).

Reactants		Products	Reference
DMS + OH	→	SO_2	(Atkinson et al., 1989)
DMS + OH	→	0.6 SO_2 + 0.4 DMSO	(Pham et al., 1995)
DMS + NO_3	→	SO_2	(Atkinson et al., 1989)
DMSO + OH	→	0.6 SO_2 +0.4 MSA	(Pham et al., 1995)
H_2S + OH	→	SO_2 + OH	(Pham et al., 1995)
CS_2 + OH	→	SO_2 + COS	(Pham et al., 1995)
COS + OH	→	SO_2	(Pham et al., 1995)
SO_2 + OH + M	→	H_2SO_4	(Pham et al., 1995)

Sulphur chemistry in GLOMAP includes eight species: DMS (dimethyl sulphide), DMSO (dimethyl sulphoxide), MSA (methane sulphonic acid), H_2S (hydrogen sulphide), COS (carbonyl sulphide), CS_2 (carbon disulphide), sulphur dioxide (SO_2) and H_2SO_4. The sulphur reaction scheme is shown in Table 2.3. The TOMCAT generated global fields of the oxidants (section 2.2.1) are interpolated between each of the four time steps occurring at 00:00, 06:00, 12:00, and 18:00 UT.

Ocean dimethyl sulphide (DMS) emissions are calculated from a monthly mean seawater concentration inventory from Kettle and Andreae (2000) using the wind speed-dependent sea–air flux parametrisation of Nightingale et al. (2000). In all chapters, 1750 and 2000 emissions of DMS modelled by GLOMAP are 17.1 Tg S a^{-1} (Table 2.2), which is at the lower end of the range of emissions (13–37 Tg S a^{-1}) reported by Kettle and Andreae (2000). An update to the Kettle and Andreae (2000) inventory by Lana et al. (2011), which used three times more samples to compile, resulted in a reported global increase of DMS concentrations of 17%. Regionally, from June–to–August surface (1000 hPa) DMS emissions may be underestimated over the Southern Ocean and Gulf of Alaska and overestimated over the Barents and Greenland Seas. While from December–to–February DMS concentrations may be underestimated over southern hemisphere sub–tropical gyres and overestimated over the Southern Ocean (Mahajan et al., 2015).

Volcanic emissions of SO_2 used in this thesis are from the AeroCom inventory, which scaled the Andres and Kasgnoc (1998) volcanic emissions inventory by a factor of 1.21 (Dentener et al., 2006) following the recommendations of Graf et al. (1998) and Textor et al. (2004). In–plume gas–to–particle conversion of SO_2 to sulphate is accounted for by assuming that 2.5% of the volcanic SO_2 emissions flux is directly emitted as sulphate (Dentener et al., 2006). In all chapters, 1750 and

2000 emissions of volcanic SO_2 modelled by GLOMAP are 12.6 Tg S a^{-1} (Table 2.2) and are emitted between 100–300 m above the surface.

For all chapters monthly mean PD SO_2 biomass burning emissions are taken from the AeroCom dataset (Dentener et al., 2006), based on the Global Fire Emissions Database v1 (van Der Werf et al., 2003). For Chapters 3 and 4 monthly mean PI SO_2 biomass burning emissions are also taken from the AeroCom dataset where emissions in most regions are scaled downwards according to population, while high latitude boreal region fires are doubled (Dentener et al., 2006). In Chapter 5 the AeroCom PI fire SO_2 emission dataset are compared to recent fire modelling estimates of emissions from two fire models (described further in Chapter 5). In–plume gas–to–particle conversion of SO_2 to sulphate is accounted for by assuming that 2.5% of the biomass burning SO_2 emissions flux is directly emitted as sulphate (Dentener et al., 2006)

Emissions from anthropogenic sources are the major present day SO_2 emission source and are assumed to have no seasonal variability in both the pre–industrial and present day. Present day industrial emissions are based on the International Institute for Applied Systems Analysis inventory and account for 49.4 Tg S a^{-1} with 24.2 Tg from power production, 19.6 Tg from industry and 5.6 Tg from transportation (Cofala et al., 2005; Dentener et al., 2006). Present day domestic emissions account for 4.8 Tg S a^{-1} (Bond et al., 2013; Dentener et al., 2006). In the pre–industrial period industrial emissions are assumed to be zero (Dentener et al., 2006), with a small domestic contribution of 0.12 Tg S a^{-1} (Bond et al., 2013; Dentener et al., 2006). Similar to volcanic SO_2 emissions, in–plume gas–to–particle conversion of SO_2 to sulphate is accounted for by assuming that 2.5% of the anthropogenic SO_2 emissions flux is directly emitted as sulphate (Dentener et al., 2006). Transport and domestic emissions are emitted into the lowest model level, whereas power plant and industrial emissions are emitted between 100–300 m above the surface.

Emissions of carbon disulphide (CS_2) and carbonyl sulphide (COS) are emitted at a constant rate. Anthropogenic sources are calculated from the molar emission ratio of SO_2 where $CS2/SO2=3\times10^{-3}$ and $COS/SO2=8\times10^{-4}$ (Pham et al., 1995; Spracklen et al., 2005a). Biogenic sources are calculated from the molar emission ratio of DMS where $CS2/DMS=1\times10^{-2}$ and $COS/DMS=1\times10^{-2}$ (Bates et al., 1992; Spracklen et al., 2005a).

2.2.3 Secondary organic aerosol

Table 2.4 Gas phase secondary organic aerosol chemistry used in GLOMAP–mode. Table modified from Mann et al. (2010).

Reactants		Products	Reference
Monoterpene + OH	→	0.13 SEC–ORG	(Pham et al., 1995)
Monoterpene + NO_3	→	0.13 SEC–ORG	(Pham et al., 1995)
Monoterpene + O_3	→	0.13 SEC–ORG	(Pham et al., 1995)

In GLOMAP modelled secondary organic aerosol (SOA) has both biogenic and anthropogenic volatile organic compound (VOC) sources. Biogenic VOCs are calculated from the monthly mean emissions of biogenic monoterpenes from the Global Emissions Inventory Analysis dataset (Guenther et al., 1995), assuming a constant emission flux throughout the month. The oxidation of monoterpenes with O_3, OH and NO_3 yields a gas–phase oxidation product (SEC–ORG) at fixed yield of 13% (Table 2.4), with reaction rates assumed to equal those of α–pinene.

Anthropogenic VOCs are calculated following Spracklen et al. (2011b) by scaling to fossil fuel carbon monoxide (CO) emissions (IPCC estimate of 450.5 Tg a^{-1}). The VOC/CO ratio is 0.29 g/g and assumes that the global total VOC equals the Emissions Database for Atmospheric Research (EDGAR) reported value (127 Tg a^{-1}).The SEC–ORG oxidation product forms SOA by condensing irreversibility onto pre-existing aerosol (Spracklen et al., 2006, 2008a). This mechanism produces 50 Tg a^{-1} of biogenic SOA and 80 Tg a^{-1} of anthropogenic SOA (Table 2.2).

2.3 Primary aerosol species

Primary aerosol are emitted directly into each mode. After which, primary particles are allowed to evolve during transport through the atmosphere (section 2.4).

2.3.1 Sea salt

Modelled emission fluxes of sea salt are calculated using the Gong (2003) parametrisation which is based on surface (10 m above sea level) wind speeds. Due to the relatively large size of sea salt particles and their high hygroscopicity, the size resolved sea salt flux only enters the soluble accumulation and soluble coarse modes. The boundary sea salt size between each mode is set at 1 micron.

2.3.2 Fossil fuel and biofuel

Anthropogenic fossil fuel and biofuel aerosol emissions follow the AeroCom recommendations (Table 2.2) and are injected in the model below 100 m. Inventories of fossil fuel and biofuel emissions contain aerosol mass only. Therefore, in order to estimate particle number concentrations a log-normal size distribution with a fixed width (σ, Table 2.1) around the peak number concentration (the number median diameter) is assumed. In this thesis the median diameter for fossil fuels combustion particles is 56 nm and for biofuels is 110 nm (Lee et al., 2013), which are larger than those suggested for AeroCom (Dentener et al., 2006), but smaller than those used by Stier et al. (2005).

2.3.3 Fire emissions

For all chapters PD monthly mean emissions of primary aerosols from fires are taken from the AeroCom dataset (Dentener et al., 2006), based on the Global Fire Emissions Database v1 (van Der Werf et al., 2003). For Chapters 3 and 4 monthly mean PI emissions are also taken from the AeroCom dataset where emissions in most regions are scaled downwards according to population, while high latitude boreal region fires are doubled (Dentener et al., 2006). In Chapter 5 the AeroCom PI fire emission dataset are compared to recent fire modelling estimates of emissions from two fire models (described further in Chapter 5).

Table 2.5. Fractional distribution (in percent) of fire emission altitudes. Tropical region is 30° S to 30° N. Temperate region is >30° N and >30° S. Eurasian sub–region is 45 to 75° N and 0 to 180° E. Canadian sub-region is 45 to 75° N and 50 to 170 ° W. Table from Dentener et al. (2006).

	Altitude range					
	0–100 m	100–500 m	500–1000 m	1000–2000 m	2000–3000 m	3000–6000 m
Agricultural	100	–	–	–	–	–
Tropical	20	40	40	–	–	–
Temperate	20	20	20	40	–	–
Boreal (Eurasia)	10	10	20	20	40	–
Boreal (Canada)	10	10	10	10	20	40

Fire emissions of aerosol and pre-cursor gases are emitted at six altitude ranges (Table 2.5), dependent upon latitude and the general vegetation biome type (Dentener et al., 2006). Similarly to fossil fuel and biofuel emissions an assumed size distribution is applied to all fire emissions, regardless of dataset, with a median particle size diameter of 110 nm (Lee et al., 2013). Again, this value is larger than the suggestion for AeroCom (Dentener et al., 2006), but smaller than the value used in Stier et al. (2005). A fixed size distribution for all datasets therefore assumes that there is no difference in median particle size in different burning regions of the world or between different types of vegetation burning that exist in some regions between different datasets examined in Chapter 5 (e.g., the fractions of agricultural vs. forest burning in mid latitudes can differ).

2.3.4 Dust

The impact of dust emissions on aerosol concentrations and climate are not diagnosed in any chapter. The following brief methodology of how dust is treated within GLOMAP is added for completeness only.

Daily varying dust emissions are prescribed using the AeroCom inventory (Dentener et al., 2006). Emissions are based on fluxes from the NASA Goddard Earth Observing System Data Assimilation System (Ginoux et al., 2001) and subsequently mapped onto the insoluble accumulation and coarse size mode (Table 2.1).

2.4 Aerosol microphysical processes

Figure 2.1 shows the micro-physical evolution of atmospheric aerosol over its lifetime. These processes influence the aerosol size, composition and atmospheric residence time. Aerosol particles are formed from gas-to-particle conversion (nucleation) of aerosols precursor gases or directly emitted. Favourable nucleation conditions are low temperature, high relative humidity and a low particle surface area. The upper troposphere is therefore an ideal environment for new particle formation to occur (Spracklen et al., 2005b).

Aerosols then grow via coagulation and condensation of vapours. Coagulation is the process of two particles colliding and forming a single new particle by ‘sticking’ together. In the atmosphere particle motion is determined by Brownian and

turbulent motion, and intermolecular forces. Coagulation facilitates the rapid growth of newly nucleated particles, which due to their small size move quickly and are often numerous, and provides an important sink for ultrafine particles with larger particles (e.g., primary particles). There is competition between nucleation and condensation in the atmosphere for the available condensable trace gases present. It is more energetically favourable for gas-phase species to condense rather than form new particles (Kulmala et al., 2004a), therefore pre-existing particles provide an important sink for trace gases. Condensation efficiently grows particles up to sizes of around 60–100 nm, after which it becomes diffusion limited (Raes et al., 2000). Growth in clean regions takes a few days to weeks, whereas in polluted regions it can occur over less than a day (Raes et al., 2000).

Once hygroscopic aerosols have grown to a certain size they can activate to form cloud droplets when the local conditions are suitable (e.g., the supersaturation). Aerosol are then removed via wet deposition (precipitation), which includes both below–cloud impaction scavenging and in–cloud nucleation scavenging. Aerosol removal also occurs via dry deposition. In general, larger particles deposit to the surface faster with an exception being ultrafine particles (< 0.05 µm) which can readily diffuse to the surface.

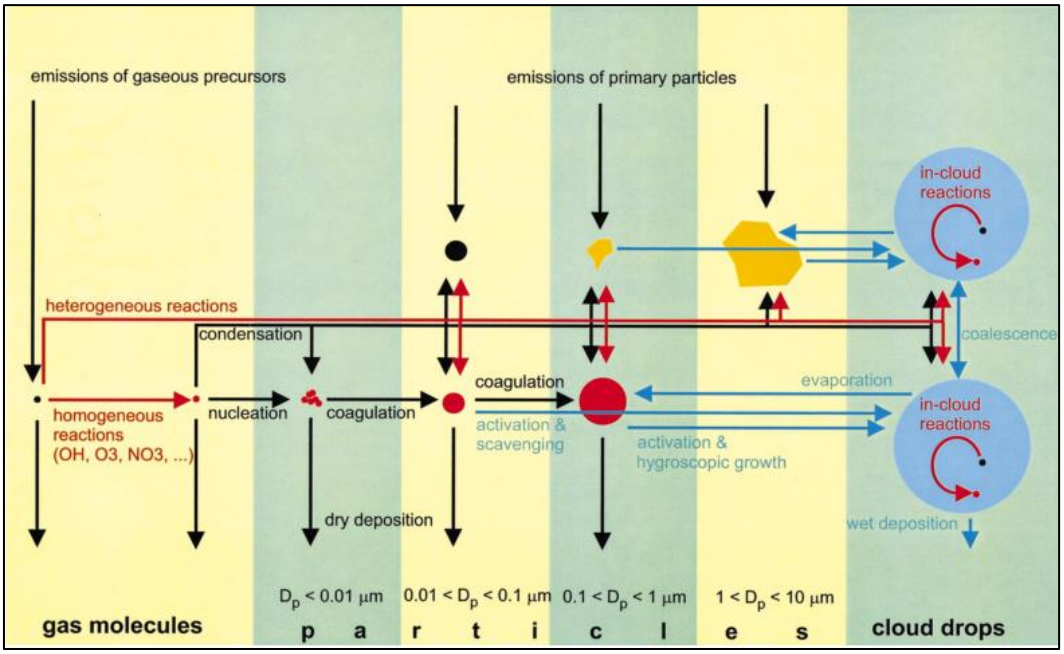

Figure 2.1. The aerosol microphysical processes that influence the size distribution and chemical composition of the atmospheric aerosol. Figure from Raes et al. (2000).

The micro-physical processes represented in GLOMAP are introduced in the following sections. A full detailed description is presented in Mann (2010).

2.4.1 Nucleation

New particle formation throughout this thesis is simulated in the free troposphere (FT) using a binary H_2SO_4—H_2O nucleation scheme from Vehkamäki et al. (2002) and in the boundary layer (BL) using a nucleation scheme where the nucleation rate depends on [H_2SO_4] (Kulmala et al., 2006).

The rate of binary nucleation is dependent on the ambient temperature, relative humidity and the [H_2SO_4]. The Vehkamäki et al. (2002) parametrisation is valid for temperatures between 230 K to 305 K and relative humidities between 0.01% to 100%. Nucleation rates under 230 K are an extrapolation of those at higher temperatures. For FT nucleation to occur a gas-phase threshold concentration must be reached, which is derived from the ambient temperature and relative humidity (Spracklen, 2005).

The model we use here does not account for the role of organic compounds in the first stages of nucleation (Metzger et al., 2010).

2.4.2 Aerosol growth

In GLOMAP particle growth can occur through the coagulation of two particles, or the condensation of low volatility gases onto the particle surface. For example sulphur dioxide and oxidised volatile organic species readily condense onto existing particles. Modelled coagulation is both inter-modal (i.e., between modes) and intra-modal (i.e., in the same mode), with the total aerosol mass remaining conserved (Mann et al., 2010; Spracklen et al., 2005b). As both nucleation and condensation compete for the available vapour concentrations, five short “competition” sub-time steps are contained within the main chemistry time step (Mann et al., 2010).

2.4.3 Aerosol activation

Throughout this thesis the subset of aerosol which can act as CCN are defined as those soluble particles with a dry diameter larger than 50 nm. This approximately corresponds to the activation of particles at 0.3% supersaturation.

Within all chapters CCN number concentrations are reported at 915 hPa (~850 m above sea level) unless otherwise stated. This height approximately corresponds to low level warm cloud base.

2.4.4 Cloud processing

GLOMAP models the in-cloud aqueous-phase oxidation of SO_2 to SO_4 within cloud droplets in non-precipitating clouds. Oxidation only occurs in those grid cells where low level warm stratiform clouds are present. Low cloud cover is prescribed from the International Satellite Cloud Climatology Project (ISCCP) climatology (Rossow and Schiffer, 1991) with cloud base assumed to be at 900 hPa globally.

2.4.5 Deposition

GLOMAP represents both the wet and dry deposition of aerosol.

Aerosols are directly precipitated out of clouds and also scavenged below cloud by falling raindrops. Large scale dynamic precipitation removes 99.9% of activated aerosol, while smaller scale sub-grid (assumed to occur in 30% of the grid cell) convective precipitation removes the aerosol fraction proportional to the fraction of cloud water converted to rain.

Aerosol dry deposition is calculated following Zhang et al. (2001) and accounts for Brownian motion, gravitational settling, interception, impaction and particle rebound. The deposition rate is dependent upon the surface roughness as defined by type (e.g., forests vs. oceans), wind speeds and size of the particle.

2.4.6 Cloud droplet number concentrations

Cloud droplet number concentrations are calculated offline from the monthly mean aerosol size distribution and assume a uniform updraught velocity of 0.15 m s^{-1} over oceans and 0.3 m s^{-1} over land (Pringle et al., 2009).

The critical supersaturation is calculated using the hygroscopicity parameter, kappa (κ), approach (Petters and Kreidenweis, 2007). A multi-component κ is obtained by weighting individual κ values by the volume fraction of each chemical component in the particles. Values of κ are assigned as follows: sulphate (0.61, assuming ammonium sulphate), sea-salt (1.28), black carbon (0.0), and particulate organic matter (0.1).

2.4.7 Radiation modelling

The PI-to-PD direct radiative forcing (DRF) and first aerosol indirect radiative forcing (IRF), also known as the cloud albedo effect, were calculated with GLOMAP output using the Suite Of Community RAdiative Transfer codes based on Edwards and Slingo (SOCRATES, Edwards & Slingo 1996), with nine bands in the longwave (LW) and six bands in the shortwave (SW). No radiation modelling was undertaken by me, only the analysis of output. Modelling was run by Dr. C. Reddington (University of Leeds) in Chapter 3 to diagnose the first aerosol indirect effect and by Dr. C. Scott (University of Leeds) in Chapter 5 to diagnose both the first aerosol indirect effect and the aerosol direct effect.

The offline configuration is driven by year 2000 monthly mean temperature and water vapour concentrations from ECMWF reanalysis data and cloud fields from the ISCCP-D2 archive (Rossow and Schiffer, 1999).

The DRF is calculated as the difference in net (SW + LW) top-of-atmosphere all-sky radiative flux between the PI and PD, based on the aerosol optical properties (scattering and absorption coefficients and the asymmetry parameter) for each size mode and spectral band (Bellouin et al., 2013).

The IRF is determined from the radiative perturbation induced by the change to CDNC between the PI and PD (Rap et al., 2013; Scott et al., 2014). To calculate the IRF, a uniform control cloud droplet effective radius (r_{e1}) of 10 μm is assumed to maintain consistency with the ISCCP derivation of the liquid water path. For each paired PI–PD experiment the effective radius (r_{e2}) for low–and–mid–level clouds (up to 600 hPa) is calculated as in Eqn. 2.2, from the monthly mean cloud droplet number fields $CDNC_1$ and $CDNC_2$ respectively (where $CDNC_1$ represents the PD simulation, and $CDNC_2$ represents the PI simulation).

$$r_{e_2} = r_{e_1} \times \left[\frac{CDNC_1}{CDNC_2}\right]^{\frac{1}{3}} \qquad (2.2)$$

2.5 Model summary

GLOMAP has been extensively evaluated against aerosol observations (Mann et al., 2010), performs well against observations of CCN in different environments (Spracklen et al., 2011a), and has been refined by comparing against a more detailed bin-resolved version of the model (Mann et al., 2012). Vertical aerosol number concentration profiles in GLOMAP have also been compared to similar models and performance was shown to be comparable (Mann et al., 2014).

This makes GLOMAP an ideal aerosol microphysics model for use in the study of natural aerosols. Due to this GLOMAP has also previously been used in various other natural aerosol studies (e.g., Schmidt et al., 2010; Scott et al., 2014; Spracklen and Rap, 2013; Woodhouse et al., 2010).

Chapter 3
Where on Earth can we observe pristine aerosol?

3.1 Introduction

It has been argued that regions in which aerosols are unperturbed by air pollution no longer exist in today's atmosphere (Andreae, 2007). If this were so then observing and characterising an atmospheric state without pollution would be very difficult, and maybe impossible in some regions, and the part of the uncertainty in the pre-industrial (PI) to present-day (PD) aerosol indirect forcing associated with this unknown baseline aerosol state may be irreducible (Carslaw et al., 2013). Even in regions dominated by natural emissions of sea spray, volcanic sulphates, marine dimethyl sulphide (DMS) or terrestrial biogenic volatile organic compounds (BVOCs), the aerosol state can still be strongly perturbed by long range transport from anthropogenic sources (e.g., Clarke et al. 2001; Browse et al. 2012; Fiore et al. 2012; Schmidt et al. 2012; O'Dowd et al. 2014). Studies of natural emissions and processes have typically focused on remote regions such as the high northern latitude boreal forest (Tunved et al., 2006), the Brazilian rainforest (Martin et al., 2010; Pöschl et al., 2010) and the Southern Ocean (Murphy et al., 1998). However, the choice of location tends to be based on the physical remoteness of the site and the strength of local natural emissions, but with little consideration as to how closely the aerosol state truly resembles unperturbed conditions.

Several definitions of pristine, natural or 'clean background' aerosol environments have been used when analysing observations, including particle number concentrations (Fiebig et al., 2014), the concentration of a particular species such as carbon monoxide or particulate black carbon (Clarke and Kapustin, 2010), the location (Pöschl et al., 2010; Tunved et al., 2006), or a combination of factors (Koren et al., 2014). However, operational definitions suffer from not knowing how much the environment is influenced by a pervasive background of anthropogenic aerosol, which is unlikely to be detectable in observations. It is also not always possible to define pristine environments in terms of the lowest observed aerosol concentration at a particular site because often such conditions are associated with strong scavenging by precipitation and will not represent and behave like the true climatological state in the PI. Remote oceans can provide an insight into how clouds respond to changes in aerosol starting from a very low aerosol baseline

(Koren et al., 2014), but are unlikely to be good analogues for aerosol in all PI regions which will often have been strongly affected by emissions from natural forest fires (Marlon et al., 2008; van der Werf et al., 2013), volcanic activity (Schmidt et al., 2012) or terrestrial biogenic emissions (Kirkby et al., 2016; Riccobono et al., 2014). There is therefore no single globally applicable aerosol state that defines the PI atmosphere. Rather, the state changes spatially and seasonally. Global models provide an alternative, and perhaps the only, way of estimating the properties and behaviour of aerosols in a PI reference state, and can at least point to where a pristine aerosol state is likely to be observable today.

The purpose of the two papers that form this chapter was twofold. First in Hamilton el al. (2014) regions of the globe were defined where PD aerosol (year 2000) looks and behaves most like it did in a PI reference state (year 1750). Second in Hamilton (2015) the analysis was extended to show how PD aerosol concentrations have changed since the PI and suggest which Global Aerosol Watch (GAW) observational stations are suitable for studying pristine aerosol environments.

The term pristine is used here to refer to regions where the PD aerosol environment still looks and behaves similarly to the PI. Pristine aerosol environments can therefore be considered to be in an unperturbed (i.e., pre–industrial) state, although the term can often be used misleadingly to imply extremely low aerosol concentrations. Anthropogenic emissions in 1750 were not zero (Dentener et al., 2006) and a 1750 reference year is therefore not truly “pre–human” (Andreae, 2007), but is appropriate for defining the properties and behaviour of aerosols in a reference state that is used for radiative forcing calculations (Schulz et al., 2006).

Two measures of similarity of aerosol between the PI and PD are used to define pristine regions based on data from GLOMAP. First, the daily aerosol states are compared. As air pollution tends to be episodic in remote regions it is not appropriate to compare longer time averages because a few polluted days will make the whole period appear mildly polluted. Secondly the aerosol response to perturbations in emissions and processes is compared. It is conceivable that two periods in the aerosol historical record could have similar cloud condensation nuclei (CCN) number concentrations (the aerosol state) but respond differently to perturbations because those two states were generated through a different series of emissions and/or processes. By comparing the responses in the PI and PD, regions where PD aerosol is ‘behaving’ like it did in the PI are identified. The similarity of aerosol responses is an essential additional factor in defining pristine regions, which cannot be addressed using observations alone.

3.2 Methods

To test the similarity of aerosol states, changes in CCN concentration between 1750 and 2000 are quantified. To test the similarity of aerosol responses in 1750 and 2000, the sensitivity of CCN to 28 model parameters representing natural and anthropogenic aerosol emissions, microphysical processes and model structures is compared (Carslaw et al., 2013; Lee et al., 2013).

To ensure that the statistics of PI–PD similarity reflect only the change in emissions and associated aerosol processes, the same (year 2008) global 3–D meteorological reanalyses in 1750 and 2000 is used, which eliminates meteorology as a source of variability between the two years. All simulations used meteorology from the European Centre for Medium–range Weather Forecasts (ECMWF) re–analyses, while low cloud cover is from the International Satellite Cloud Climatology Project (ISCCP) climatology (Rossow and Schiffer, 1991).

Emissions for both the PI and PD are listed in Table 2.2. Anthropogenic fossil fuel emissions are assumed to be zero in the PI, although a small anthropogenic biofuel component to the atmosphere exists (Dentener et al., 2006). Natural emissions of sea spray, BVOC (which form SOA) and volcanic sulphur dioxide are the same in the PI and PD. Pre-industrial emissions of biofuel and biomass burning follow the Dentener et al. (2006) recommendations for AeroCom which were derived by scaling emissions with human population data.

A variance–based sensitivity analysis of PI CCN concentrations to perturbations of 28 model parameters covering emissions, microphysics and model structures was performed in the same way as the PD analysis of Lee et al. (2013). The 28 model parameters and their ranges are defined in Table 3.1, with a full description of what each parameter does in the model in Lee et al. (2013). Scaled parameters are calculated by multiplying by a factor between the minimum and maximum given in the uncertainty range column. Absolute parameters were calculated by setting the parameter to a fixed value between the minimum and maximum given in the uncertainty range column. The parametric uncertainty was calculated by performing a Monte Carlo sampling of validated Bayesian emulators conditioned on an ensemble of 168 model simulations covering the joint parameter space of the 28 model parameters (Table 3.1), with combinations of parameter settings defined by a Maximin Latin Hypercube experimental design. The Bayesian emulator then describes the relationship between the modelled CCN and the setting of the 28 perturbed parameters across the defined uncertainty space. The main effect values were calculated using variance decomposition of 140,000 Monte Carlo CCN

samples drawn from the emulator, generating a probability density distribution of CCN concentrations caused by the uncertainty in the model input parameters, including their interactions (Lee et al., 2013), under the assumption that the sources of uncertainty in the PI are the same as in the PD (Table 3.1).

The perturbed parameter GLOMAP ensemble (Carslaw et al., 2013; Lee et al., 2013) and the single hourly–output simulations for 1750 and 2000 were set up in an identical way and also used 2008 ECMWF meteorology in each modelled time period. Parameters relating to biomass burning emissions are assigned as natural aerosol in both PI and PD. Accurate source type identification of atmospheric biomass burning aerosol, with a similar fuel origin, is currently impossible to disentangle in the atmosphere once the aerosol becomes well mixed. In combination with the similar assumption of PI biomass burning emissions, it is therefore expected that the identification of pristine aerosol in fire–dominated environments will be an upper limit.

To identify grid cells with similar CCN sensitivity in the PI and PD, the goodness of fit correlation (coefficient of determination) of the 28 PI and PD parameter sensitivities (main effects) was calculated. The goodness of fit is based on the 1:1 line by setting the predicted value in the residual sum of squares calculation equal to the observed value (i.e., the expected PD main effect = the initial PI main effect) and not on the best fit line. Those grid cells with an $r2 \geq 0.9$ are then considered as having a pristine “PI-like” sensitivity (i.e., the CCN sensitivity to all 28 parameters is behaving similarly in both time periods). Although it is possible for the CCN response to a single parameter to be of an equal and opposite sign of magnitude, this is unlikely and does not alter the concept that the sensitivity of the aerosol to the full 28-parameter ensemble is similar.

Radiative forcing values were obtained from the Carslaw et al. (2013) study and linearly interpolated onto the 2.8° by 2.8° GLOMAP grid to allow direct comparison with both the simulation and sensitivity analysis results (i.e., identified pristine regions). Low-cloud fraction is taken from a climatology of observations created by the International Satellite Cloud Climatology Project (ISCCP-D2) and linearly interpolated onto the 2.8° by 2.8° GLOMAP grid.

In these offline experiments, the second aerosol indirect (cloud lifetime) effect is not calculated.

Table 3.1. Parameter descriptions, uncertainty ranges and median values as used in both the pre–industrial and present–day simulations. For the emissions, the median value of the scaling parameter means the emissions in Table 2.2 were used. Symbols relate to those seen in Figure 3.13 and 3.14.

Parameter description	Uncertainty range	Median value	Effect	Symbol/ Fig. 3.13/14
Volcanic SO_2 emission flux	0.5-2	1	Scaled	
Biogenic monoterpene production of secondary organic aerosol	5-360 Tg POM a^{-1}	50 Tg POM a^{-1}	Absolute	
Sea spray mass flux	0.2-5	1	Scaled	
DMS emission flux	0.5-2	1	Scaled	
Biomass burning mass emission rate (BC/OC)	0.25-4	1	Scaled	
Biomass burning emitted median dry diameter (BC/OC)	50-200 nm	110 nm	Absolute	
Fossil fuel mass emission rate (BC/OC)	0.5-2	1	Scaled	
Fossil fuel emitted median dry diameter (BC/OC)	30-80 nm	56 nm	Absolute	
Biofuel mass emission rate (BC/OC)	0.25-4	1	Scaled	
Biofuel emitted median dry diameter (BC/OC)	50-200 nm	110 nm	Absolute	
Mass fraction of SO_2 converted to new sulphate particles in sub-grid power plant plumes	0-1%	0.0012%	Scaled	
Emitted number median dry diameter of new sub-grid sulphate particles	20-100 nm	40 nm	Absolute	
Anthropogenic SO_2 emission flux	0.6-1.5	1	Scaled	
Anthropogenic VOC production of secondary organic aerosol	2-112 Tg POM a^{-1}	80 Tg POM a^{-1}	Absolute	
Boundary layer nucleation rate co-efficient	$3.2x10^{-7}$ – $2x10^{-4}$ s^{-1}	$2.6x10^{-7}$ s^{-1}	Absolute	
Free tropospheric nucleation rate	0.01-10	1	Scaled	
Ageing	0.3-5 monolayer	1 monolayer	Absolute	
Accumulation modal width (soluble/insoluble)	1.2-1.8	1.5	Absolute	
Aitken modal width (soluble/insoluble)	1.2-1.8	1.5	Absolute	
Mode separation diameter (nucleation/Aitken)	9-18 nm	10 nm	Absolute	
Mode separation diameter (Aitken/accumulation)	0.9-2 x activation diameter	1.5	Absolute	
Cloud drop activation dry diameter	50-100 nm	75 nm	Absolute	
pH of cloud drops (controls SO_2 + O_3)	pH 4-6.5	pH 5.5	Absolute	
pH of cloud drops (SO_2 + O_3)	pH 3.5-5	pH 4	Absolute	
Nucleation scavenging offset dry diameter	0-50 nm	25 nm	Absolute	
Nucleation scavenging fraction (accumulation mode) in mixed and ice clouds (temperature < -15°C)	0-1	0.5	Scaled	
Dry deposition velocity (Aitken mode)	0.5-2	1	Scaled	
Dry deposition velocity (accumulation)	0.1-10	1	Scaled	

3.3 Results and discussion

3.3.1 Properties of the pre-industrial aerosol

Figure 3.1 shows monthly mean modelled PI CCN concentrations. Contrary to previous suggestions (Andreae, 2007), modelling results suggests that a significant land-ocean contrast in CCN concentrations could also have existed in the PI. Averaged over a year, the mean PI CCN concentrations over Northern Hemisphere (NH) land regions are 36% higher than the Southern Hemisphere (SH) (NH = 186 cm^{-3} and SH = 137 cm^{-3}), while over ocean regions they are almost identical (NH = 61 cm^{-3} and SH = 64 cm^{-3}). The PI land–ocean contrast in CCN concentrations is particularly large in July, lying between 0–100 cm^{-3} over most extratropical ocean regions and 100–500 cm^{-3} over the majority of the land, with peak CCN concentrations greater than 2500 cm^{-3} in African Savannah burning regions and greater than 5000 cm^{-3} in Siberian boreal regions. Another factor affecting the PI land/ocean contrast is the higher abundance of biogenic organic

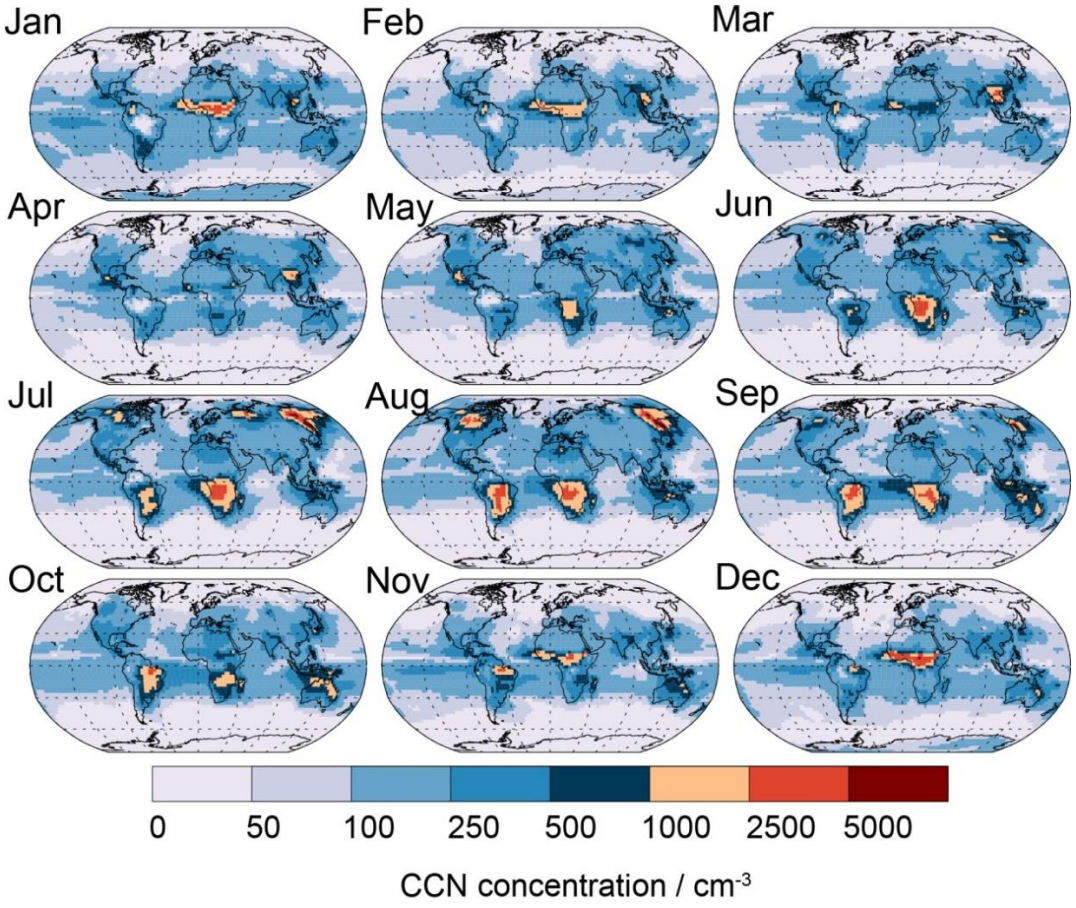

Figure 3.1. Monthly mean pre-industrial (1750) cloud condensation nuclei (CCN) concentrations. CCN concentrations are defined as the aerosol concentration with a dry diameter above 50 nm and calculated at cloud base (~915 hPa).

compounds over land, which causes the growth of small nucleated particles to CCN sizes (Merikanto et al., 2009). The model does not account for the role of organic compounds in the first stages of nucleation itself, which would further increase the land–ocean contrast (Kirkby et al., 2016; Riccobono et al., 2014).

The uncertainty (standard deviation) in PI CCN concentrations (Figure 3.2) is generally lower than the simulated CCN concentrations (Figure 3.1). Peak uncertainties occur in regions were fire emissions are having a large impact on the aerosol state due to the large uncertainty associated with emissions (Table 3.1). In the absence of anthropogenic emissions in the PI, the contribution natural emissions make to the uncertainty in CCN is higher than in the PD, reported in Lee et al. (2013), particularly in the NH. For example, over the summertime North Atlantic biomass burning emissions account for nearly half the uncertainty in the PI, but less than 10% in the PD and while DMS emissions account for up to a quarter of the uncertainty in spring in the PI NH, they are a negligible source of uncertainty in those regions in the PD.

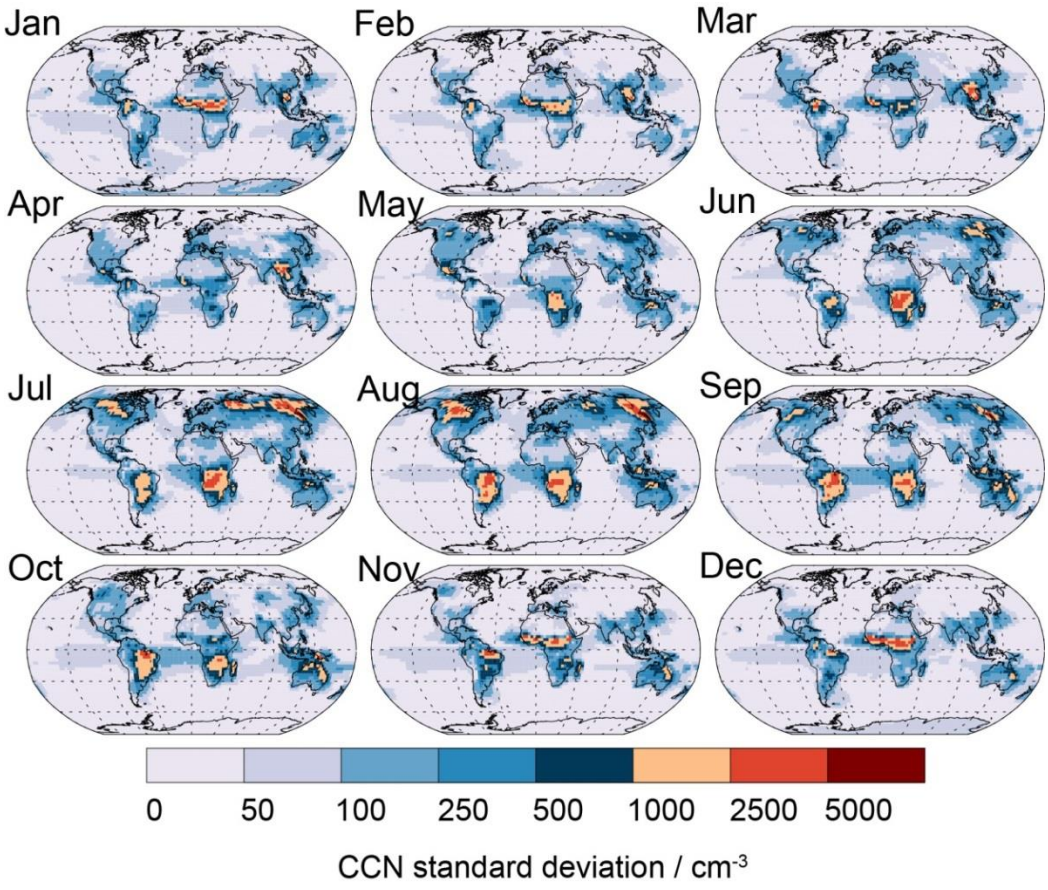

Figure 3.2. Uncertainty (standard deviation) in monthly mean pre-industrial (1750) cloud condensation nuclei (CCN) concentrations. CCN concentrations are defined as the aerosol concentration with a dry diameter above 50 nm and calculated at cloud base (~915 hPa).

Modelled uncertainty in PI CCN concentration over marine regions is typically from 20 to 40% (standard deviation divided by the mean, shown in Figure 3.3) between ±60° latitude, up to about 70-90% at higher latitudes and over 100% near the Antarctic continent and very high latitude Arctic regions. In some continental regions uncertainties exceed 100% of the mean in regions dominated by fires. To further assess how structural uncertainties potentially alter the pristine regions presented in the following sections future studies using a range of models would need to be undertaken.

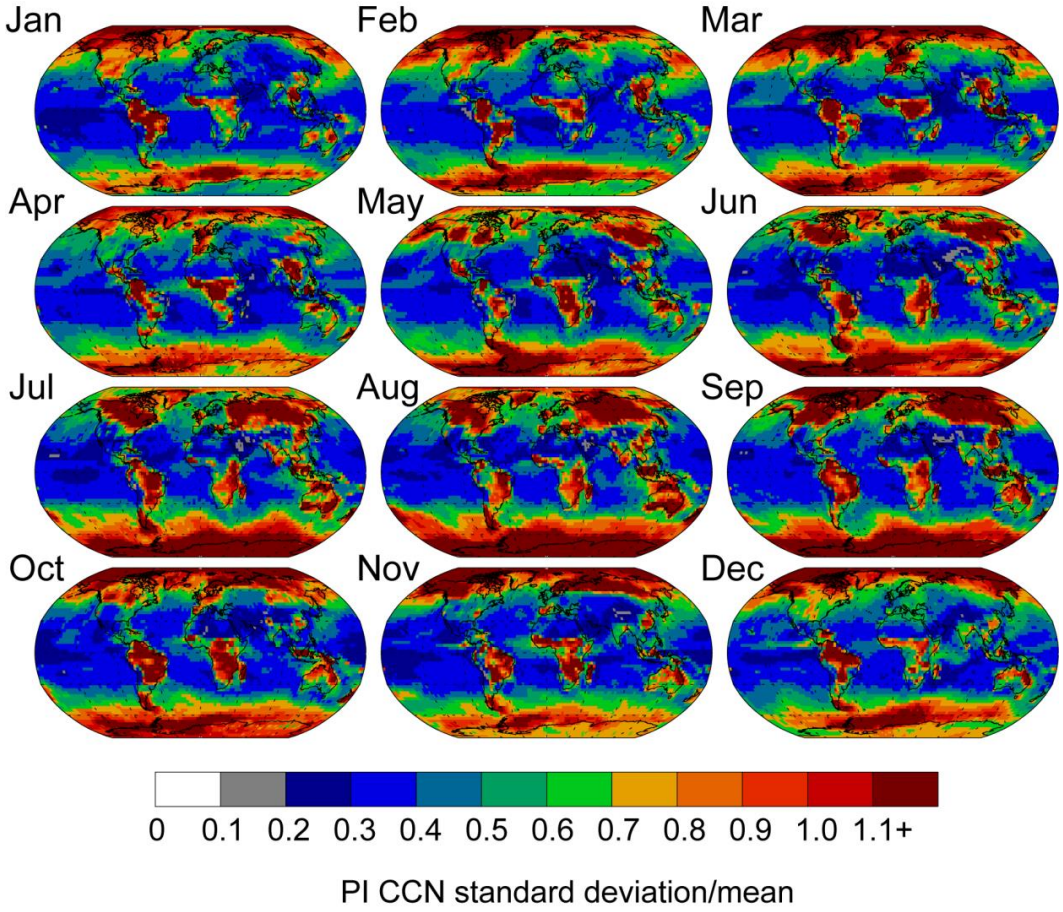

Figure 3.3. Pre-industrial (1750) cloud condensation nuclei (CCN) relative standard deviation (CCN standard deviation/CCN concentration). CCN concentrations are defined as the aerosol concentration with a dry diameter above 50 nm and calculated at cloud base (~915 hPa).

3.3.2 Changes in 1750 to 2000 aerosol concentrations

Figure 3.4 shows the monthly mean simulated percentage change in CCN number concentrations between 1750 and 2000. For most of the year a clear hemispheric contrast exists between the NH and SH. The largest increases in PD CCN are in the NH, where the majority of pollution occurs, and, in particular, over the low to mid-latitude region increases are generally over 100%, but can exceed 1000% in highly polluted continental regions. Although the SH is less polluted than the NH, on a monthly average, a pervasive background of anthropogenic aerosol exists across most regions of the world. So as to be able to detect when episodic pollution events are impacting aerosol concentrations in remote regions a shorter daily time resolution is used in Section 3.2.2 when identify pristine aerosol regions.

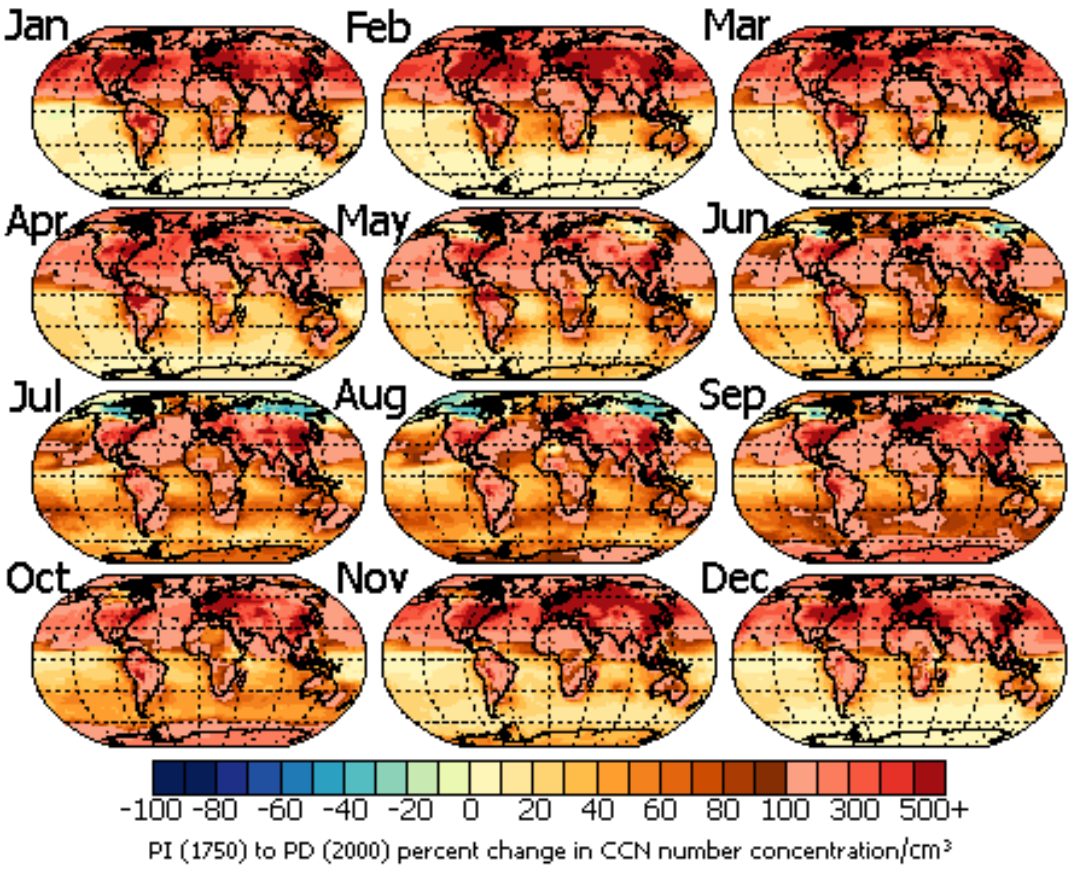

Figure 3.4. The pre–industrial (1750) to present–day (2000) monthly mean percent change in cloud condensation nuclei (CCN) number concentrations at 915 hPa.

Histograms (Figure 3.5) of PI and PD CCN concentrations show that although the occurrence of high CCN concentrations is similar in the PI and PD, the most frequent oceanic CCN concentrations are centred around 80 cm^{-3} compared to about 180 cm^{-3} over land. The PD histograms show a much greater influence of pollution over land compared to oceanic regions, with the most frequent CCN concentration remaining around 80 cm^{-3} over the ocean, but increasing to more than 500 cm^{-3} over land. Despite the differences between PI and PD aerosol concentrations, there is considerable overlap of the CCN histograms, particularly over oceans at low CCN concentrations, suggesting that regions exist today that could be analogues for PI environments.

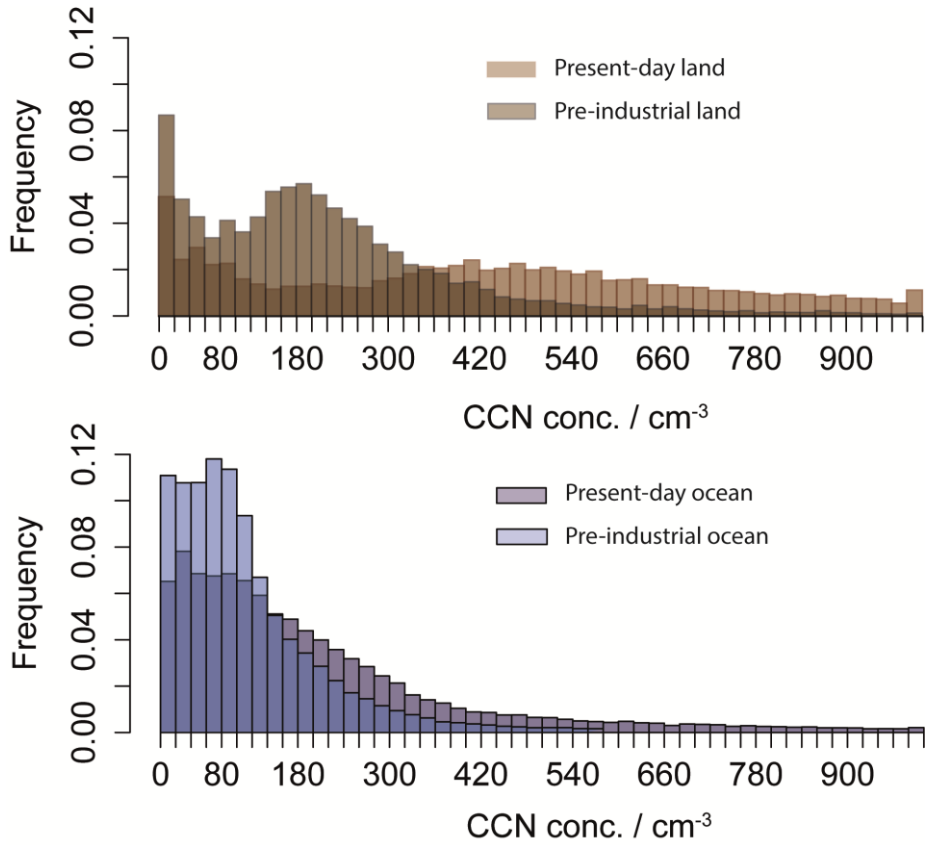

Figure 3.5. Pre-industrial (1750) and present-day (2000) global modelled annual mean cloud condensation nuclei (CCN) concentrations over land and ocean grid cells, calculated from daily mean CCN concentrations at cloud base (~915 hPa). The third colour indicates overlap of the two distributions. The maximum CCN bin concentration is set to 1000 cm^{-3}, although a small fraction exists at higher concentrations.

3.3.3 The occurrence of pristine days

Figure 3.6 shows the similarity of CCN concentrations in the PI and PD in terms of the number of days that concentrations are within ±20%. The threshold of ±20% in concentration is based on the estimated CCN measurement uncertainty across the majority of datasets compiled by Spracklen et al (2011a).

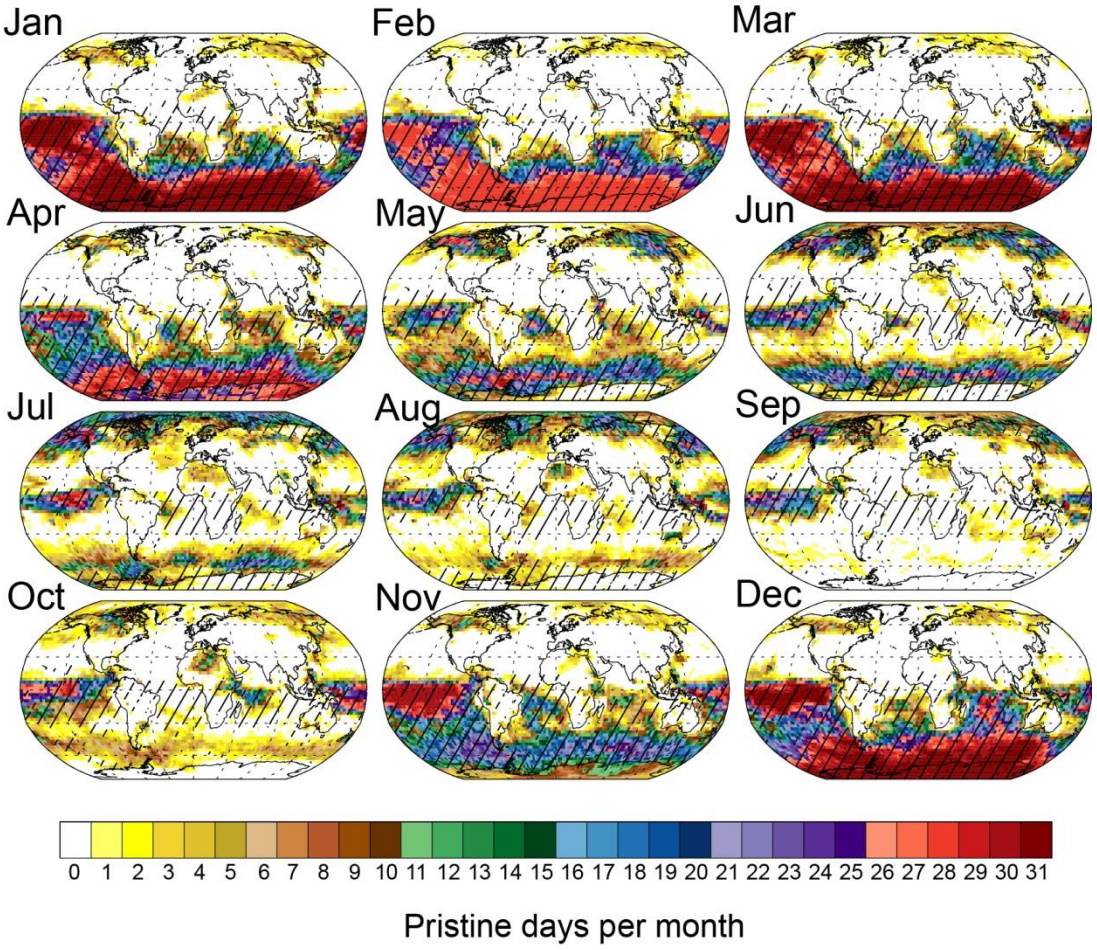

Figure 3.6. The occurrence of pristine days over a year, based on two definitions: colours show the number of days per month on which pre–industrial (PI) and present–day (PD) cloud condensation nuclei (CCN) concentrations differ by no more than ±20% in that grid cell at cloud base (~915 hPa). Stippling shows regions where the sensitivities of PI and PD CCN to 28 model parameters are similar ($r^2 \geq 0.9$) in that grid cell at cloud base. Pristine regions are those which exhibit both a similar PI and PD CCN concentration and a similar PI and PD response to the 28 parameters.

Table 3.2. Fraction of the Earth defined as pristine (pre–industrial (PI) to present–day (PD) cloud condensation nuclei number concentration (CCN) ±20% and similar PI–to–PD CCN response to 28 parameters covering natural and anthropogenic emissions, processes and model structures). Values in parentheses show the pristine fraction when the CCN number concentration change only is considered.

	Pristine fraction				
	Global	Ocean	Land	Northern Hemisphere	Southern Hemisphere
Jan	**0.27** (0.32)	**0.34** (0.40)	**0.10** (0.13)	**0.02** (0.06)	**0.53** (0.59)
Feb	**0.27** (0.32)	**0.34** (0.40)	**0.10** (0.11)	**0.02** (0.04)	**0.53** (0.61)
Mar	**0.27** (0.31)	**0.33** (0.39)	**0.09** (0.12)	**0.00** (0.03)	**0.53** (0.60)
Apr	**0.18** (0.25)	**0.21** (0.30)	**0.08** (0.12)	**0.00** (0.03)	**0.35** (0.46)
May	**0.10** (0.17)	**0.13** (0.20)	**0.02** (0.09)	**0.02** (0.08)	**0.18** (0.26)
Jun	**0.07** (0.16)	**0.10** (0.19)	**0.01** (0.10)	**0.03** (0.11)	**0.12** (0.21)
Jul	**0.05** (0.14)	**0.06** (0.16)	**0.02** (0.08)	**0.06** (0.15)	**0.04** (0.13)
Aug	**0.04** (0.12)	**0.05** (0.13)	**0.02** (0.08)	**0.05** (0.16)	**0.03** (0.08)
Sep	**0.04** (0.08)	**0.05** (0.09)	**0.01** (0.07)	**0.04** (0.12)	**0.04** (0.05)
Oct	**0.05** (0.11)	**0.07** (0.14)	**0.01** (0.05)	**0.03** (0.09)	**0.07** (0.13)
Nov	**0.20** (0.25)	**0.28** (0.32)	**0.01** (0.06)	**0.03** (0.08)	**0.37** (0.42)
Dec	**0.26** (0.33)	**0.32** (0.40)	**0.09** (0.12)	**0.02** (0.06)	**0.49** (0.59)
Annual	**0.12** (0.21)	**0.16** (0.26)	**0.02** (0.10)	**0.02** (0.08)	**0.22** (0.34)

The occurrence of pristine CCN regions in the PD atmosphere is highly variable in space and time, with the frequency of pristine days lying between 0 and 100% in a given month. Averaged over a full year, approximately one-third (Table 3.2) of the SH has CCN concentrations similar to the PI, with a maximum spatial coverage over SH ocean regions in the SH summer when every day of the month approaches pristine conditions. In contrast, less than 9% of the NH is pristine, with a maximum coverage of about 15%, also in the summer. In many major shipping regions (e.g., Capaldo et al. 1999) anthropogenic perturbations to aerosol concentrations are large enough that the region is classed as non-pristine. The equatorial Pacific Ocean is the most persistently pristine environment, most likely due to the dominant local marine emission source and effective barrier to NH inter-hemispheric transport of anthropogenic pollution provided by the intertropical convergence zone. In agreement with observational (Clarke and Kapustin, 2010) and modelling studies (Penner et al., 2012), the southern Pacific Ocean (approx. 20-6^{o}S, 90-180^{o}W) is identified as a large region close to pristine, especially during SH summer when monthly mean PD CCN concentrations in this region are in the range of 53-285 cm^{-3} (median 104 cm^{-3}), when the main natural source of CCN is from DMS-derived

sulphate aerosol (Korhonen et al., 2008). A Southern Ocean summertime band of pristine CCN exists between 50-65°S, with generally low PD CCN concentrations of 20-153 cm^{-3} (median 58 cm^{-3}), when natural emissions of sea spray are the dominant aerosol source (McCoy et al., 2015; Murphy et al., 1998). The mid-latitude Pacific and Atlantic Oceans deviate from a pristine state for more of the year than at higher and lower latitudes, mainly due to assumed increases in fire emissions from South American and African tropical fire regions (Bowman et al., 2009), which are assumed to be due to increased anthropogenic activity. Generally, SH continental land masses have sparse regions of pristine CCN concentrations.

In the NH, prolonged pristine periods generally occur only over continental regions above 60°N, such as in boreal Canada (Pierce et al., 2012) and Russia (Chi et al., 2013), where aerosol is affected strongly by natural forest fire emissions. Here, CCN concentrations are highly variable, but generally range from 100-1000 cm^{-3}. The high Arctic (75°N and above) is frequently pristine during the NH summer, with low CCN concentrations in July of 39-142 cm^{-3} (median 55 cm^{-3}), but strongly and persistently polluted during winter and spring, consistent with the seasonal cycle of Arctic haze controlled by scavenging processes (Browse et al., 2012). There are almost no marine pristine days during NH winter and spring and very few regions are persistently pristine over a month. In NH mid-latitude regions there are no pristine days at any time of the year. In particular, the North Pacific Ocean is impacted by transport of pollution from East Asia to North America (Yu et al., 2012) and is a region where we find no pristine days in the main transport periods.

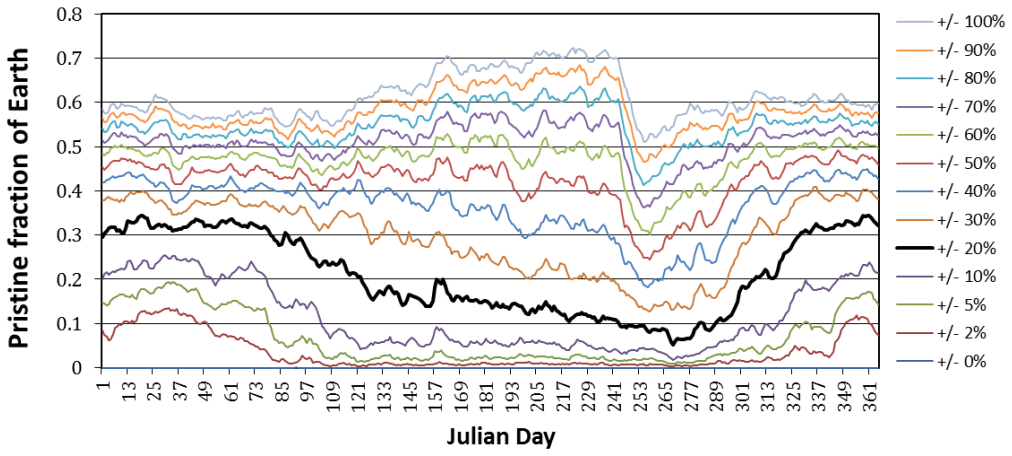

Figure 3.7. The fraction of the Earth defined as pristine based on the pre–industrial to present–day cloud condensation nuclei (CCN) number concentration change being within a certain threshold. Thresholds vary from ±0% to ±100%. Results are for every day over a full year with CCN concentrations taken at 915 hPa in every grid cell of the model.

Confidence in the extent and location of pristine regions depends on the modelled CCN uncertainty as well as the assumed tolerance used to compare PI and PD CCN number concentrations, set at ±20% (as above). Figure 3.7 shows the daily fraction of the Earth defined as pristine when this threshold is set to values ranging between ±0% to ±100%. This threshold is particularly sensitive to the onset of the biomass burning season in the SH due to the large flux of aerosols emitted in this region (Figures 3.1 and 3.4). Figure 3.8 shows the effect that changing the tolerance to 10%, 30% and 50% for January, April, July and October has on the spatial distribution of pristine regions. This range of tolerances is comparable to the modelled relative CCN uncertainty, which is approximately 20-50% in the main pristine regions (Figures 3.3 and 3.6). Increasing the threshold increases the marine fraction of the Earth which is defined as pristine, however continental regions are relatively insensitive to changes below 50% due to the large increases in pollution increasing CCN number concentrations in these regions beyond this threshold (Figure 3.4).

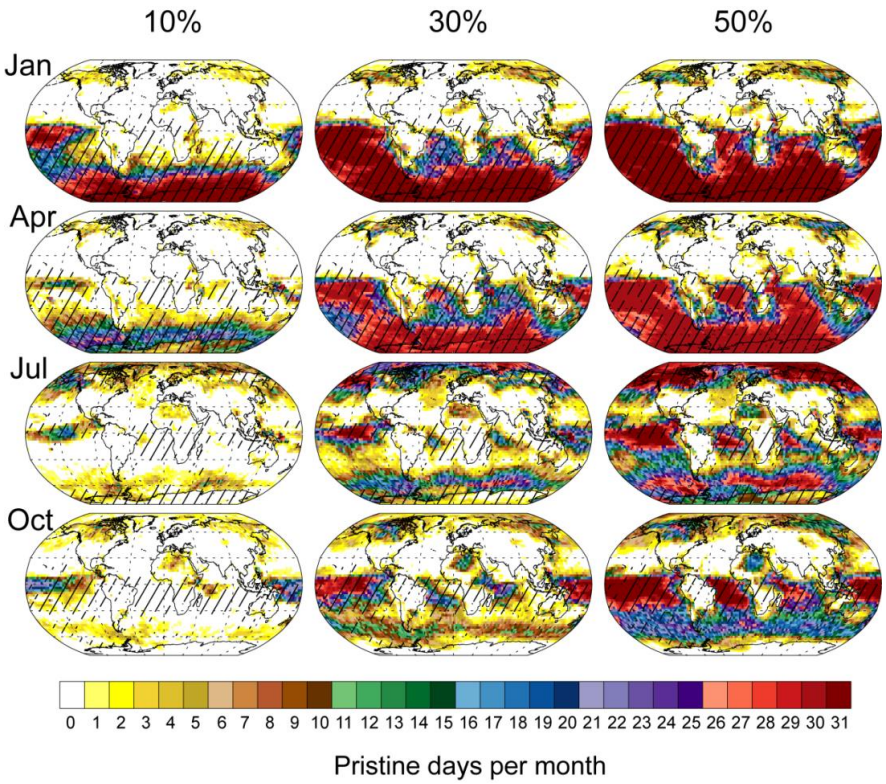

Figure 3.8. The occurrence of pristine days in January, April, July, and October based on two definitions. Colours show the number of days per month on which pre–industrial (PI) and present–day (PD) cloud condensation nuclei (CCN) number concentrations differ by either ±10%, ±30%, or ±50% in that grid cell at cloud base (~915 hPa). Stippling shows regions where the sensitivities of PI and PD CCN to 28 model parameters are similar ($r2 \geq 0.9$) in that grid cell at cloud base.

In all months of the year the pristine fraction of the Earth (PD aerosol concentrations ±20% of their PI levels) also depends on the particle size. Figure 3.9 shows the fraction of the Earth that is defined as being pristine as a function of aerosol particle size, i.e. counting all particles above this size. Anthropogenic aerosols tend to occur at smaller particle sizes resulting in the fraction of the Earth defined as pristine being smallest within the Aitken mode (aerosol particle sizes of 10-100 nm), with a minimum pristine coverage when the particle size lies between 50-100 nm. Natural aerosols dominate at increasingly larger particle sizes, due to sea salt and dust emissions containing significant quantities of large particles, resulting in a steady increase in the pristine fraction of the Earth with increasing particle size within the accumulation mode (aerosol particle sizes of 100-1000 nm). At the boundary with coarse mode aerosol (aerosol particle size of >1000 nm) pristine coverage of the Earth is over 90% in all months of the year. As ice-nuclei are typically large (>500 nm) aerosol particles, such as dust (Atkinson et al. 2013), the very high pristine fraction of the Earth which is shown at these larger aerosol sizes could be important when considering changes to ice-nuclei concentrations over the industrial period. There is little seasonality in pristine coverage within the naturally dominated accumulation size range compared to a distinct seasonality in the anthropogenically effected Aitken size range.

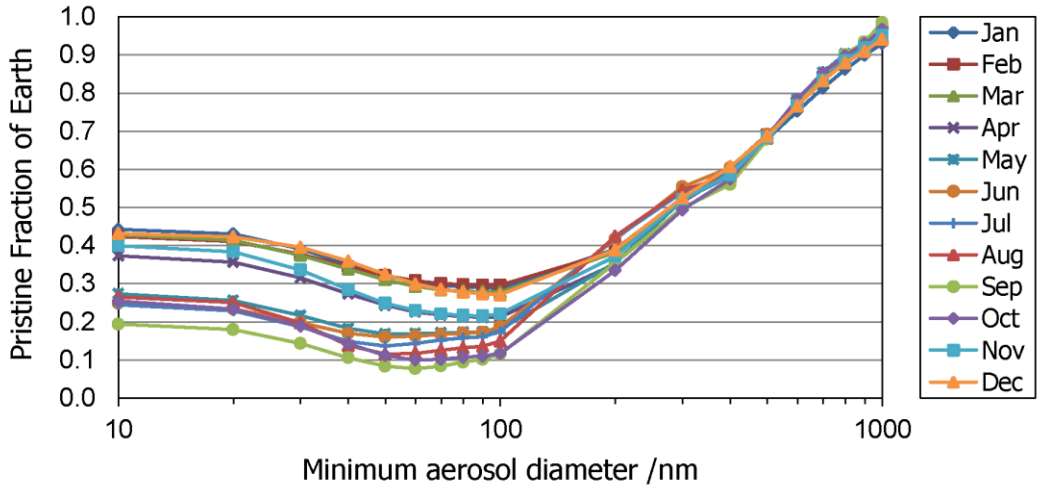

Figure 3.9. Pristine fraction of the Earth (1750 and 2000 aerosol concentrations are similar [±20%]) as a function of the aerosol size of interest.

An analysis of the vertical profile of pristine regions shows that the distribution of pristine days is similar at ~2.5 km above sea level (Figure 3.10), while at ~5 km above sea level long range transport of anthropogenic emissions cause changes in the spatial distributions of SH pristine regions (Figure 3.11). However, these free tropospheric aerosols do not affect cloud-base CCN concentrations in the boundary layer, and if they are mixed down to lower altitudes then they will be included already in the analysed fields at 1 km altitude.

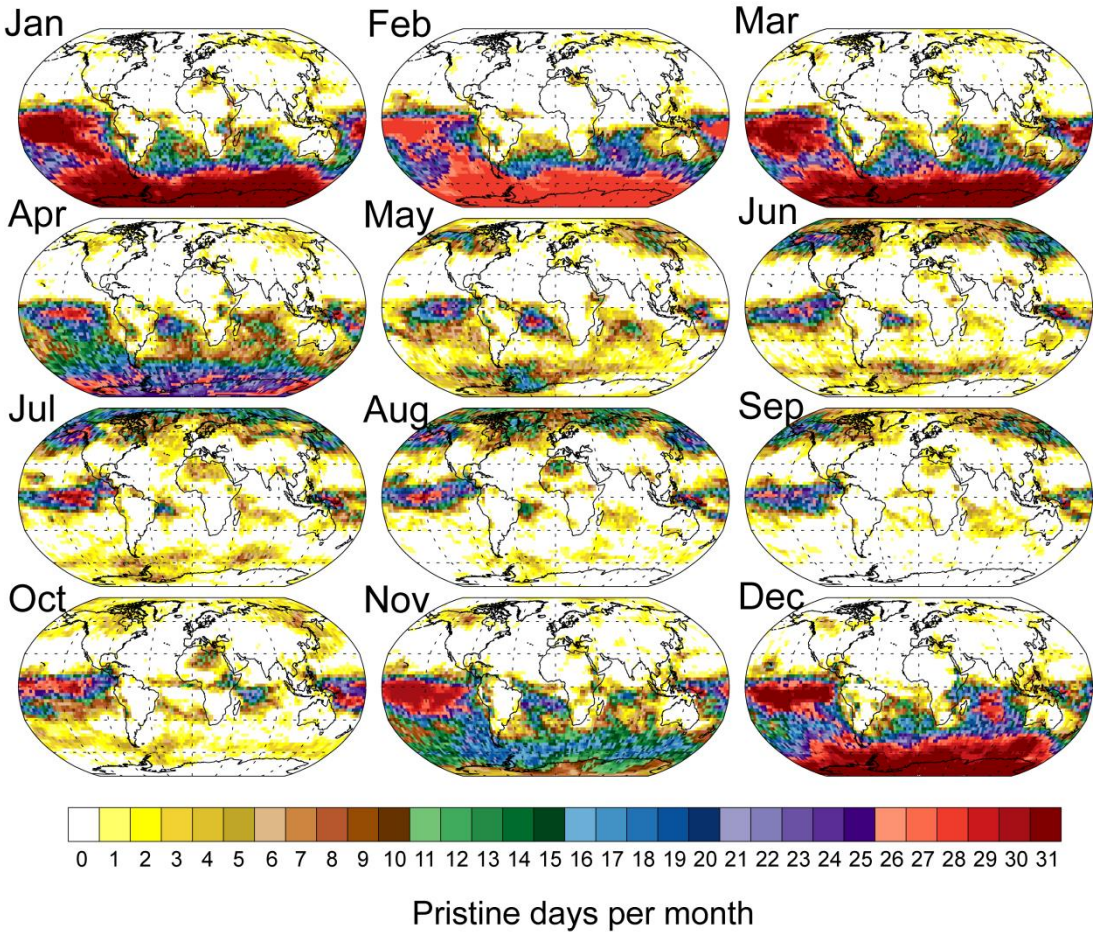

Figure 3.10. The occurrence of pristine days over 1 year. Colours show the number of days per month on which pre–industrial and present–day cloud condensation nuclei concentrations differ by no more than ±20% in that grid cell at ~2500 m above sea level.

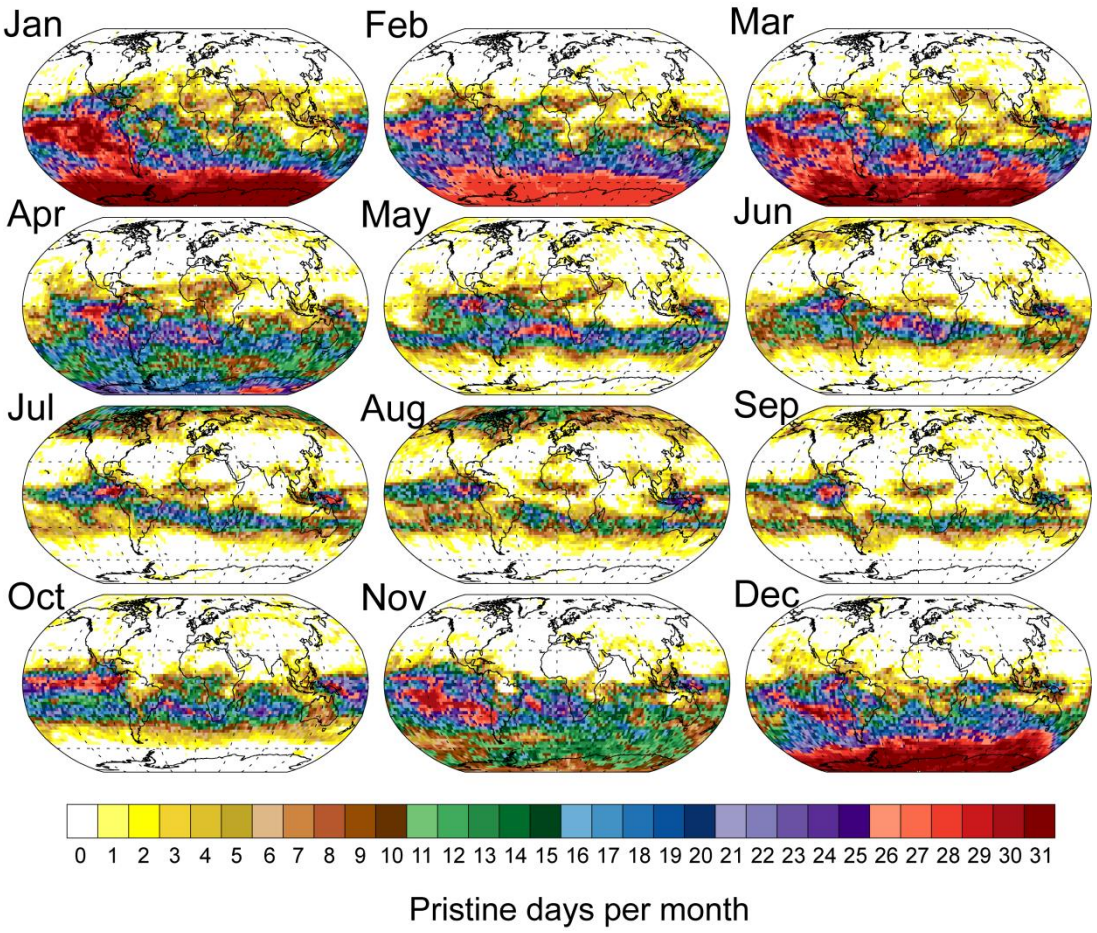

Figure 3.11. The occurrence of pristine days over 1 year. Colours show the number of days per month on which pre–industrial and present–day cloud condensation nuclei concentrations differ by no more than ±20% in that grid cell at ~5000 m above sea level.

The optimum pristine region, defined as a low relative modelled CCN uncertainty (Figure 3.3) and a high number of pristine days (Figure 3.6), is the central Pacific. At American Samoa comparisons of GLOMAP total aerosol number concentrations were compared to observations in Mann et al. (2010) and were shown to be very similar (b vs. observations: 0.05). The modelled seasonal cycle in DMS flux to the atmosphere is well captured when compared to observations from Amsterdam Island and Cape Grim. However, sea salt concentrations are slightly over estimated in the Southern Ocean. Although relative uncertainties (Figure 3.3) can be fairly high in some pristine regions, model uncertainties are expected to be correlated in the PI and PD, giving more confidence in the model results than indicated. While meteorological variability is likely to cause interannual variability in the precise location of pristine regions, the principal pristine regions (the remote Pacific, Southern Ocean, Arctic, etc.) will be more climatologically persistent features.

3.3.4 Present–day observational sites close to a pre–industrial aerosol state

Ideally observations of pristine aerosol should be made in regions as similar to the PI as possible. Unfortunately the majority of regions with a pristine aerosol environment are located in marine regions, where making measurements is logistically more difficult than on the land. However, modelling results suggest that certain existing measurement stations are located within potentially suitable regions. Figure 3.12 shows four Global Atmosphere Watch (GAW) baseline aerosol measurement station locations where daily PI and PD CCN concentrations are similar. There are two SH locations that include Amsterdam Island (Figure 3.12a) and American Samoa (Figure 3.12b) and two NH locations that include the high-latitude measurement stations of Alert (Figure 3.12c) and Barrow (Figure 3.12d). Under the assumption that the boundary layer is well mixed, the CCN concentrations at 915 hPa and the CCN concentrations in lower model levels (where stations typically exist) are comparable. Due to model resolution the grid cells that contain the island locations are treated as ocean. As the air masses reaching these islands also travel over the surrounding ocean regions, it is assumed that this discrepancy will have little to no effect on the analysis. In general, both the island locations are more similar in their CCN profiles throughout the whole of the year than the Arctic stations which are typically only pristine during the summer months.

Amsterdam Island is situated close to the Southern Ocean and located in a grid cell which is particularly close to a PI aerosol state. This is a region of the world that would particularly benefit from previously untaken measurements of CCN concentrations and, ideally, with a focus on how natural ocean emissions, such as DMS, interact with aerosols and the climate without influence from pollution. America Samoa is located in the remote South-Western Pacific and modelled results also show this as a good choice for understanding pristine aerosol environments. At both Alert in Northern Canada and Barrow in Alaska PD CCN number concentrations are lower over the summer months than in the PI, with the reduction being more pronounced in Barrow than Alert, due to the assumed 50% reduction in boreal wildfire emissions in the AeroCom inventory (Dentener et al., 2006). During the winter months long range transport of pollution builds up in the Arctic regions consistent with the seasonal cycle of Arctic haze which is controlled by scavenging processes (Browse et al., 2012). Nevertheless both of these NH observational sites are potential candidates for measuring aerosol in a pristine environment for at least part of the year.

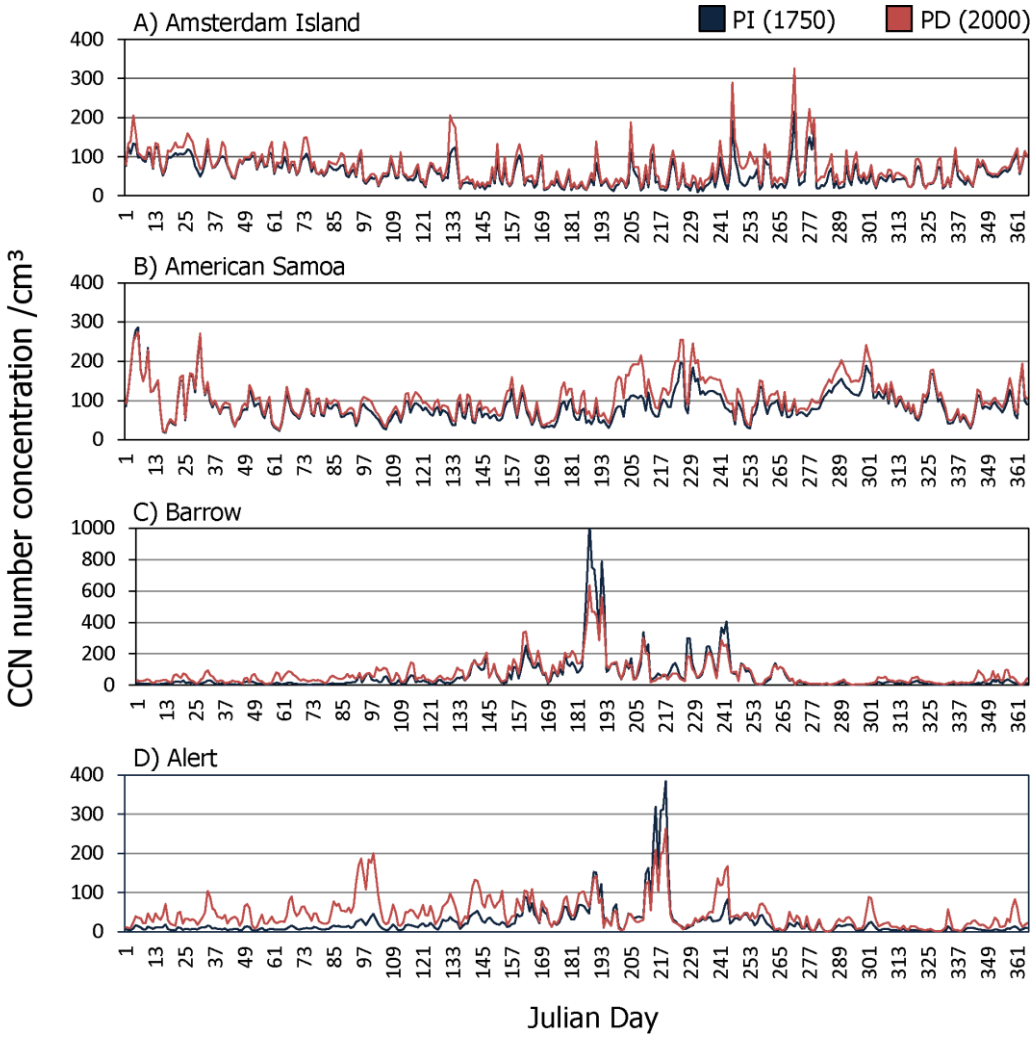

Figure 3.12. Daily mean cloud condensation nuclei number concentrations over one year in the pre–industrial (PI) and present–day (PD) at 4 atmospheric monitoring stations a) Amsterdam Island, b) American Samoa, c) Barrow and d) Alert.

3.3.5 Changes in CCN sensitivity between 1750 and 2000

Stippling in Figure 3.6 shows regions where the aerosol sensitivity to perturbations of 28 model parameters covering emissions, microphysical processes and model structures (Lee et al., 2013) is similar in 1750 and 2000. The parameter sensitivities in each grid cell at cloud base (915 hPa) were calculated by variance decomposition of the CCN distributions that were used to generate the uncertainty in CCN concentrations (Figure 3.2). The fractional contribution to variance of each parameter is termed the main effect index (Lee et al., 2012, 2013). The PI and PD main effect indices for the 28 parameter perturbations in each grid cell are correlated (see Methods) and regions are defined as being pristine, somewhat arbitrarily, if the coefficient of correlation is greater than 0.9. Figure 3.13 shows these correlations at four representative sites.

In regions where CCN concentrations exhibit about 20 or more pristine days in a month the CCN response to model parameters is also similar in both periods. For regions with about 10-19 days of pristine CCN concentration, there is partial overlap with regions with similar CCN sensitivity, while for regions with less than 10 days per month of pristine CCN concentrations CCN sensitivities are now different to the PI.

The equatorial Pacific is the largest region that is closest to pristine all year round in terms of the similarity of the aerosol state and the aerosol sensitivity, while other regions vary seasonally between being pristine and not. Other regions with a high number (20 or more) of pristine days and similar CCN sensitivity in one or more months include parts of Alaska and Yukon, the Southern Ocean, Melanesia, south-west Greenland and the southern Indian Ocean.

Figure 3.13 shows the change in PI to PD CCN sensitivity at four grid cells representing four different sites. Melanesia (Figure 3.13a) has a very similar CCN sensitivity and state in 1750 and 2000, where 99% of modelled days have PD CCN concentrations within ±20% of PI concentrations. Prevailing winds in this region originate over the Pacific Ocean bringing clean background air masses and natural marine aerosol (Savoie et al., 1989). Figure 3.13a shows that both 1750 and 2000 CCN sensitivities are dominated by the same parameters relating to natural emissions and aerosol microphysical processes (volcanic SO_2 and biogenic secondary organic aerosol (SOA) as well as model uncertainties in the Aitken mode width, boundary layer nucleation rates, CCN activation diameter and the pH of cloud droplets). In all months the fraction of variance attributable to anthropogenic

emissions is less than about 1%. CCN concentrations and behaviour in this location are therefore clearly driven by natural processes.

The eastern Atlantic (Figure 3.13b) has a different CCN response and state in the two periods. It is located in a region of high aerosol-cloud radiative forcing (Carslaw et al., 2013). Many of the main effect indices have changed over the industrial period, indicating an anthropogenic influence on the behaviour of the aerosol. In particular, anthropogenic SO_2 emissions and production of SOA from anthropogenic compounds contribute more to CCN variance in the PD than in the PI and natural emissions of DMS and biomass burning contribute less. This reduction in sensitivity to natural emissions will suppress natural aerosol-climate feedbacks (Spracklen and Rap, 2013).

The Brazilian rainforest (Figure 3.13c) has a similar CCN response but dissimilar state in the two periods. Although the aerosol state is strongly anthropogenically perturbed by increased biomass burning emissions, these emissions dominate the aerosol sensitivity in both the PI and PD (Figure 3.13c). While our model results suggest that fires are the largest contributor to PI CCN concentrations major uncertainties exist as to the magnitudes of historic biomass burning emissions (van der Werf et al., 2013). While our model results suggest that fires are the largest contributor to PI CCN concentrations major uncertainties exist as to the magnitudes of historic biomass burning emissions (Marlon et al., 2008). However, in many fire-dominated regions the response of CCN to changes in emissions is similar in both the PI and PD (e.g., Figure 3.13c) and these regions are still likely to be useful analogues of PI CCN behaviour.

North east China (Figure 3.13d) has a very different CCN response and state in the two periods. Annual mean CCN concentrations at this site are the furthest from PI CCN baseline concentrations of any other location. While PI CCN concentrations are sensitive to the flux and size of biofuel emissions (from early human activity) and biogenic SOA, PD CCN concentrations are sensitive to the flux and size of fossil fuel emissions and the fraction of sulphate formed on sub-grid scales from anthropogenic SO_2 emissions.

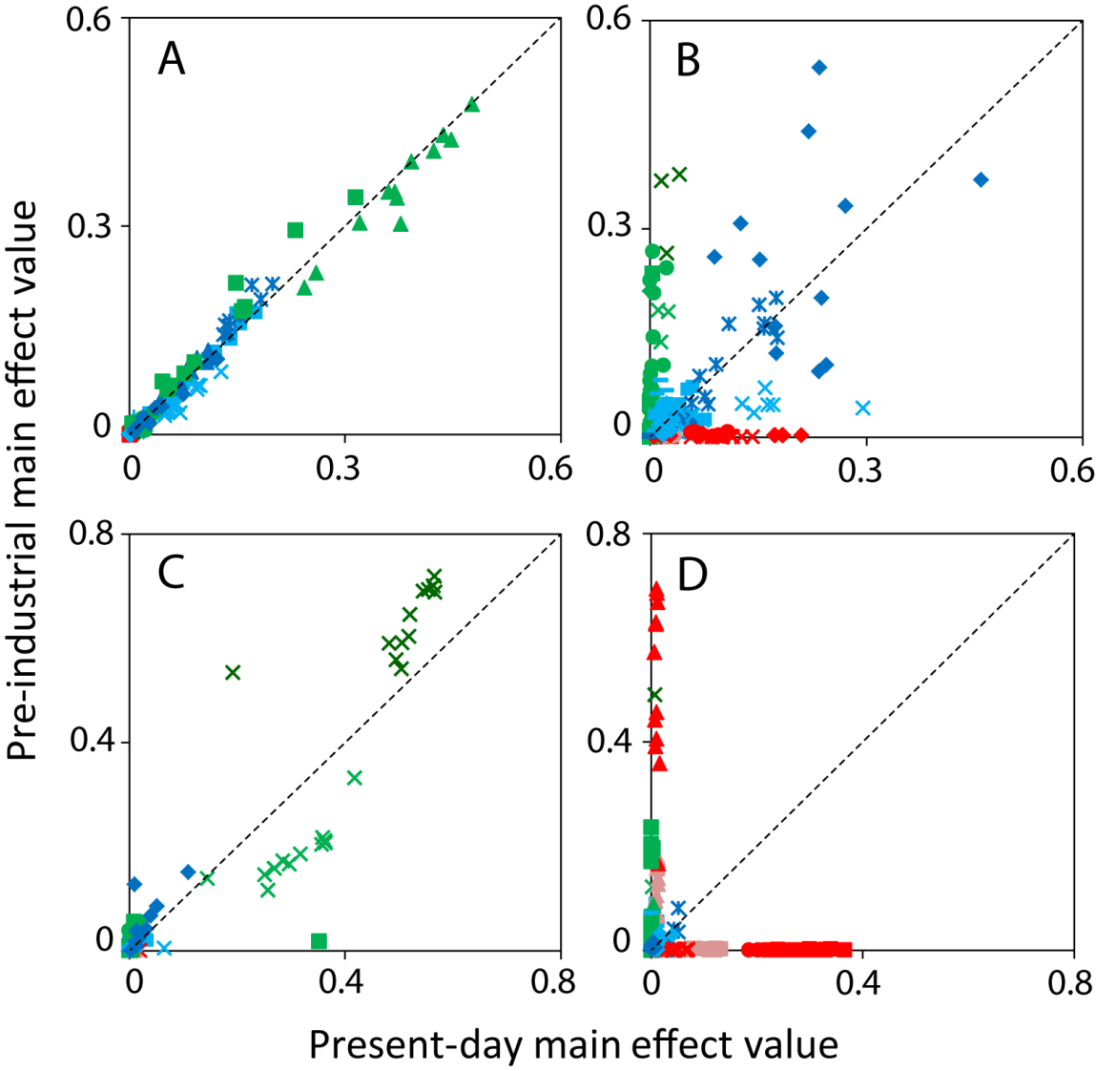

Figure 3.13. The similarity of cloud condensation nuclei sensitivities in the pre–industrial and present–day to 28 parameters covering natural emissions (green) anthropogenic emissions (red) and processes (blue) for every month in the year at four different sites: a) Melanesia (1°S, 151°E), b) eastern Atlantic (38°N, 21°W), c) Brazilian rainforest (1°S, 66°W) and d) north east China (38°N, 111°E). For more information on individual marker descriptions see Table 3.1.

Model results spanning the grid cells 14°S to 22°S and 121°W to 130°W, which overlaps the most with the pristine region studied by Koren et al. (2014) at 13 °S to 22 °S and 121 °W to 130 °W, suggest that even in these remote regions PD CCN concentrations in July are up to 40% higher than in the PI, mainly due to increases in anthropogenic biomass burning emissions over the industrial period. In addition, Figure 3.14 shows that the CCN response to volcanic SO_2 emissions in the region has approximately halved since the PI and an additional PD contribution from anthropogenic SOA concentrations can be seen.

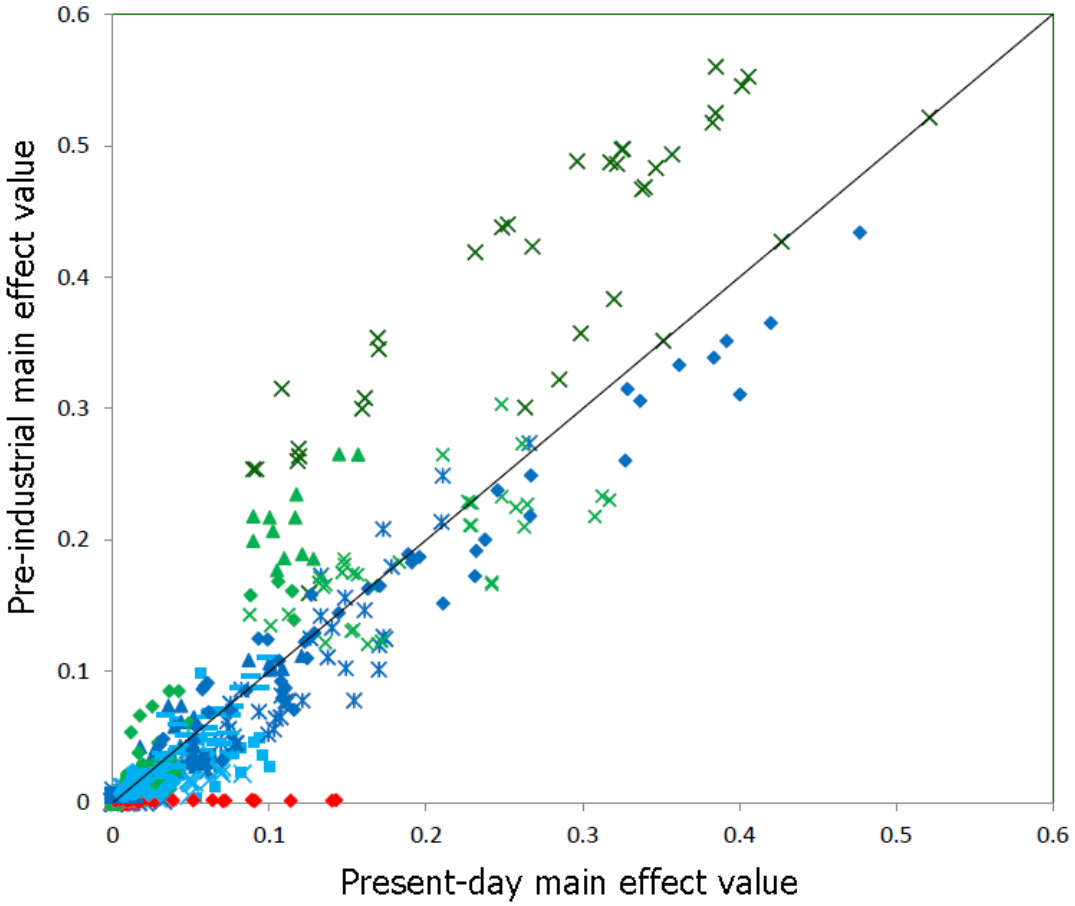

Figure 3.14. The similarity of annual mean cloud condensation nuclei sensitivities in the pre–industrial and present–day to 28 parameters covering natural emissions (green) anthropogenic emissions (red) and processes (blue) for every month of the year at 14°S to 22°S and 121°W to 130°W. For more information on individual marker descriptions see Table 3.1.

3.3.6 The overlap of pristine regions and aerosol-cloud radiative forcing

Aerosol measurements under pristine conditions would be most useful if they were made in regions where there is an aerosol-cloud radiative forcing, so that both the clean and perturbed aerosol-cloud processes could be observed. However, on average, such regions are of course not pristine today. To assess the overlap of forcing and pristine conditions, Figure 3.15 shows the relationship between 1750–to–2000 monthly mean aerosol indirect radiative forcing (Carslaw et al., 2013) and the number of pristine days per month. As expected, the general relationship shows that regions with the highest monthly mean forcing have the lowest number of pristine days (grey markers in Figure 3.15). For example, grid boxes with greater than -5 Wm^{-2} forcing have generally less than 5 pristine days per month. When the additional constraint of similarity of CCN sensitivities is applied (tan markers in Figure 3.15) it is possible to observe pristine days only in regions with a monthly mean forcing less than about -2 to -3 Wm^{-2}, which is in the lowest quartile of the forcing estimates.

If the analysis is not restricted to observing pristine aerosol in regions of forcing, but just in regions of low cloud, then extensive regions can be found with pristine days of 0 to 31 per month. The black markers and maps in Figure 3.15 show pristine regions with higher than average low cloud cover (fraction ≥0.3). These pristine low-cloud conditions generally occur over the major marine stratocumulus decks in the SH. It is in these regions where aerosol and related process measurements would be most useful in constraining the PI baseline using PD observations. However, in making aerosol-cloud measurements there is a compromise to be reached between a useful number of observable pristine days and the magnitude of the forcing in that region. Regions with a small number of pristine days will enable strong cloud perturbations to be observed, while regions with a high number of pristine days will experience only weak or brief aerosol perturbations.

These results show that, although cloud radiative forcing and pristine regions are in general spatially anti-correlated, meteorological variability means that in regions with non-zero radiative forcing there are days that are likely to approach PI aerosol conditions.

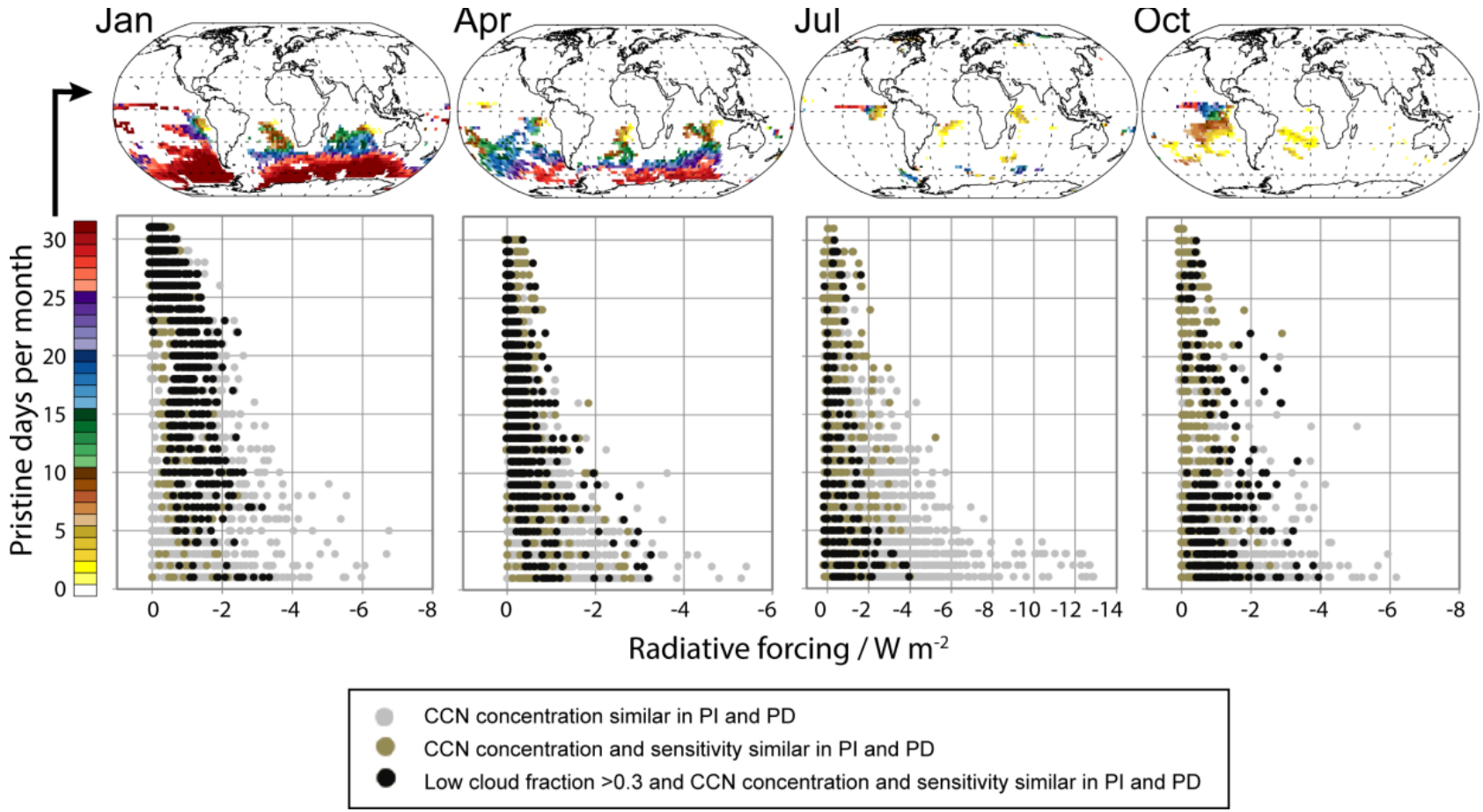

Figure 3.15. The relationship between 1750-to-2000 monthly mean aerosol indirect radiative forcing and the occurrence of pristine aerosol conditions. Maps show number of days in which pristine conditions (PI:PD cloud condensation nuclei (CCN) number concentrations within ±20% and similar response to the 28 parameter in both time periods) and average low cloud fraction (≥ 0.3) overlap.

3.4 Conclusions

If the large uncertainty in aerosol-cloud radiative forcing between PI and PD periods is to be constrained by measurements, it is important to characterize aerosol in regions of today's atmosphere that most closely resemble PI conditions. While there is likely to always be uncertainty associated with predicting the PI atmosphere, simply because natural emissions may have changed with time, regions have been identified in today's atmosphere that are similar enough to PI conditions to be explored further. The joint analysis of changes in CCN concentration alongside the changes in the sensitivity of CCN to emission and process perturbations provides a complete model picture of where on Earth we can observe pristine aerosol concentrations and behaviour.

Anthropogenic activity has greatly increased aerosol number concentrations since 1750, and in doing so reduced the aerosol number fraction associated with natural aerosol. Simulated annual mean global modelled CCN number concentrations, at low level warm cloud base (915 hPa), have increased by a factor of 2.2 over the industrial period (1750–to–2000). Due to the different hemispheric distributions of anthropogenic pollution emissions, increases in CCN number concentrations are larger in the NH.

This study has identified regions and seasons with the highest likelihood of observing pristine aerosol in terms of the number of model days per month pristine aerosol could be observed. However, ultimately it is necessary to define pristine aerosol based on measurements because measurements are needed for model evaluation. There is no universal operational definition of pristine aerosol because natural aerosols vary substantially. The mass concentration of a species associated with anthropogenic emissions is often used as an anthropogenic tracer (e.g. carbon monoxide (Clarke and Kapustin, 2010) or black carbon (O'Dowd et al., 2004)). But such a definition is appropriate only if the species is not part of the local natural aerosol – clearly not the case if natural forest fire aerosols are being studied.

Model results have been shown here to be useful in identifying those regions that are potentially suitable sites for making observations of natural aerosol in pristine-like environments. Pristine sites are often marine in nature and located in the SH which has suitable island locations for taking measurements from. Some high latitude NH pristine regions, such as Alaska and Yukon, also exist but these pristine environments are more transient than in the SH. Identified pristine regions may not be the only places to observe PI-like aerosol behaviour. Although results suggest that the region of the Pacific studied by Koren et al. (2014) has a different aerosol

state and response to parameter perturbations today compared to the PI, it may still behave in a way that is sufficiently similar to the PI to be informative. However, clouds appear to be highly sensitive to aerosols at very low concentrations (Carslaw et al., 2013; Koren et al., 2014; Schmidt et al., 2012) and strong regime shifts can occur in some aerosol-cloud systems (Mechoso et al., 2014; Rosenfeld et al., 2014), so even small perturbations of the aerosol state away from PI conditions may be important.

Differences in modeled aerosol removal processes have been shown to cause a large diversity in simulated BC concentrations in remote regions (Mann et al., 2014). Browse et al. (2012) investigated how improving scavenging processes in GLOMAP affected Arctic aerosol concentrations and seasonality. The authors found that in summer, when Arctic pristine regions are at a maximum (Figure 3.8), inclusion of aerosol scavenging by drizzle effectively 'filtered' the aerosol north of 60°. Inclusion of such a scheme could therefore further increase pristine regions duration and extent during the spring-summer time in the Arctic region.

Ageing processes are another source of uncertainty with the potential to effect the duration and extent of pristine regions by altering the lifetimes of anthropogenic emissions. The lifetime of BC in GLOMAP is 6.6 days (Mann et al. 2010), which is very similar to the mean of 6.5 days documented in Textor et al. (2006) for AeroCom models. This suggests that the long-range transport of anthropogenic aerosol to remote regions is well represented in GLOMAP. Different ageing rates, defined by how many layers of soluble material are required to transform an insoluble aerosol particle to a soluble one was also examined in the sensitivity analysis. A significant change between the PI and PD in the response of CCN number concentrations to the ageing rate would be seen by a change in the regions that are stippled in Figure 3.8. Furthermore in Figures 3.14 and 3.15 ageing (round blue circles) is not apparent as an important parameter, a result which is consistent with the global analysis in Lee et al. (2013) where ageing is ranked the least important of all 28 parameters in terms of aerosol (CCN number concentrations) sensitivity to perturbations of the parameter.

The analysis has focused on modelled daily mean regional CCN concentrations at cloud base. In reality, precipitating shallow clouds can strongly scavenge aerosol on timescales shorter than 1 day (Muhlbauer et al., 2014; Wood et al., 2008), leading to transient and localised conditions of very low aerosol concentration, even when the region is generally perturbed relative to the PI state by anthropogenic aerosol. The question arises whether such PD locally scavenged clean environments can be

used to experimentally evaluate modelled aerosol-cloud interaction as an analogue of the regional-scale response to changes in aerosols that occurred between the PI and PD. Given the different behaviours of single clouds and regional-scale cloud systems (Stevens and Feingold, 2009), it is unlikely that local processes will be informative about regional PI–to–PD changes like those studied here. It is also important to recognise that pristine CCN environments could still be perturbed by light-absorbing aerosols either within or above the clouds (Ackerman et al., 2000; Wilcox, 2010). Such effects, and associated fast adjustments of the cloud system, may alter the extent of PI-like aerosol-cloud environments shown in this study. Furthermore, pristine aerosol days may be associated with different meteorological conditions to polluted days, which would make it difficult to separate meteorological and aerosol influences on cloud behaviour in PD observations.

Pristine low-cloud regions are almost entirely in the SH. To reduce the uncertainty in regions of NH forcing we need to characterise the natural aerosol state either directly in these perturbed NH regions (which seems challenging) or in regions of the SH that are appropriate analogues for the NH. From a model uncertainty reduction perspective, an appropriate analogue implies that the parameters controlling CCN sensitivity in the PI SH are the same as those controlling sensitivity in the NH. Our PI simulations of CCN suggest that CCN concentrations may have been higher in the NH than the SH, because of a larger influence of terrestrial emissions. Further research is needed to determine whether these differences limit what we can learn about NH aerosol from SH measurements.

The PI NH/SH contrast, combined with the rarity of pristine days in the NH, may mean that we may have to accept that some of the PI–to–PD aerosol-cloud forcing uncertainty will be irreducible. Regardless of how well we can observe and simulate aerosol-cloud interaction in today’s atmosphere, a large part of the forcing uncertainty – that part associated with the unknown baseline aerosol state – will remain.

Chapter 4
Classification of natural emission regimes in the pre–industrial (1750) and present–day (2000) atmosphere using cluster analysis

4.1 Introduction

To observe and understand natural aerosol interactions in the Earth system, as well as their impacts on climate, it is necessary to know where and when natural emissions are playing a dominant role in affecting aerosol properties. A difficulty in studying natural aerosol is that the anthropogenic perturbation (Spracklen and Rap, 2013) to the climate and Earth system has affected regions, and hence environments, in different ways (Regayre et al., 2015). Aerosols with a predominantly natural composition can often be observed close to strong local emission sources, like wildfires. Nevertheless, we are often interested in how the emissions affect aerosol and cloud properties in remote locations. In these environments, far from well-defined aerosol sources, it is much more difficult to unambiguously separate natural aerosol environments from those with an anthropogenic influence because particles become mixed over long time scales. Detection of natural environments becomes even more challenging because many natural emissions lead to formation of low volatility gases like sulphuric acid or low volatility organic compounds that can condense onto anthropogenic and natural particles (Keskinen et al., 2013) or nucleate to form new ones (Riccobono et al., 2014; Spracklen et al., 2006). The microphysical evolution of such an aerosol system means that observationally there is no way to detect the boundaries of a natural aerosol environment. Various chemical tracers can be used to stratify aerosol measurements, such as carbon monoxide (Clarke and Kapustin, 2010), black carbon (O'Dowd et al., 2014) or even particle concentrations (Fiebig et al., 2014; Koren et al., 2014), but none of these tracers are uniquely natural or anthropogenic. For example, wildfires also produce black carbon and carbon monoxide emissions.

One approach to detecting such natural aerosol regimes is to use a model to identify locations that are most likely to represent natural environments by assessing the aerosol response to all emissions. Chapter 3 identified present–day (PD) regions where the aerosol environment is close to a pre–industrial (PI) state.

However, it didn't investigate which, if any, natural emissions are controlling cloud condensation nuclei (CCN) number concentrations.

In this chapter natural emission regimes for biomass burning, biogenic volatile organic compounds (BVOC), dimethyl sulphide (DMS), volcanic sulphur dioxide and sea spray are defined in terms of being the dominant emission (or combination of two) controlling CCN number concentrations. Natural regimes are calculated for both the PI and PD for three months representative of the seasonal variation: January, April and July. October is omitted due to biomass burning emissions peaking in this period (i.e., tropical dry season) and dominating terrestrial emissions. Each natural regime presented is defined such that all other modelled natural and anthropogenic emissions are deemed to have a negligible impact on modelled CCN number concentrations within the geographical space determined by the regime extent. Geographical regions where the same natural regime exists in both the PI and PD may be useful "natural laboratories" in which the effects of natural emissions on CCN could be studied in a PI-like state.

4.2 Methods

In order to define natural emission regimes, cluster analysis methods (Jain et al., 1999) are applied to the global model parameter sensitivity dataset of Lee et al. (2013), which was also used in Chapter 2. The statistical methodology in Lee et al. (2013) is based on the principles of variance decomposition, through which the contributions of uncertain parameters to the uncertainty in the model output of interest can be estimated. In every grid cell, 140,000 samples over the full 28-dimensional parameter uncertainty space were used to attribute the uncertainty (variance) in CCN number concentration to each of the investigated 28 parameters (Table 3.1).

A Monte Carlo assessment of model behaviour across a 28-dimensional parameter space is too computationally expensive, so a statistical representation using validated Gaussian process emulation (Currin et al., 1991) was constructed in each model grid cell to represent the relationship between CCN and the model parameters over the perturbed ranges (Lee et al., 2012). As in Chapter 2 the main effect values (Box 1) are used throughout this chapter.

Box 1: The fractional contribution to the variation in modelled CCN number concentrations given the uncertainty in each of the input parameters (Table 3.1) is termed the main effect index and it is these main effect contribution values which are then used throughout this chapter.

This statistical approach has been successfully applied to the GLOMAP model in several published studies to quantify how expert-elicited input parameters affect the uncertainty in CCN number concentrations (Lee et al., 2012, 2013), aerosol number concentrations, and aerosol-cloud radiative forcing (Carslaw et al., 2013; Regayre et al., 2014). The same techniques have also been applied to a cloud microphysics model to explore uncertainty in convective cloud properties (Johnson et al., 2015).

4.2.1 Clustering methodology

Cluster analysis techniques are a widely used tool in many weather and climate studies (Jolliffe and Philipp, 2010), but are rarely employed in aerosol-Earth system-climate studies. Here average-linkage agglomerate hierarchical cluster analysis (Kalkstein et al., 1987) is used to generate the geographical locations in which modelled natural emissions (Table 3.1) are controlling CCN number concentrations, based on the 28 main effect values from each parameter over the full set of 8192 model grid cells that make up the globe. Cluster analysis is a well-used exploratory data analysis technique that partitions data step-wise into subsets called clusters. In general, given N items to be clustered and a distance (or similarity) matrix, the most similar pair of clusters is merged at each step into a new single cluster (for the average linkage method this results in the minimum statistical variance in the distance measure within the new cluster while at the same time producing the maximum variation between different clusters) until the whole data set is merged into one single cluster.

Figure 4.1 shows the decision tree used to generate each natural emission regimes geographical location, starting with the input data to the final selection, in three stages (lanes). Lane 1 details the step-wise methodology of how the cluster analysis was undertaken. Lane 2 details how clusters with a natural emission fingerprint of interest were identified. Lane 3 details how the final selection of clusters was undertaken to define the total geographical extent of the regime.

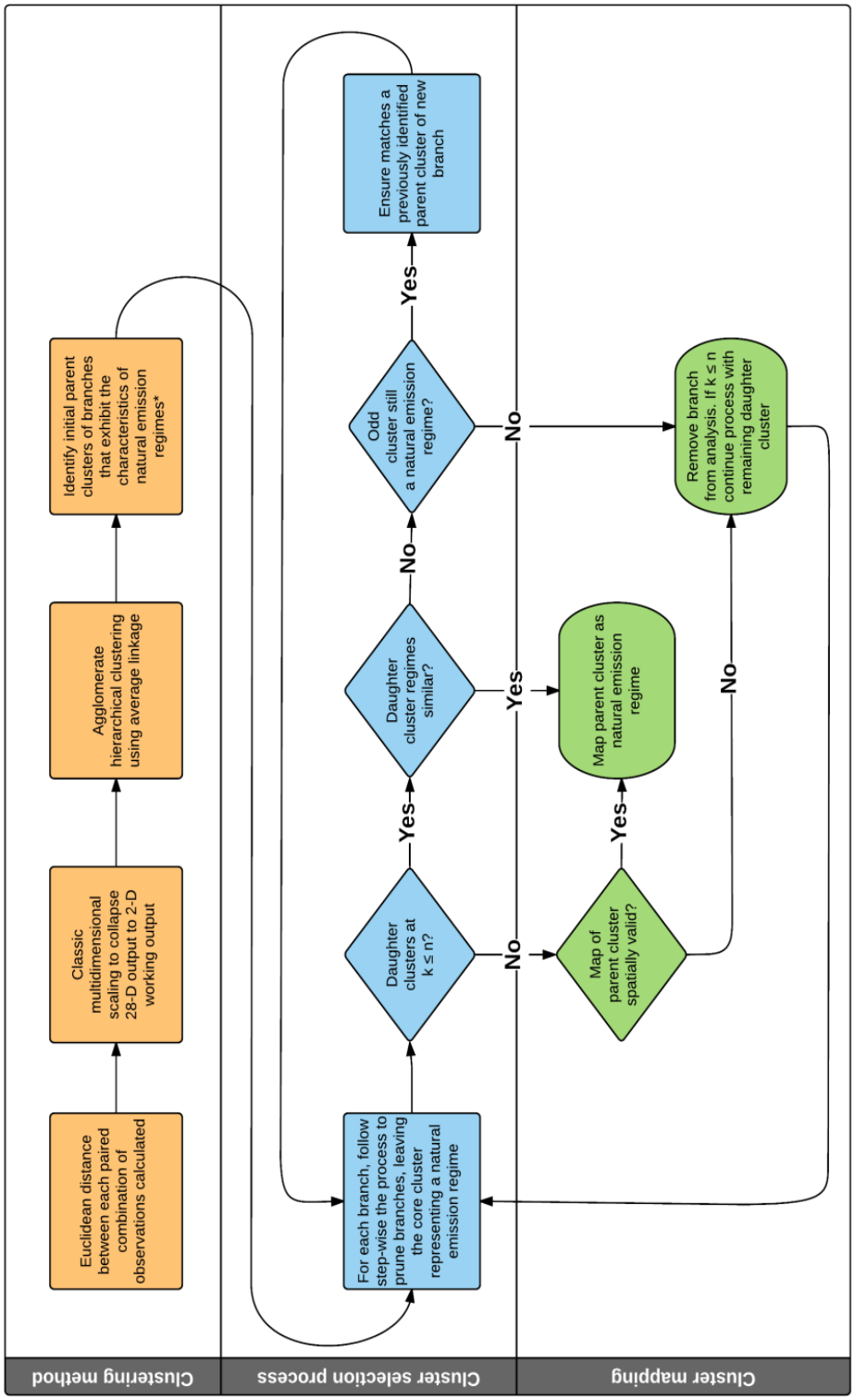

Figure 4.1. Three lane decision tree detailing the methodology used in this study to evaluate and create the clusters representing natural emission regimes (*cloud condensation nuclei number concentrations only sensitive to emissions from one or two natural emission sources).

4.2.2 Clustering method (Figure 4.1: Lane 1)

Across all grid cells, the Euclidian distance between every pair of parameter main effect values is calculated for all 28 input parameters considered. As each of the 28 parameter's main effect values are on the same scale (0-1) the Euclidian distance (norm) limits any prospect of bias towards one emission type over another as equal importance is given across all 28 dimensions. The calculated Euclidian distances from all 28 parameters are then collapsed to two dimensions using classic multi-dimensional scaling (Torgerson, 1952) prior to clustering in order to match the desired geographical distribution (longitude-latitude). Schematic 4.2a is a hypothetical case showing the distances obtained for two parameters and seven grid cells. Agglomerative hierarchal clustering of this two-dimensional output using average linkage, which minimises within-cluster variance while at the same time maximising between-cluster variance, is then used to create the dendrogram (a two-dimensional graphical representation of the resulting cluster breakdown represented as a tree of relationships) from which all clusters of interest were identified (Section 4.2.3). Schematic 4.1b-f illustrates the following detailed description of how a cluster of interest is identified, using the hypothetical case in 4.1a.

A dendrogram contains k hierarchical levels, which are explored to identify clusters of interest. In this study there is a maximum of k = 8192 hierarchical levels (the total number of grid boxes to be classified, which make up the global data set). Starting at k = 1, for each consecutive split of a branch within the dendrogram the total number of hierarchical levels increases by one. At k = 1 there is one cluster containing all the grid cells (e.g., Schematic 4.1c) and their main effect values. Each successive split of a cluster produces two new daughter clusters on the next hierarchical level (e.g., Schematic 4.1d-e). The grid cells contained within the parent cluster are distributed between the two daughter clusters. In any given cluster, the mean main effect for each parameter is calculated as the mean of the main effect values (for that parameter) from all grid boxes contained within that cluster. Hence, the mean main effect values of each of the 28 parameters changes from the parent cluster to the subsequent daughter clusters at each split in the dendrogram. In each cluster a main effect threshold value of 0.05 is defined such that any parameter whose mean main effect is less than this threshold value is omitted from consideration and deemed as having no significant impact on CCN number concentrations across that cluster. In Schematic 4.1f, the blue grid cells relate to the hypothetical cluster that is identified as a potential natural emission cluster (Section 4.2.3) and subsequently mapped (Section 4.2.4).

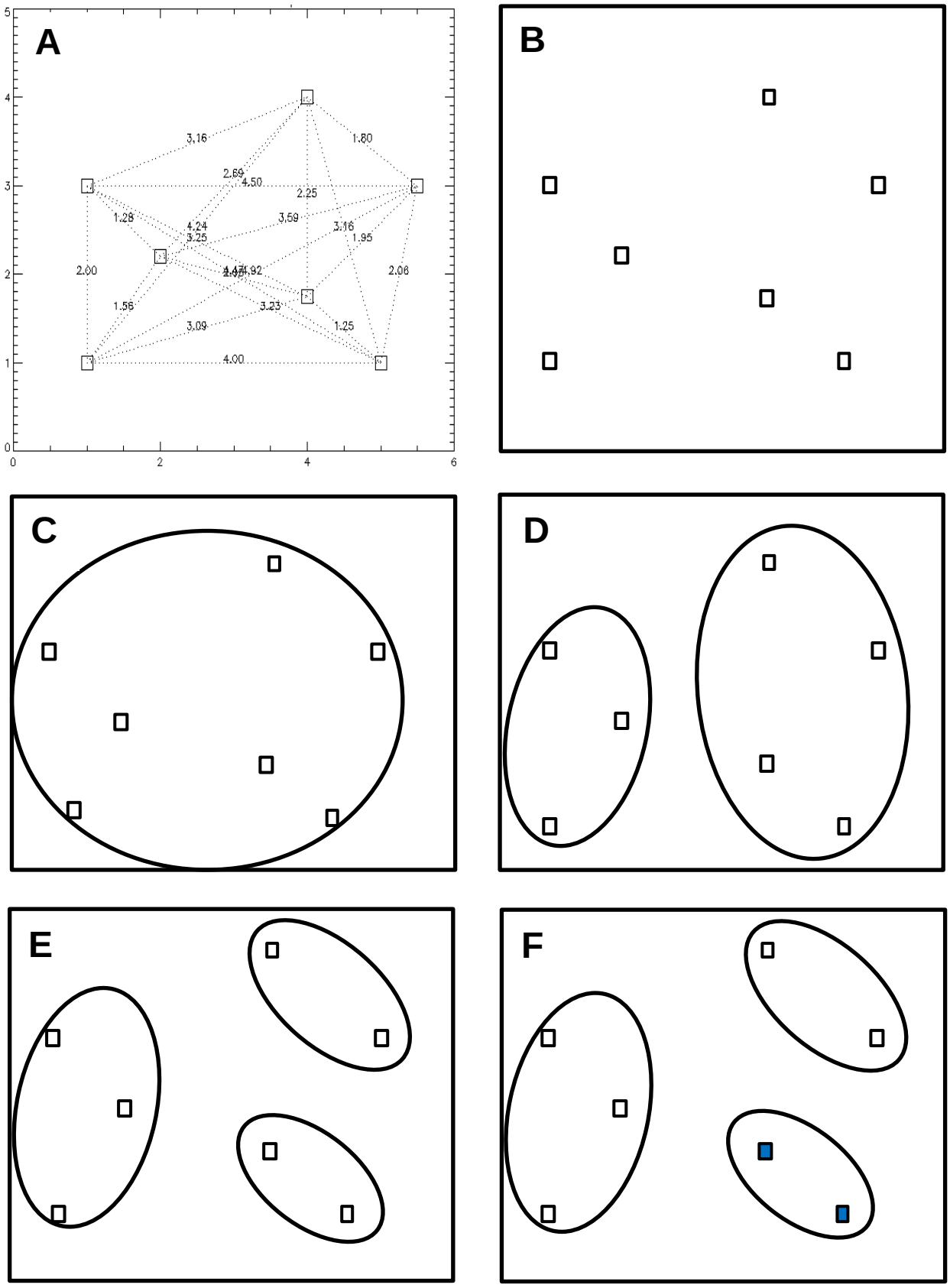

Schematic 4.1. **A**: Hypothetical case showing the Euclidian distances obtained for a case with two parameters and seven grid cells (squares). **B**: Seven grid cells which will be clustered**. C:** All grid cells in one cluster (*k*=1 on the dendrogram). **D-E**: Splitting of a parent cluster into two daughter clusters (*k*=2 and 3). **F:** Grid cells that would be mapped if the cluster was potentially part of a natural emission regime.

Before exploratory analysis of the series of daughter clusters within a branch of the dendrogram can begin an initial parent cluster characterised by the desired properties must be isolated to start the exploratory analysis from. In this study the desired cluster characteristic is that either one (for a single pure natural emission cluster) or two (for a combined natural emission cluster) natural emissions mean main effect values are the only explanatory emission variables in controlling CCN number concentrations (i.e. CCN number concentrations are deemed as being insensitive to all other emissions). Here, an initial parent cluster is defined through agreement with the following set of criteria:

1) $k \leq 100$
2) Fulfils this study's requisite of a natural emission "fingerprint" *viz*,
    a) All anthropogenic emissions have a mean main effect value of < 0.05
    b) One or two natural emission parameters have a mean main effect value of ≥ 0.05
3) The hierarchical level above (if present) does not also have the same natural emission fingerprint (see Point 2)

In this study two parameters are associated with biomass burning emissions: particle size and emission flux. Following point 2b above, biomass burning regimes are not evaluated with a second natural emission. Regimes composed of clusters with more than two natural emissions affecting CCN number concentrations (for example sea spray, DMS and volcanic emissions can be spatially co-located in certain ocean regions) are excluded from the discussion so as to focus on those natural regimes which are most practical for future study in the field.

4.2.3 Cluster selection process (Figure 4.1: Lane 2)

Once an initial parent cluster is identified, each following pair of daughter clusters is explored stepwise to a maximum of *n* pairs (where *n* corresponds to a maximum limit of hierarchical levels that the exploratory data analysis occurred over, with *n* =1 being the initial solo cluster containing all data). The aim of the decisions in the cluster selection process (Lane 2) is to reduce the number of falsely positive assigned grid cells, over the sum of hierarchal levels investigated, within a natural emission regime so as to define the geographical extent of that regime as best as possible. Cluster analysis is designed so that at each increasing hierarchical level each cluster becomes more defined, therefore the likelihood of each successive set of daughter cluster being a false positive assignment lowers. The overall general

spatial pattern of natural emission regimes was found in practice to be well defined by n =100.

The decisions in this lane (Lane 2) lead to four ways that a branch, defined as the portion of the dendrogram starting with the parent cluster and containing all its potential daughter clusters to be investigated, can be trimmed (removed) over the range of k = 2 to n, which are:

1. If a separate parent cluster for a different natural emission regime is located within the branch investigated (i.e. the new parent cluster is at a higher hierarchical level number in the dendrogram than the initial parent cluster currently being investigated), then the branch is trimmed at this point. This then allows the decision tree to be followed starting at this point for the new parent cluster.
2. A branch is considered for removal from analysis if a cluster no longer contains any mean main effect emission values ≥ 0.05.
    i. The geographical location of those grid cells within the branch determining whether or not to remove them.
3. A branch is removed from analysis if one or more of the mean main effect values for any of the anthropogenic emissions become ≥ 0.05.
4. A branch is removed from analysis if the number of natural emission parameters with a mean main effect value of ≥ 0.05 increases to 3 or more.

4.2.4 Cluster mapping (Figure 4.1: Lane 3)

The above methodology produces regimes comprised of one or more clusters within them. Usually a regime consists of more than one cluster (i.e. all clusters have the same natural emission fingerprint as per Point 2 in Section 4.2.2) and the difference between these clusters is then due to a significant shift in the mean main effect values of the microphysical process parameters, the model structure parameters, the natural emission parameters or a combination of them.

Each cluster's geographical extent, as defined by the sum of the grid cells within the cluster membership, was examined to check the cluster was well defined before being committed to the regime. Occasionally the deselection of a cluster occurred when it was apparent the cluster represented noise, i.e. a random selection of grid cells with no apparent spatial cohesion with the other clusters within that regime.

4.3 Results and Discussion

Figure 4.2 shows how the natural aerosol regimes are defined in terms of the fractional contribution of each natural emission flux to the CCN variance (the main effects) from all grid cells within all clusters in the regime. The geographic spread of the model grid cells in each regime are shown in Figures 4.3, 4.6, 4.7, 4.9 and 4.11 and the geographical coverage is summarised in Table 4.1.

Each violin in Figure 4.2 represents a box plot with a rotated probability density function calculated from the natural emission main effect value across all grid cells identified in each natural aerosol regime. As described in Section 4.2.2, for a cluster to be classed as being in a particular regime the mean main effect value across all grid cells from the corresponding natural emissions within that cluster is defined to be ≥ 0.05, while all other emissions are < 0.05. For example, the BVOC regime for January in the PI (Figure 4.2 top left) has a mean main effect across all grid cells in the regime of 0.3, meaning that 30% of the variance in CCN is accounted for by variations in BVOC emissions. The contribution of BVOCs to CCN variance varies across the grid cells up to a maximum of nearly 70%. So in some of the grid cells in this regime BVOC emissions strongly dominate CCN uncertainty, while in others the effect is weaker. Nonetheless, grid cells in each cluster comprising the regime were identified through cluster analysis to be behaving similarly and so all belong in the BVOC emission-controlled regime.

The biomass burning regime is defined in terms of two parameters: the particle emission flux and the emitted particle size. This regime occurs in all three examined months and in both the PI and PD. As shown in Figure 4.2, it is the emitted particle size that most strongly determines CCN number concentrations. The DMS and sea spray regimes occur in two of the three months and the PD regimes of both emissions generally have more a bi-modal distribution than the PI regimes. In winter and spring in the PI a BVOC regime exists, but in the PD the BVOC influence on CCN number concentrations is supressed due to increased anthropogenic activity. Similarly volcanic regimes only occur in the PI and no single volcanic emission regime occurs in any month suggesting that volcanic SO_2 emissions are well mixed throughout the atmosphere and not concentrated in particular regions.

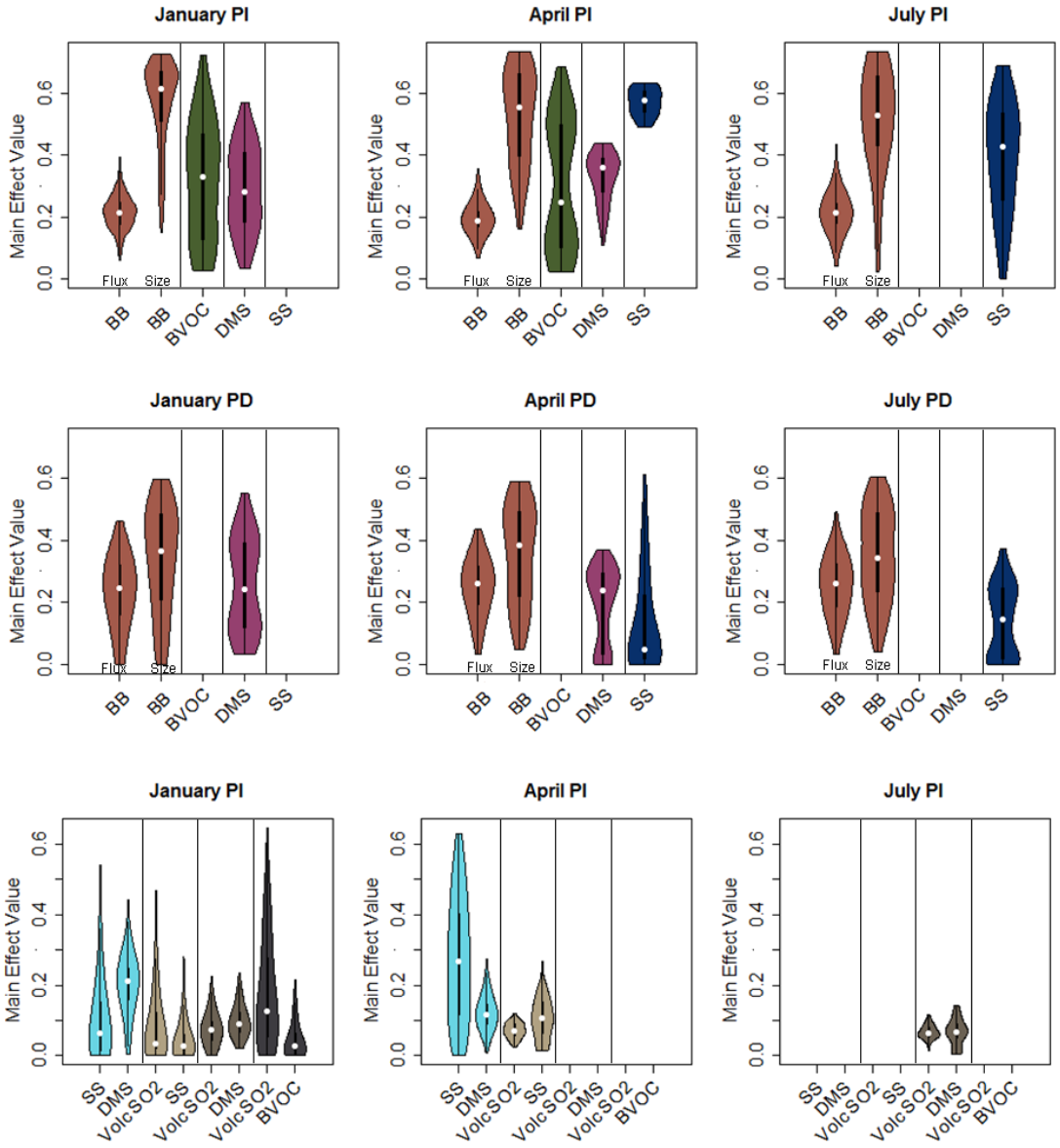

Figure 4.2. Violin plots of the emission main effect values from all grid cells in each natural emission regime presented in this study. Each violin shows a box plot with a rotated probability density function calculated from the natural emission main effect values across all grid cells identified in each natural aerosol regime. Each regime is coloured identically (and matches the corresponding maps) with pre–industrial (PI) pure natural emission regimes in the top rows, present–day (PD) pure natural emission regimes in the middle row and the dual natural emission regimes in the third row (only present in the PI).

Although industrial emissions are assumed to be zero in the PI the global sum of natural emission regimes in each month in Table 4.1 does not reach close to 100% due to clusters with either zero or three or more natural emissions controlling CCN number concentrations being omitted from study. An increase in the geographical coverage of the biomass burning regime from PI to PD is due to increased fire emissions over this period. There are also increases from PI to PD in the pure DMS and sea spray regimes which are accounted for not by an increase in natural emissions, but by the suppression of the PI joint emission regimes in the PD which allows the relevant pure natural regime to expand slightly into regions of low anthropogenic influence. Comparison of the coverage of PD natural regimes with PD pristine aerosol environments in the previous chapter shows that both PD natural regimes and pristine aerosol environments are mainly a SH phenomenon. The tropical PD biomass burning regime does not coincide within a pristine aerosol environment due to the modelled increases in CCN number concentrations over the industrial period. Therefore the sum global coverage of pure natural emission regimes is larger than the sum global coverage of pristine aerosol environments.

In the following sections, pure natural emissions regimes, in which CCN number concentrations are sensitive to the modelled perturbations from a single natural emission only, are first discussed. Then, we consider the regimes with a combination of two natural emissions. In the case of biomass burning, two parameters (emissions flux and particle size) relating to this emission were explored. However, as both these parameters have the same emission source, the biomass burning regime is discussed as a single emission regime. Each cluster with the same natural emission fingerprint (Point 2 section 4.2.2) is coloured identically in the presented results to show the total approximate geographical coverage for each of the identified natural emission regimes.

Table 4.1. The global percentage area coverage of each pure natural emission regime and their total in January, April and July in the pre-industrial (1750) and present-day (2000).

		Global percent coverage					
	Natural emission	Pre-industrial			Present-day		
Environment	**regime**	Jan	Apr	Jul	Jan	Apr	Jul
Terrestrial	Biomass burning	7.5	12.8	28.1	13.8	16.9	27.2
	BVOC	10.6	7.4	-	-	-	-
Marine	Dimethyl sulphide	18.6	3.8	-	19.9	5.6	-
	Sea spray	-	0.4	12.6	-	8.3	1.3
Global	All single regimes	36.7	24.4	40.7	33.7	30.8	28.5

4.3.1 Pre-industrial and present-day biomass burning regimes

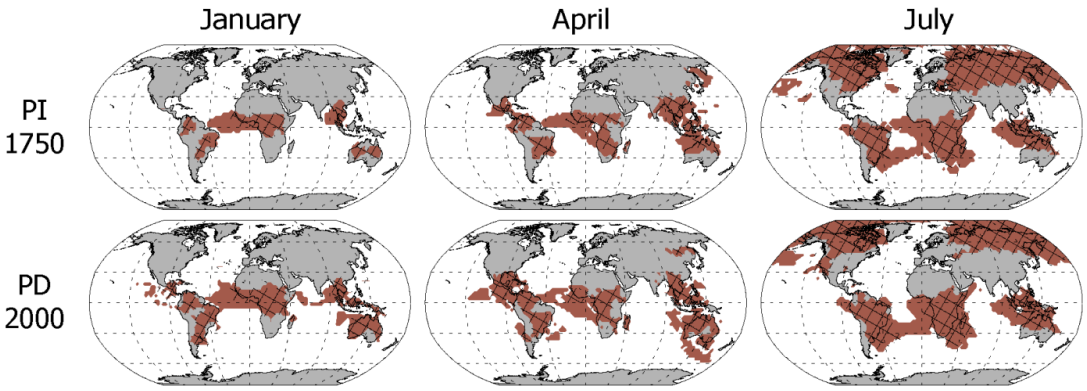

Figure 4.3. Spatial extent of the biomass burning regime in January, April and July in the pre-industrial (1750) and present-day (2000). Regime determined sensitivity of cloud condensation nuclei concentrations (CCN) to biomass burning emissions (black carbon and organic carbon) being dominant compared to all other analysed emission parameters at 915 hPa. Cross hatching indicates the portion of the biomass burning regime where CCN concentrations are sensitive to biomass burning emission fluxes and particle size parameters only (i.e. all other 26 perturbed parameters are assumed to have no significant influence on concentrations).

Figure 4.3 shows that in all months across the tropical continental and nearby ocean regions from ~15°N to ~30°S biomass burning flux and particle size are the dominant emission parameters contributing to CCN number concentrations. The cross-hatched regions are those clusters where the two biomass burning emission parameters are the only parameters controlling CCN concentrations (i.e. all 26 other investigated parameters have a mean main effect value within the cluster of < 0.05). In the PD a large fraction of tropical biomass burning emissions will be directly related to anthropogenic activity (Dentener et al., 2006), however results in Chapter 3 (Figures 3.8 and 3.13) show that in most tropical regions the overall CCN response to the 28 perturbed parameters has remained similar between PI and PD regardless of the total biomass burning emission differences. The biomass burning regime is generally restricted to the vicinity of the main biomass burning regions (e.g., van der Werf et al., 2010) despite the fact that the particles can be transported long distances through the free troposphere (Labonne et al., 2007). This long range transport results in mixing with other aerosol species, meaning that the strong influence of the emission parameters diminishes with distance so that a pure biomass burning regime no longer exists.

As fire emissions vary depending upon the fuel source (Andreae and Merlet, 2001), each of the main biomass burning regions (the Amazon, African savannah, Australasia and high latitude Boreal regions) are discussed. Human land cover change and land use intensification (e.g., Ellis et al., 2013) is not explicitly accounted for within the AeroCom emissions used in this chapter (Dentener et al., 2006). Therefore, the extent of the PI biomass burning regime is likely to be a lower limit if fire activity was higher in the PI (van der Werf et al., 2013 and Chapter 5).

Figure 4.3 shows that in tropical regions there is little overall spatial change to the pattern of the tropical biomass burning regimes between the PI and PD, due to PI tropical fire emissions being calculated based on the scaling back of PD fire emissions with changes in human population (Dentener et al., 2006). This methodology also probably overestimates fire emissions in Amazon and Indonesian deforestation regions (Brito et al., 2014; Cochrane, 2003) by carrying over this anthropogenic source of PD fire occurrence to the PI. The tropical PI biomass burning regime shown in Figure 4.3 is therefore likely to be a maximum spatial coverage for this time period. Outside these arcs of deforestation, Figure 4.3 suggests that the way aerosol responds to tropical biomass burning emissions has remained relatively similar over time (Hamilton et al., 2014). The biomass burning regime also covers Central America, reaching a spatial maximum in April which is earlier in the year than the Amazonian biomass burning season.

From January to July in Africa, there is a southerly shift in the biomass burning regime extent from the tropical northern hemisphere (NH) through to the tropical southern hemisphere (SH), which corresponds to the dry season in each hemisphere. The NH dry season is influenced by the position of the inter-tropical convergence zone (ITCZ) over the four months centred on January while in the SH the dry season is controlled by the interoceanic confluence lasting 4-5 months with a peak in July (Cachier and Ducret, 1991). In Figure 4.3 the Congo rainforest is contained within the biomass burning regime in all explored months, suggesting that rainforest vegetation is continually exposed to transported biomass burning emissions. Modelled PI CCN number concentrations in this region are over 100 cm^{-3}, and exceed over 1000 cm^{-3} for a third of the year (Figure 3.1). The large (50-500%) modelled increases in PI-to-PD CCN concentrations (Figure 3.4) suggests that changes to fire emissions over the industrial period could be impacting diffuse radiation (Mercado et al., 2009), net photosynthesis rates and primary productivity (Rap et al., 2015) within the rainforest.

In the extra-tropical regions differences can be seen in Figure 4.3 between the spatial extent of the PI and PD biomass burning regime over Australia and the NH boreal regions. These differences account for the majority of the fractional global spatial coverage reduction in PD July (Table 4.1) compared to January and April which both see an increase in PD regime coverage (Table 4.1). The difference between PI and PD regime coverage is a result of PD industrial emissions and the assumption that high latitude PI boreal fire emissions are double PD emissions (Dentener et al., 2006). Figure 4.3 shows that PI July fire emissions dominate CCN number concentration variance over North American and Russian continental regions above ~30°N while in the PD the biomass burning regime covers only the higher latitude NH region above ~50°N. In Australia the PD regime extends further southward in April, compared to the PI, and incorporates the southeast Australian region.

Downwind of African and Australasian biomass burning regions the biomass burning regime is characterised by the biomass burning emission and dry deposition parameters (Figure 4.4). In contrast CCN number concentrations are generally insensitive to dry deposition downwind of South American biomass burning regions. As the behaviour within clusters is statistically similar, understanding how the negative correlation between source and sink of biomass burning aerosol (Figure 4.5) impacts the atmospheric state, e.g. local cloud microphysics (Kaufman et al., 1998; Rosenfeld, 1999) and the strength of the Hadley circulation (Tosca et al., 2013), may be logistically easier in continental South Australia rather than within identified marine regions.

Events such as the El Niño Southern Oscillation (ENSO) and Indian Ocean Dipole are important considerations in many studies of fire variability (Field et al., 2009; Fuller and Murphy, 2006; Giglio et al., 2010; van der Werf et al., 2008a, 2008b). While the large range (0.25-4) around which biomass burning emissions were perturbed (Table 3.1, Lee et al., 2013) is assumed to capture changes in modelled fire emissions in response to climate variability, e.g. drought can over double fire emissions compared to non-drought years (Reddington et al., 2015), it does not explicitly capture spatial changes to fire activity, e.g. during drought years, usually in response to ENSO, a third or more of the Amazon is susceptible to fire (Nepstad et al., 2004). Therefore the impact of large-scale climate variability on biomass burning emissions was not diagnosed within this study and measurements made under different meteorological conditions, especially extremes such as ENSO, are important considerations for future studies.

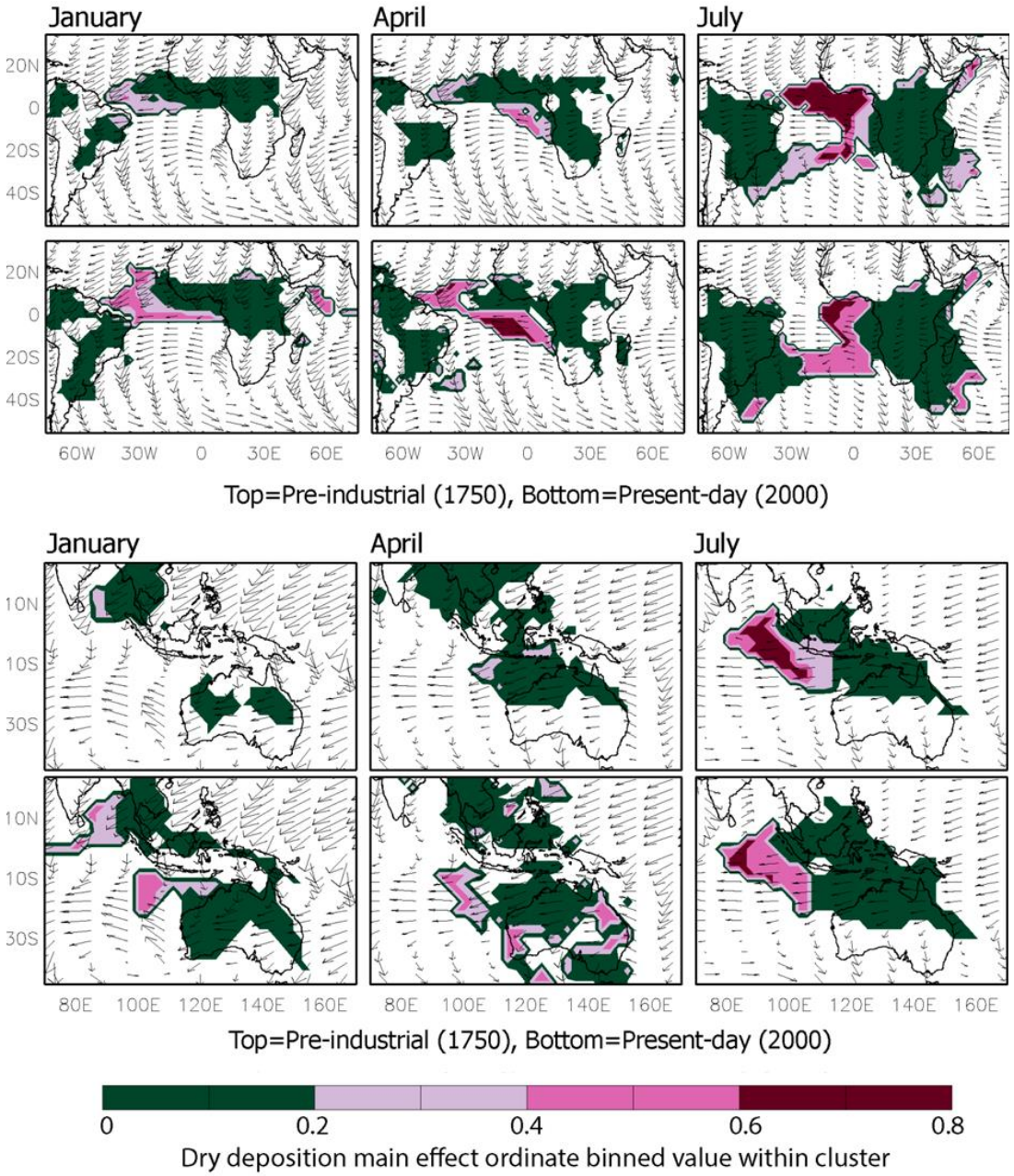

Figure 4.4. Clusters within biomass burning regime over the Atlantic and Indian Ocean regions identified by the mean dry deposition main effect ordinate value in increasing 0.2 value bins. Figure is overlaid with the ERA-interim analysis winds for 2008.

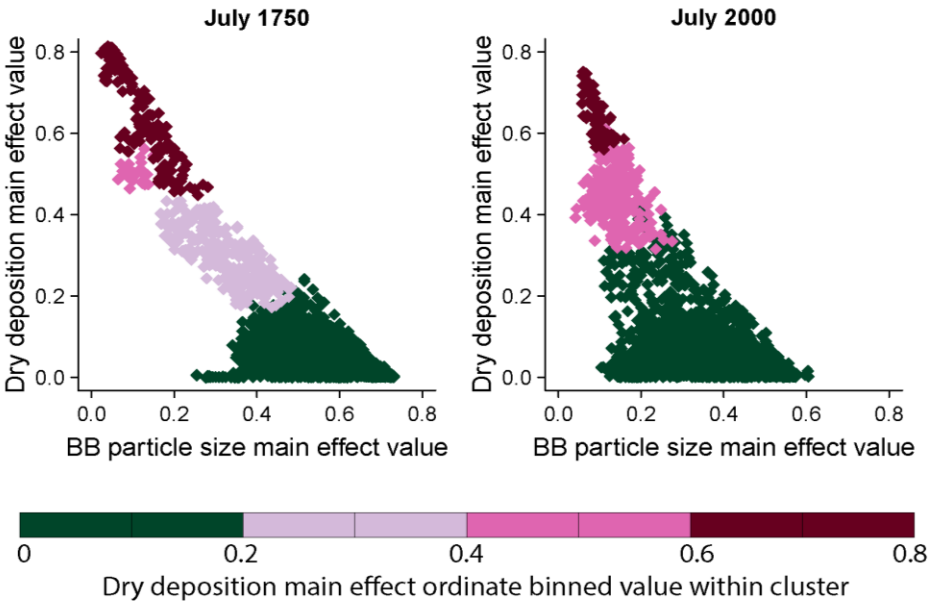

Figure 4.5. Example distribution of pre-industrial (1750) and present-day (2000) July biomass burning (BB) particle size main effect values plotted against dry deposition main effect values for each grid cell across the biomass burning regimes shown in Figure 4.3. Colours and legend represent the cluster membership shown in Figure 4.4 for each grid cells.

4.3.2 Pre-industrial and present-day biogenic volatile organic compound regimes

Figure 4.6 shows that a pure BVOC emission regime occurs only in January and April in the PI atmosphere and not at all in the PD atmosphere. The lack of a PD BVOC regime in any of the studied months is most likely due to the intermittent transport of pollution to boreal regions making the region appear mildly polluted on the monthly mean time scale used within the sensitivity analysis. Other explanations include this analysis not accounting for particle formation enhancement by organic material within the continental boundary layer (Metzger et al., 2010). For example, in the recent study by Regayre et al. (2014), which uses a similar methodology to calculate CCN sensitivities to a perturbed parameter ensemble but included this parametrisation, BVOC emissions were found to have a higher impact on the uncertainty in CCN number concentrations than in the results from Lee et al. (2013) used here. The lack of a PD BVOC regime is also probably affected by the simple treatment of SOA within the model.

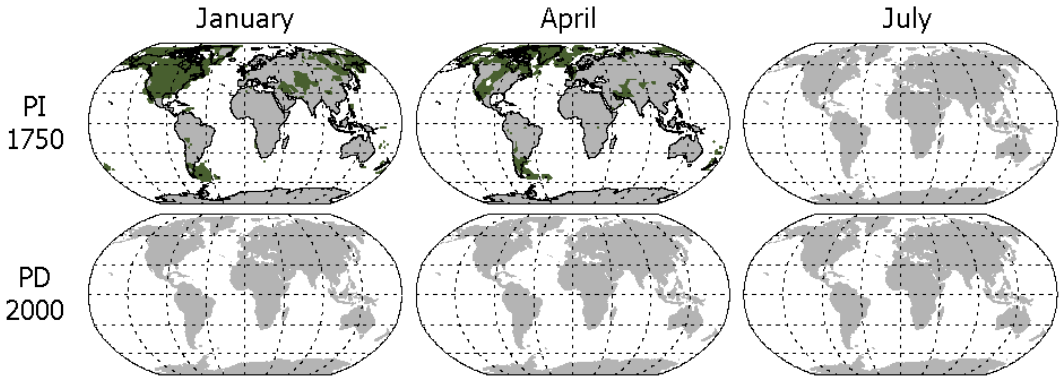

Figure 4.6. Spatial extent of the biogenic volatile organic compounds regime in January, April and July in the pre-industrial (1750) and present-day (2000). The regime is determined by the sensitivity of cloud condensation nuclei concentrations to the terrestrial biogenic emissions parameter being dominant compared to all other analysed emission parameters at 915 hPa.

In January the PI BVOC regime covers 10.6% of the globe and occurs over all of New Zealand, North America and the adjoining north-eastern Siberia region, parts of Greenland, Central Eurasia, and around South America. There are small shifts in this pattern in April, notably also encompassing the high latitude continental and marine North Atlantic, which results in a reduced overall coverage of 7.4% of the globe. The seasonal occurrence of the BVOC regime runs counter to the factors that control BVOC emissions, which are light availability, leaf area index and temperature (Guenther et al., 2012). Modelled PI CCN concentrations in boreal winter and spring across the high latitude NH BVOC regime are usually very low (< 100 cm^{-3}, Figure 3.1), suggesting only a small wildfire influence on CCN number concentrations during this period. By July the BVOC regime disappears as wildfire emissions are the prevalent aerosol particle emission source within the region.

Once aerosol has become well mixed in the atmosphere, apportioning anthropogenic SOA and biogenic SOA to their respective sources is difficult (Heald et al., 2011). The lack of a PD BVOC regime suggests that the study of BVOC emissions on aerosol concentrations requires the maximum exclusion of anthropogenic influence in regions close to pristine conditions (e.g., Chapter 2). Logically such regions are near forests, where BVOC emissions can contribute up to half of the total PD aerosol burden in boreal regions (Tunved et al., 2008) or in the Amazon during the wet season where observations suggest BVOCs dominate aerosol concentrations (Martin et al., 2010; Pöschl et al., 2010). In the previous chapter results showed that pristine aerosol environments above ~60°N could

potentially be observed up to a third of the month in January and around half the month in April.

4.3.3 Pre-industrial and present-day dimethyl sulphide regimes

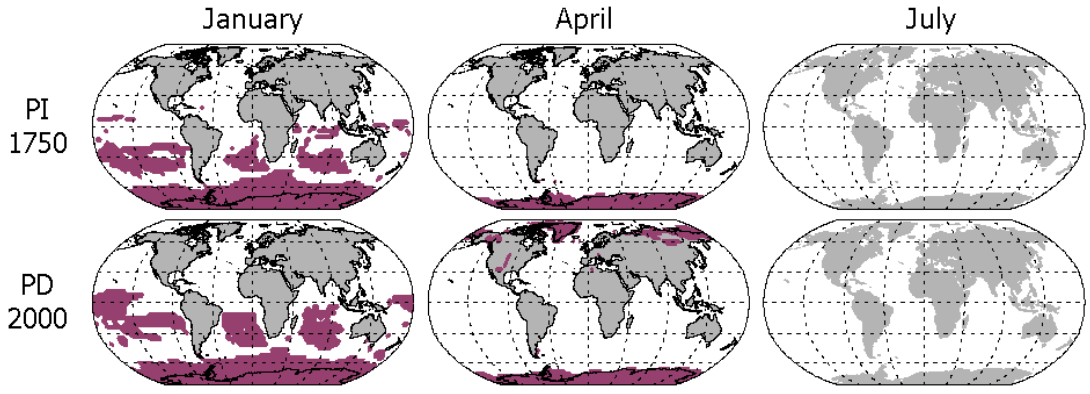

Figure 4.7. Spatial extent of the dimethyl sulphide regime in January, April and July in the pre-industrial (1750) and present-day (2000). The regime is determined by the sensitivity of cloud condensation nuclei concentrations to the dimethyl sulphide emissions parameter being dominant compared to all other analysed emission parameters at 915 hPa.

The DMS emission-dominated regime is almost entirely a southern hemisphere phenomenon (Figure 4.7) but, unlike BVOC emissions, occurs in both the PI and PD. This is likely due to the ITCZ providing an effective barrier to the southward transport of NH continental pollution and that a large fraction of SH DMS emissions are located in remote marine regions, far from SH pollution sources. In January, when ocean biological activity and corresponding DMS sea water concentrations are high (Kettle and Andreae, 2000; Lana et al., 2011), the DMS regime encompasses the main SH subtropical ocean gyre regions as well as the Southern Ocean and continental Antarctica. There are only minor changes between the PI and PD patterns of the DMS regimes which are mainly accounted for by the joint PI DMS and volcanic natural emission regime (Section 2.5) not being present in the PD. In April, as biological activity in the SH decreases towards Austral autumn, the DMS regime is reduced in both the PI and PD to cover Antarctica and the Weddell Sea. In the PD the DMS regime extends beyond that of the PI to cover Greenland and parts of high latitude continental Siberia and Yukon as well as the neighbouring

seas. In the PI those NH regions are part of the BVOC emission regime (Figure 4.6). One possible explanation for this change in regime is that continental anthropogenic emissions act to supress the continental BVOC regime by providing particles to condense upon, thus allowing a marine DMS emission regime close to strong DMS emission sources to occur instead. By July in the SH ocean DMS concentrations are at their seasonal low (e.g., Read et al., 2008; Sciare et al., 2000) and no clusters are identified in this hemisphere. In the NH, DMS concentrations reach a high in the Northwest Atlantic region (Yang et al., 2009), however modelled NH fire emissions dominate in this region at this time of year (Figure 4.3) so no clusters are identified in this hemisphere either. Furthermore, similar to the BVOC regime, the lack of a PD NH DMS regime in July will also be partly due to a small yet pervasive pollution component to the modelled atmosphere. Studies which observationally account for intermittent pollution and wildfire aerosol plumes could still study the DMS impact on CCN number concentrations in the pristine region the previous chapter highlighted along the coast line from Alaska to Yukon.

Figure 4.8 shows each of the model parameters controlling changes to CCN number concentrations in January (mean main effect > 0.05) in the three main geographical locations where the DMS regime occurs: 1) all SH sub-tropical ocean gyres, 2) the Southern Ocean, 3) Antarctica. The four parameters are: 1) DMS emission flux, 2) aerosol dry deposition rate, 3) pH of cloud droplets (which affects in-cloud production of sulphate from oxidation of sulphur dioxide by ozone), 4) the width of the Aitken mode. These plots show that the Southern Ocean and Antarctic regions have almost identical parameter sensitivities in the PI and PD. These are therefore ideal regions for exploring DMS-controlled environments essentially unperturbed since the PI. In contrast, the sensitivity of CCN to DMS in the PD subtropical gyre region is reduced by about one-half compared to the PI, with a corresponding rise in dry deposition sensitivity.

A recently updated DMS climatology by Lana et al. (2011) used three-times more samples to compile than the earlier Kettle et al. (2000) study used in this sensitivity analysis. The result is that, globally, seawater DMS concentrations are now estimated to be 17% higher than those in Kettle et al. (2000). Although this global mean increase in DMS concentrations lies within the ±50% perturbed range (Table 3.1), regional differences between the emissions are much larger and Woodhouse et al. (2013) have previously shown that such regional differences in emissions are likely to be very important for CCN sensitivity to DMS emissions. Furthermore, a recent comparison of the two DMS climatologies by Mahajan and Fadnavis (2015) showed that, in their model, an increase in DMS sea–water concentrations in the

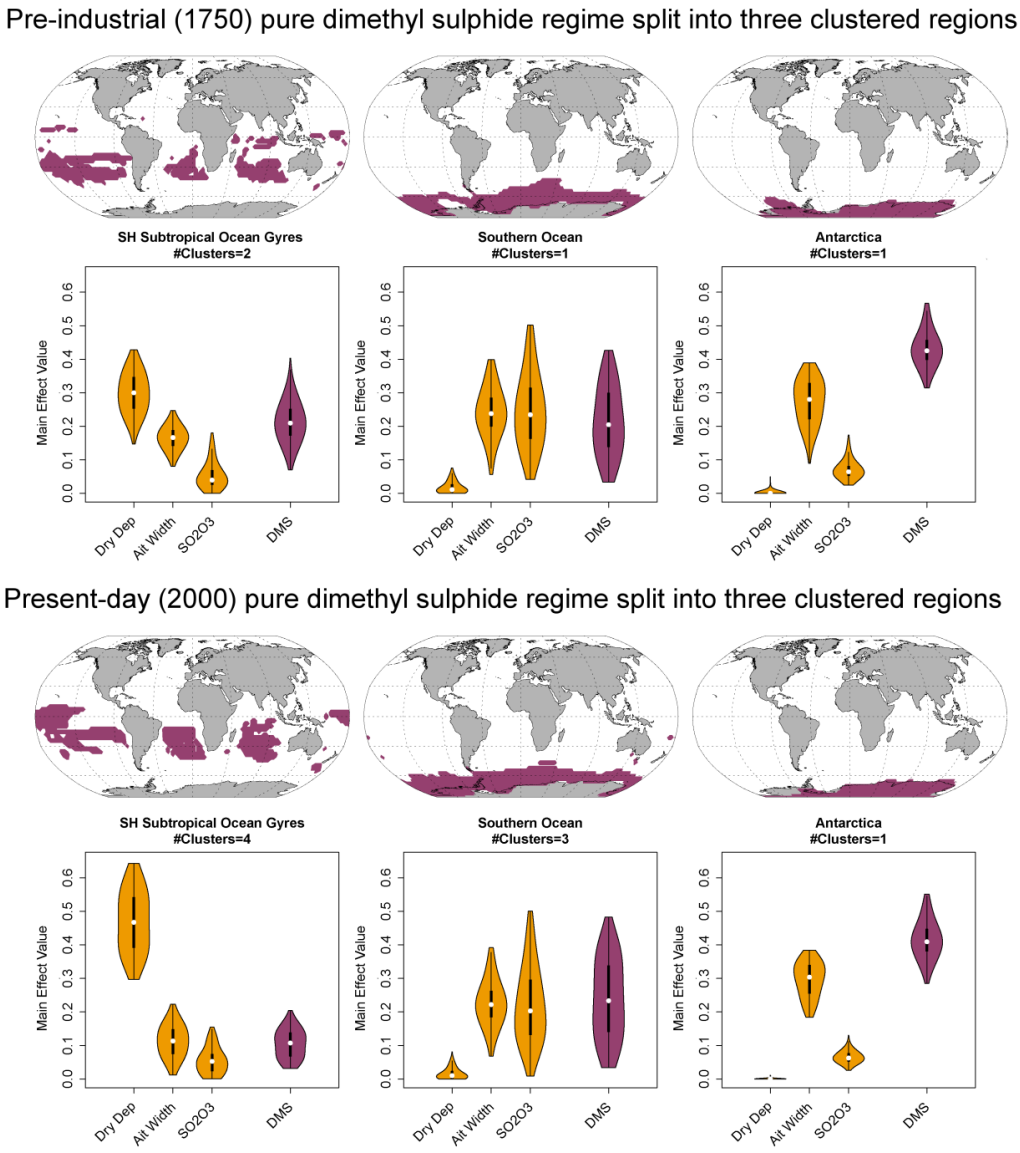

Figure 4.8. Violin plots showing box plots and the probability density distribution for the four perturbed parameters which dominate the sensitivity of cloud condensation nuclei number concentrations in the DMS regime in pre–industrial (PI) and present–day (PD) January across three distinct regions: southern hemisphere subtropical gyres, Southern Ocean and Antarctica (cluster geographical extent shown above plot). The parameters are: the DMS emission flux, the aerosol dry deposition rate, the pH of cloud droplets (which affects in-cloud production of sulphate from oxidation of sulphur dioxide by ozone), and the width of the Aitken mode. Each violin plot is constructed from the sum of all main effect values across all grid cells within the clusters (cluster membership numbers shown) that reside in their respective geographical regions.

Indian subtropical gyre region led to large increases in sulphate, aerosol concentrations and finally cloud drops concentrations in the region. Therefore future studies of DMS effects on aerosols and clouds should not be solely confined to the Southern Ocean, but rather include the lower latitude sub-tropical gyre regions as shown in Figure 4.8 where the climate response to DMS is possibly higher (Mahajan et al., 2015) and the potential for a climate feedback is possible (Charlson et al., 1987).

4.3.4 Pre-industrial and present-day sea spray and dimethyl sulphide regimes

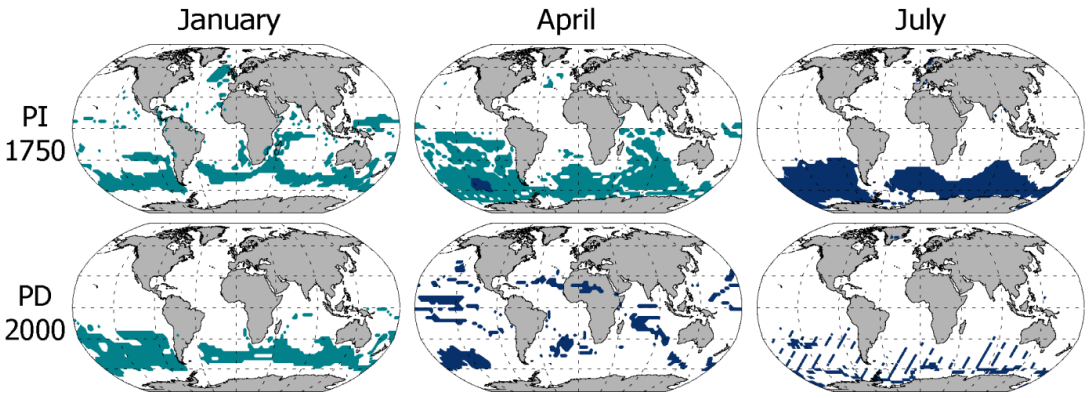

Figure 4.9. Spatial extent of both the single emission sea spray regime (dark blue regions) and the joint sea spray/dimethyl sulphide regime (light blue regions) in January, April and July in the pre-industrial (1750) and present-day (2000). The stippled region in PD July shows the extent of the sea spray and anthropogenic volatile organic compound regime. The regimes are determined by the sensitivity of cloud condensation nuclei concentrations to either the sea spray parameter or both the sea spray and the dimethyl sulphide emissions parameters being dominant compared to all other analysed emission parameters at 915 hPa.

Figure 4.9 shows both the pure sea spray regime (dark blue) and the regime in which both sea spray and DMS control CCN (light blue). As with the pure DMS regime in Figure 4.7 the spatial pattern of the January joint sea spray/DMS emission regime is almost identical in the PI and PD during this peak period of biological activity. The joint sea spray and DMS regime covers the majority of the ocean between the DMS regime's upper SH subtropical ocean gyres section and lower Southern Ocean section (shown in Figure 4.7), and transects through the region where the Cape Grim marine observatory station in Tasmania collects

natural marine aerosol measurements. In the PI there is additional coverage of this joint regime in the north-east Atlantic which covers the area where well established NH marine observations of natural aerosol are collected from Mace Head (O'Dowd et al., 2014; Reade et al., 2006).

The joint sea spray/DMS regime also dominates much of the SH in April in the PI, but in the PD it completely disappears leaving only the pure sea spray element of the regime situated across many major global wind flow regions where sea spray emissions peak. As both DMS sea water concentrations and winds are matched in both time periods this change in regime between PI and PD suggests that study into how anthropogenic activity changes aerosol sensitivity to DMS emissions could be investigated in Austral autumn in this region.

In July, weak biological activity and the strong circumpolar wind flow in the Southern Ocean means that the flux of sea spray to the atmosphere dominates CCN sensitivity. While both this study and the recent study by McCoy et al (2015) demonstrate that sea spray is the dominant emission controlling CCN number concentrations in July in the Southern Ocean region, with the exception of a small pure sea spray regime centred around 60°S, a small pervasive anthropogenic component is also present. The region containing this additional anthropogenic secondary organic aerosol component (Lee et al., 2013) is shown by the hatching on the Figure 4.9 plot for July PD. Results in the previous chapter showed that the aerosol environment in this region is pristine for up to 20 days per month in July, i.e. the anthropogenic aerosol component is present for approximately a third of the month, so a sea spray dominated CCN environment could be found by eliminating days with clear signals of anthropogenic SOA pollution. Assuming aerosol measurement conditions are representative of a "pristine" aerosol state the extent of the PD sea spray regime is then be regarded as the same as the PI and as shown in Figure 4.10 is defined when modelled winds reach a threshold speed (9 ms^{-1} in the South Pacific and 10 ms^{-1} in the remainder).

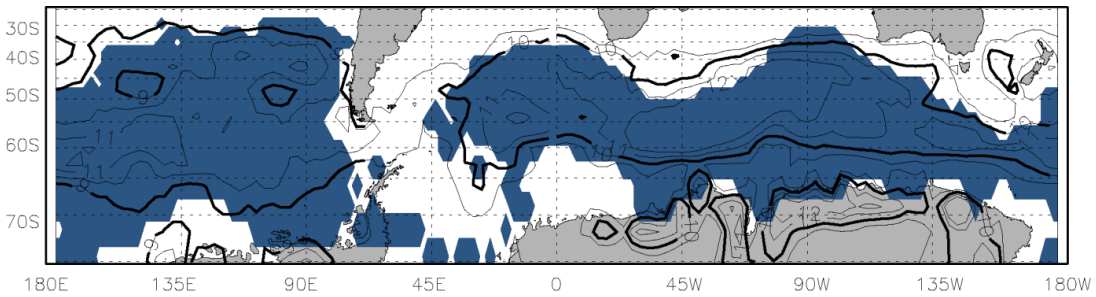

Figure 4.10. July sea spray regime for the Southern Ocean region shown for the pre-industrial (the potential extent of the present-day regime is the same under pristine aerosol conditions, which exist for up to 20 days per month) over-laid with modelled wind speed contours from ECMWF reanalysis.

4.3.5 Pre-industrial volcanic emission regimes

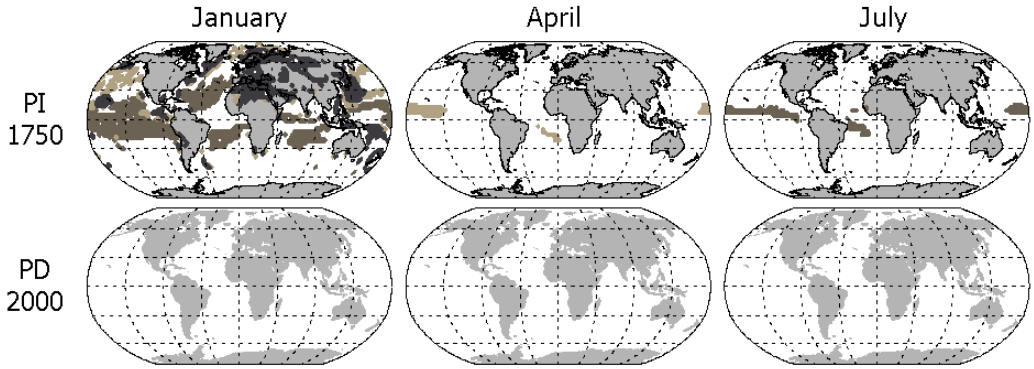

Figure 4.11. Spatial extent of the three double volcanic SO_2 emission regimes (light grey in combination with sea spray, grey in combination with dimethyl sulphide and dark grey in combination with biogenic volatile compounds) in January, April and July in the pre-industrial (1750) and present-day (2000). The regime is determined by the sensitivity of cloud condensation nuclei concentrations to the volcanic SO_2 emissions parameter and also the sea spray, dimethyl sulphide or biogenic volatile compounds emissions parameters being dominant compared to all other analysed emission parameters at 915 hPa.

Volcanic emissions are important in defining the PI CCN state (Carslaw et al., 2013; Schmidt et al., 2012). However, analysis of emission sensitivities reveals no regions in the PI or PD where CCN number concentrations are controlled solely by volcanic emissions. Rather, CCN concentrations are always controlled by volcanic

emissions combined with emissions of sea spray, dimethyl sulphide or BVOCs (Figure 4.11). In the PD, volcanic emissions become dominated by anthropogenic emissions, so no volcanically influenced regime exists.

Results suggest that while volcanic emissions are almost twice as efficient than DMS emissions at producing CCN in GLOMAP (Schmidt et al., 2012), there may be limited locations where the study of how cloud base CCN number concentrations respond to volcanic emissions in isolation. This is possibly due to the high fraction of volcanic emissions being injected into the free troposphere, resulting in a longer lifetime per unit of sulphur emitted than DMS emissions, and hence becoming well mixed with other emissions.

In January, all three joint emission volcanic regimes are present. Together they cover a large portion of the NH, especially in marine regions. In April and July a volcanic regime only occurs across the equatorial Pacific, in combination with marine emissions of sea spray and DMS respectively. The equatorial Pacific band shown in all three months represents the region where volcanic SO_2 has the largest impact on modelled CCN number concentrations and is also a highly pristine PD location (Figure 3.6). At latitudes higher than 30°S there are no volcanic regimes as biological sulphate emissions are dominating (Rap et al., 2013).

4.4 Conclusions

This chapter has built upon the previous chapters results which showed where and when the atmospheric aerosol state is similar in the PI and PD. However, the previous chapter's analysis did not diagnose which, if any, of the natural emissions studied was controlling that state, or discuss the location and change over time between natural emission regime boundaries.

In order to improve modelled historical and future climate projections a sound understanding of natural aerosol properties from targeted observational studies is required. Cluster analysis, a tool which enables large data sets to be sorted in a categorical manner, was used to explore the global model parameter sensitivity dataset of Lee et al. (2013) to identify those geographical regions and periods in which the variance in CCN number concentrations is controlled by specific natural emissions with little-to-no influence from other emission types.

The sensitivity of CCN number concentrations to the 28 parameters related to emissions, microphysical processes and model structures which were explored showed that natural emission regimes for BVOC and volcanic sulphur emissions

occurred in the PI only, while natural regimes for biomass burning, DMS and, to a small degree, sea spray occur in both the PI and PD. The observational study of BVOC, volcanic and Southern Ocean sea spray emissions in isolation is likely to require extra consideration of transported pollution and wildfire emissions or choosing study periods with little-to-no transported emissions present. The sum geographical coverage of the single natural emission regimes peaks in July in the PI (approximately 41% coverage of the globe) which is the same month as the PD minimum (approximately 29%). This suggests that suppression of natural aerosol interactions with the climate by anthropogenic activity (Spracklen and Rap, 2013) peaks during the summer.

A large portion of the PI-to-PD uncertainty in cloud-aerosol radiative forcing stems from uncertainties about how natural emissions and processes affect aerosol concentrations in the unobservable PI atmosphere. Most PI regimes shown in this chapter also overlap to some extent within regions of high PI-to-PD aerosol-cloud radiative forcing uncertainty (Carslaw et al., 2013). This suggests that reducing some of the uncertainty in aerosol-cloud radiative forcing could be achieved through reducing the uncertainty in how natural emissions affect aerosol properties in PD regimes which overlap with PI regimes also covering these radiative uncertain regions. However, due to the issue of equifinality (Beven, 2006) any forcing uncertainty reduction is likely to be less than the reduction in the uncertainty in the natural emissions impact on CCN number concentrations itself (Lee et al., 2016) and so a portion of the PI–to–PD radiative forcing uncertainty may still be irreducible. Furthermore, even with a reduction in uncertainties that natural emissions have on aerosol concentrations, the uncertainty relating to microphysical processes still remains and so measurements under different meteorological conditions than those used in this study, especially extremes such as ENSO, are also important considerations of future studies.

In tropical regions, PI and PD CCN number concentrations are controlled by biomass burning emissions with a clear regime existing in both time periods. Over boreal regions the PD regime is reduced to higher latitudes compared to the PI and accounts for the majority of the spatial change in biomass regimes over time. Over tropical continental regions CCN concentrations are sensitive only to the biomass burning emissions, while over downwind ocean regions CCN is controlled by a combination of emissions and deposition.

Over the majority of the SH ocean regions it is DMS and sea spray emissions that are controlling CCN number concentrations, with the relative importance depending

on seasonal variations in biological activity and wind speeds. The SH sub-tropical gyre region was identified to be within the DMS regime highlighting that studies of DMS effects on aerosols and clouds should not be confined to the Southern Ocean, but rather include these lower latitude regions where the climate response to DMS is possibly higher (Mahajan et al., 2015) and the potential for a climate feedback is possible (Charlson et al., 1987). The relationship between wind speed threshold and the sea spray regime extent provides an additional constraint to the boundary conditions in which studies such as sea spray-climate feedbacks (Dunne et al., 2014) or sea spray geoengineering (e.g., Bower et al., 2006; Pringle et al., 2012) can operate which is observationally simple to assess. The current contribution of industrial sulphate to the atmosphere rapidly declines after ~35° south (McCoy et al., 2015). As future industrialisation of the SH will increase the anthropogenic component over SH oceans advantage of the fact that CCN concentrations in the mid-latitude SH ocean regions are currently predominantly driven by natural emissions would be best taken in the near future.

Global climate model simulations currently underestimate cloud albedo over the Southern Ocean compared to satellite observations (Stephens and L'Ecuyer, 2015; Trenberth and Fasullo, 2010). The result of which is that the SH energy budget is incorrect and therefore regional sea surface temperatures and large-scale circulation patterns poorly represented. These deficiencies impede evaluation of how the Southern Hemisphere will respond to future climate change and any systematic bias between PD and PI simulations also increases the uncertainty in an already uncertain PI atmospheric state. Determining the contributions to this bias from natural emissions is yet to be made. Results show that the relative importance of long range transport of pollution on cloud base CCN number concentrations over the Southern Ocean is at a minimum in the Austral summer, when CCN concentrations are at their peak (Ayers and Gras, 1991) and primarily controlled by the local DMS flux, while in winter it is mainly sea spray driven with an additional small anthropogenic component.

Evaluation of the capacity of global climate models to reproduce observed aerosol concentrations requires information on the locations of the natural emission regimes they are representing. This is important not only for evaluating model skill but also for highlighting where further understanding of natural processes or boundary conditions is required. Incorporation of prior knowledge on the location and duration of natural aerosol regimes will also help focus observational studies on when and where the response in aerosol concentrations has a minimal contamination from other emission sources.

Chapter 5
The influence of pre-industrial fire emissions on the magnitude of the anthropogenic aerosol radiative forcing over the industrial period

5.1 Introduction

Global fire activity is strongly governed by human activity and climate (Bowman et al., 2009; Pechony and Shindell, 2010). The present–day (PD) pattern of fire is relatively well understood based on global satellite measurements of burnt area (e.g., Giglio et al. 2010). However, despite the prominent role of fire in past and present climate (Ward et al., 2012), current understanding of pre–industrial (PI) fire emissions is limited (van der Werf et al., 2013). Proxy records (Figure 5.1) show that fire activity varied considerably over the last five hundred years, declining from 1500 to a low in the 1600s, then rising again to a peak around 1850 before declining to PD levels (Marlon et al., 2008, 2016; McConnell et al., 2007; Wang et al., 2010). The charcoal record is a global proxy of fire activity, while ice core carbon monoxide (CO) measurements from Antarctica are a proxy for fire emissions within the Southern Hemisphere, due to CO lifetime not facilitating inter-hemispheric mixing. The methane record does not follow the same pattern (Ferretti et al., 2005), but a follow–on study by Houweling et al. (2008) has shown that the ice core methane record is also sensitive to anthropogenic fossil fuel emissions.

Figure 5.1 suggests that PI fire emissions may have been similar to the PD, if not higher, which is contrary to both the AeroCom 1750 (Dentener et al., 2006) and the Coupled Modelling Inter-comparison Project (CMIP) 1850 (Lamarque et al., 2010) datasets in which PD fire emissions are a factor 1.3 to 3.0 times greater than the PI. Both datasets assume a positive relationship between population density and fire occurrence to create PI emissions from known PD emissions. However, advances in global fire modelling (Hantson et al., 2016) suggest a significantly different pattern of fire occurrence under PI conditions, and consequently higher emissions. Furthermore, anthropogenic land cover change has not previously been accounted for, although it is known that total burnt area increases when the fuel bed is less fragmented by human activity (Bistinas et al., 2013; Knorr et al., 2014; van der Werf et al., 2013).

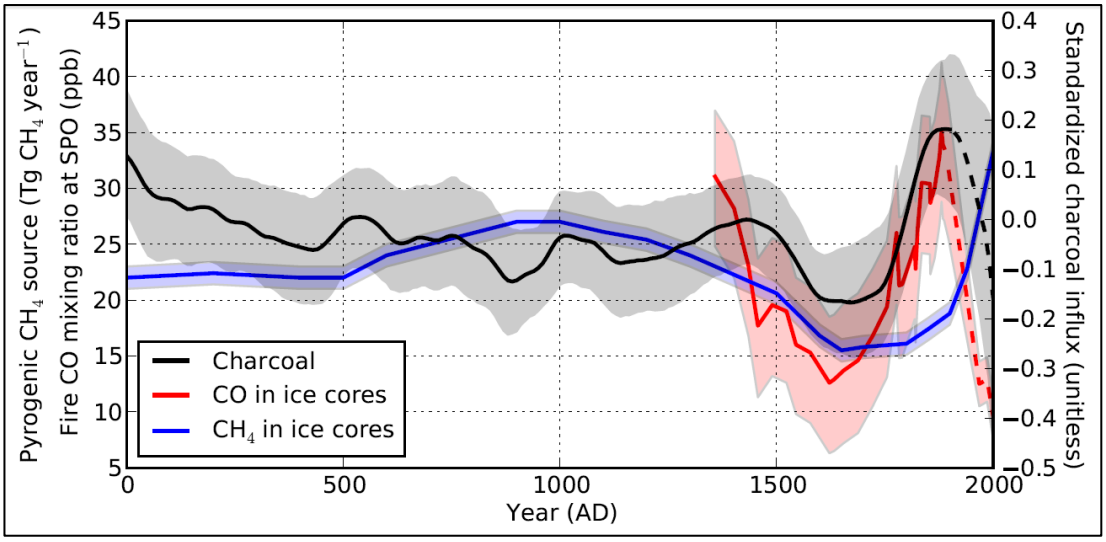

Figure 5.1. Variability in biomass burning over the last two millenia based on a global compilation of charcoal sediment records (Marlon et al., 2008) and Antarctic ice core records of carbon monoxide (CO) (Wang et al., 2010) and methane (CH_4) (Ferretti et al., 2005). Shaded areas indicate reported uncertainty. Figure from van der Werf et al. (2013).

To quantify how assumptions about PI fire emissions affect historical aerosol radiative forcing three datasets of black carbon (BC), particulate organic matter (POM) and sulphur dioxide (SO_2) emissions were compiled and then tested in GLOMAP. Fire emissions are defined as the sum of emissions from natural wildfires and those due to anthropogenic activity.

5.2 Fire modelling

Large-scale fire models aim to include representations of three main processes (Pfeiffer et al., 2013):

1. Occurrence of fires
2. Behaviour of fires
3. Impacts of fire on the local vegetation

Estimates of fire aerosol and gas emissions up to the global scale, depending on the complexity of the model, are calculated from the modelled amount of dry matter burnt. The magnitude of the flux also depends on the total burnt area, itself a function of the fire intensity, fuel abundance, fire spread, and fire related weather

conditions. Fire-weather encompasses modelled conditions which either promote or suppress fires, mainly: lightning ignition, relative humidity, recent precipitation, temperature, and wind.

In order to provide a more realistic range of PI fire emissions, which cannot be directly observed, this chapter compares two fire models driven by distinct philosophies with those in the widely used AeroCom dataset (Dentener et al., 2006).

The first fire model LMfire was run by Prof. J. Kaplan (University of Lausanne) to provide dry matter burnt data. Aerosol and gas emissions from this data were then calculated for use within GLOMAP. The second fire model SIMFIRE–BLAZE was run by Dr. S. Hantson (Karlsruhe Institute of Technology) and provided an alternative set of aerosol and gas emissions, which were then compared to the LMfire model emissions.

5.2.1 LPJ–LMfire fire model

The LMfire model is an update to the SPITFIRE (SPread and InTensity of FIRE) combustion model (Thonicke et al., 2010) and is coupled to the Lund-Potsdam-Jena (LPJ, Sitch et al. 2003) dynamic global vegetation model (DGVM). The model calculates the amount of dry matter burnt from nine plant functional types (PFTs).

The LMfire model is currently the only fire model specifically designed to simulate fire in the PI period (Pfeiffer et al., 2013) and performs well when reproducing PD boreal fire behaviour (Pfeiffer et al., 2013), a PD region analogous to the PI. The LMfire model simulates natural wildfires from lightning ignition and includes a unique representation of fires generated by PI hunter–gatherers, as well as both agricultural and pastoral societies. The rate of fire spread accounts for passive fire suppression due to anthropogenic land fragmentation.

In order to simulate meteorological variability, monthly mean anomalies of precipitation, temperature, wind speeds and lightning flash rate are added to a baseline 1770 climatology (Pfeiffer et al., 2013). LMfire incorporates the KK10 land use data set (Kaplan et al., 2011) with agricultural and pastoral burning held constant so that the variability in fire emissions is due to natural wildfire variability only. The final LMfire dataset used in the thesis incorporates the 150 year emission mean and four decadal datasets which are used to estimate the natural variation in fire emissions, defined as the minimum and maximum of emissions for the tropical (30° N to 30° S) and extra-tropical (>30° N and >30° S) regions.

5.2.2 LPJ–GUESS–SIMFIRE–BLAZE

The SIMFIRE–BLAZE (Nieradzik et al. 2017, *in prep*) model incorporates the SIMFIRE (SIMple FIRE model, Knorr et al. 2014) combustion model and is coupled to the LPJ-GUESS DGVM (Smith et al., 2001). Ignition is controlled by the SIMFIRE module and depends on lightning or 'a match'. Population density determines both the anthropogenic fire ignition (the 'match') and suppression. The average annual maximum fraction of Absorbed Photosynthetically Active Radiation (fAPAR) from satellite measurements is used as a proxy for total available biomass in a region. Total burnt area is simulated by SIMFIRE and has been empirically optimised against PD observations of burnt area, biome type and population densities (Knorr et al. 2014). SIMFIRE–BLAZE simulates dry matter burnt from the fire intensity and fractional fluxes from each carbon pool's fuel abundance (e.g., live wood, dead wood or litter). The SIMFIRE–BLAZE fire model does not simulate agricultural fires. SIMFIRE–BLAZE is then configured to run under PI conditions. Emissions used in this chapter are calculated as the mean of a 1750–to–1770 transient simulation, which spans the time period between AEROCOM and LMfire.

5.2.3 Anthropogenic land use and land cover change

An important difference between each fire model is the representations of anthropogenic land cover and land use change over the industrial period within the host DGVM. The SIMFIRE–BLAZE simulation incorporates the Hundred Year Database for Integrated Environmental Assessments (HYDE 3.1) dataset (Klein Goldewijk et al., 2011), which linearly extrapolates historical land cover change based on 1961 land use, resulting in increased anthropogenic land use in western Europe in 1750 (Ellis et al., 2010, 2013; Kaplan et al., 2011). The LMfire simulation incorporates the KK10 dataset (Kaplan et al., 2011), which assumes a Boserupian view of non-linear land use intensification where low population densities lead to fast anthropogenic land expansion (Ellis et al., 2013; Kaplan et al., 2011). The LMfire simulation therefore features significantly more anthropogenic land use in the early PI period than SIMFIRE–BLAZE (Figure 5.2), particularly over Eurasia, India, southeast Asia and Africa (Ellis et al., 2013; Kaplan et al., 2011).

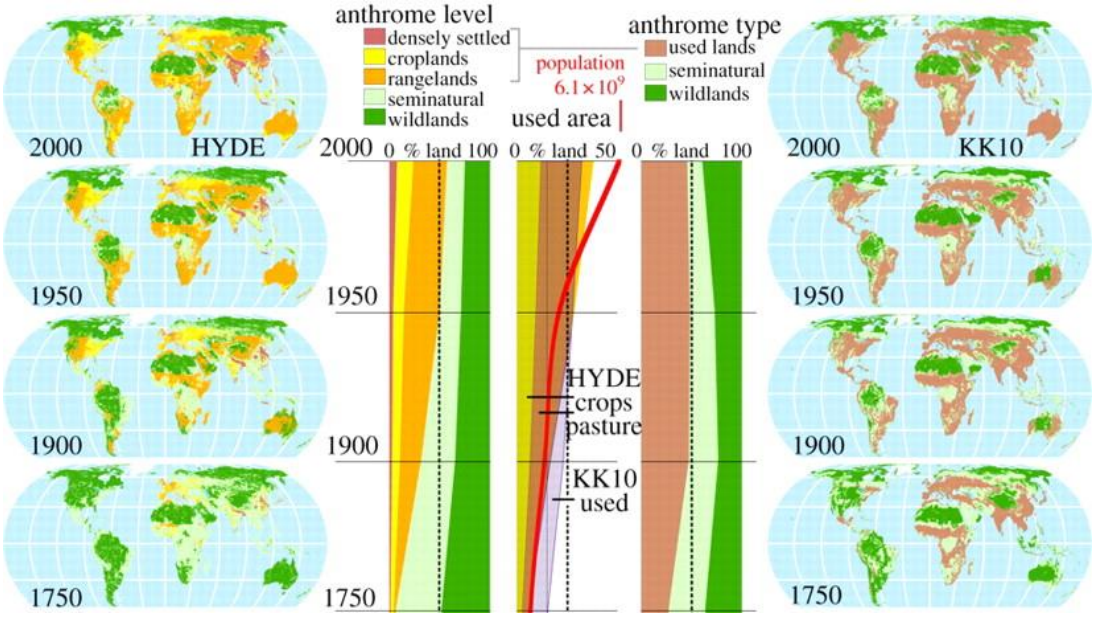

Figure 5.2. Anthropogenic transformation of the terrestrial biosphere over the industrial era. Left: Global anthrome level maps and area changes derived from HYDE land-use and population data. Right : anthrome type maps and area changes from KK10 land-use data. Centre: global crops and pasture land area fraction from HYDE and KK10 overlaid with global trends in human population. Figure from Ellis (2011).

5.3 Methods

Emissions E of aerosol or gas species x are calculated as in equation 5.1, from LMfire or SIMFIRE–BLAZE simulated output of kg of dry matter burnt for the j^{th} vegetation fuel type (i.e. canopy or plant functional type). The emission factors EF used to calculate fire emissions of black carbon (BC), organic carbon (OC) and sulphur dioxide (SO_2) are shown in Table 5.1.

$$E_x = \sum EF(x, j) \tag{5.1}$$

Table 5.1. Emission factors for black carbon (BC) and organic carbon (OC) are from Li et al. (2012). Emission factors for sulphur dioxide (SO_2) are from van der Werf et al. (2010).

	Emission factor/ g species per kg dry matter burnt		
Plant functional type	**BC**	**OC**	**SO_2**
Tropical broadleaf evergreen	0.56	4.3	0.71
Tropical rain-green	0.47	3.2	0.71
Temperate needleleaf evergreen	0.56	9.1	1.0
Temperate broadleaf evergreen	0.56	9.1	1.0
Temperate broadleaf summergreen	0.56	9.1	1.0
Boreal needleleaf evergreen	0.56	9.1	1.0
Boreal summergreen	0.56	9.1	1.0
C3-Type grass	0.56	9.1	0.37
C4-Type grass	0.47	3.2	0.37

The effect of PI fire emissions from these two models are compared with the widely used AeroCom 1750 data set (Dentener et al., 2006), which calculates PI fire emissions in most regions by scaling down fire emissions from the Global Fire Emissions Database (year 2000) according to the local PI to PD changes in population density. AeroCom emissions do not represent the lower bound of PI fire emissions in the literature which is held by Crutzen and Zimmerman (1991) who suggested them to be 10% of PD levels. To test the sensitivity of PI fire emission estimates to natural climate variability the 150 year emission dataset of LMfire was partitioned into 15 decadal mean fire climatologies, each representing a plausible PI fire landscape. As tropical and extra-tropical fires belong to distinct regimes with different characteristics, four different scenarios based on the maximum and minimum emissions from each were selected.

All aerosol modelling was performed using GLOMAP. All other emissions are consistent with previous chapters (Table 2.2). Anthropogenic fossil fuel emissions are assumed to be zero in the PI, although a small anthropogenic biofuel component to the atmosphere exists (Dentener et al., 2006). Natural emissions of sea spray, BVOC (which form SOA) and volcanic sulphur dioxide are the same in the PI and PD. Pre-industrial emissions of biofuel follow the Dentener et al. (2006) recommendations for AeroCom which were derived by scaling emissions with human population data. Similarly, cloud condensation nuclei (CCN) number concentrations are defined as in previous chapters as the number concentration of soluble particles with a dry diameter equal to or greater than 50 nm at 915 hPa, approximately cloud base for stratiform low level clouds. GLOMAP has previously been used to model CCN concentrations in various studies involving biomass

burning aerosols (Hamilton et al., 2014; Regayre et al., 2014; Spracklen et al., 2011a) and has been shown to perform well against CCN observation data in different environments (Mann et al., 2012).

Differences in the type of vegetation burning in each model will impact the properties of aerosol and gas species emitted to the atmosphere. Table 5.1 shows the ratio of BC:OC emitted during fires from different vegetation types. The SIMFIRE–BLAZE model does not model agricultural fires and therefore a difference between LMfire and SIMFIRE–BLAZE in regions of agricultural fires is that the OC:BC ratio could larger in LMfire compared to SIMFIRE–BLAZE. Furthermore, land cover change from PI to PD can also alter the BC:OC ratio between the two time periods. The assumed fire size distribution (see Section 2.3.3) uses a median particle size diameter of 110 nm (Lee et al., 2013), which does not account for any differences in mean particle sizes due to differing fuel types. For example, emissions from agricultural burning will have a different mean particle size to those from woody fuels.

The same (year 2008) global 3-D meteorological reanalyses in 1750 and 2000 is used, which eliminates meteorology as a source of variability between the two years. All simulations used meteorology from the European Centre for Medium–range Weather Forecasts (ECMWF) re–analyses, while low cloud cover is from the International Satellite Cloud Climatology Project (ISCCP) climatology (Rossow and Schiffer, 1991).

5.4 Results and Discussion

5.4.1 Pre-industrial fire emissions

The three fire emission datasets produce a wide range of PI aerosol and gas emissions (Table 5.2). Figure 5.3 shows that AeroCom fire emissions are lower in the PI than the PD at latitudes below about 50°N because they are scaled by population. In contrast, although the LMfire and SIMFIRE–BLAZE modelled PI emissions differ substantially, they are both higher than PD emissions at almost all latitudes outside the tropics. The majority of fire emissions originate in tropical Savannah regions where biomass accumulates during the wet season and provides plenty of fuel to burn during the dry season. This annual burning cycle has likely remained similar over the industrial period and explains the similarity of PI and PD emissions in that region.

Table 5.2. Fire aerosol and gas emissions for each of the three main pre–industrial (PI) experiment datasets, four PI climate sensitivity scenarios and single present–day (PD) dataset (used in the calculation of PI-to-PD aerosol radiative forcing).

Scenario	BC	POM	SO_2
PI AeroCom	**1.03 Tg a^{-1}**	**12.80 Tg a^{-1}**	**2.92 Tg a^{-1}**
PI LMfire mean	***5.19 Tg a^{-1}***	***90.34 Tg a^{-1}***	***5.27 Tg a^{-1}***
PI Tropics Max	*5.14* ***Tg a^{-1}***	*87.25* ***Tg a^{-1}***	*5.24* ***Tg a^{-1}***
PI Tropics Min	*5.02* ***Tg a^{-1}***	*86.56* ***Tg a^{-1}***	*5.08* ***Tg a^{-1}***
PI xTropics Max	*5.61* ***Tg a^{-1}***	*98.56* ***Tg a^{-1}***	*5.69* ***Tg a^{-1}***
PI xTropics Min	*4.92* ***Tg a^{-1}***	*84.22* ***Tg a^{-1}***	*4.88* ***Tg a^{-1}***
PI SIMFIRE–BLAZE mean	**3.30 Tg a^{-1}**	**46.36 Tg a^{-1}**	**4.25 Tg a^{-1}**
PD AeroCom	**3.10 Tg a^{-1}**	**34.70 Tg a^{-1}**	**8.20 Tg a^{-1}**

PI $_{Aerocom}$= 1750, PI $_{SIMFIRE–BLAZE}$= 1750-1770, PI $_{LMfire}$= 1770 and PD = 2000. BC= Black Carbon, POM=Particulate Organic Matter and POM= 1.4*organic carbon, SO_2= Sulphur dioxide. Tropics= 30°N to 30°S, xTropics= > 30°N and > 30°S.

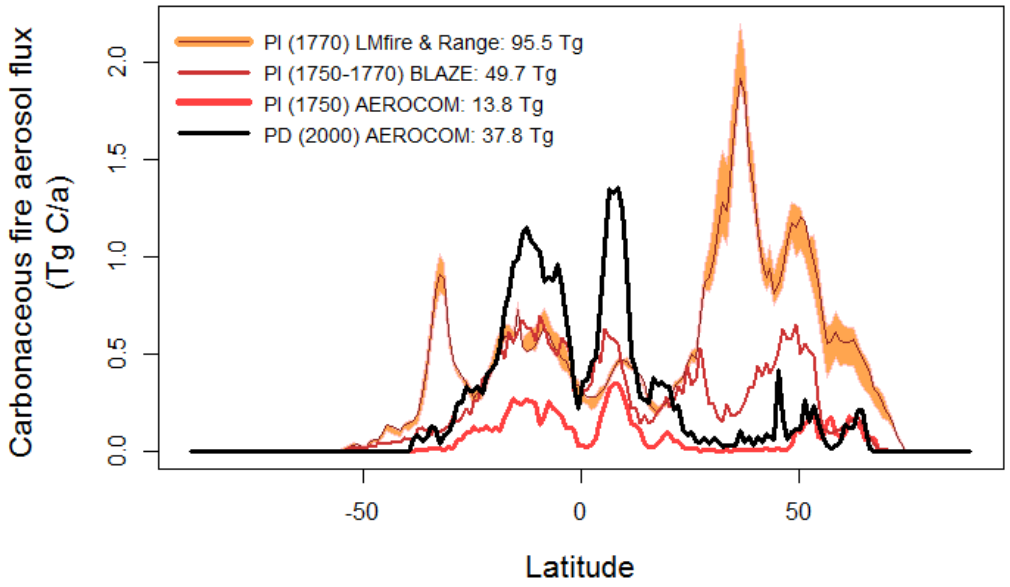

Figure 5.3. Pre-industrial (PI) and present-day (PD) emissions of black carbon and particulate organic matter as a function of latitude. The emissions are shown as the mass flux of carbon from both species. The annual flux is given in the legend. PI fire emissions derived from three fire data sets: LMfire, SIMFIRE–BLAZE and AeroCom. PD fire emissions are from the AeroCom inventory for the year 2000. The range around LMfire represents a plausible range in the natural variability of PI fire emissions derived from the maximum and minimum in emissions from the four distinct decadal mean fire climatologies

Different representations of anthropogenic land cover and land use change over the industrial period in each fire dataset contribute significantly to the difference in PI emissions at northern mid-latitudes (Figure 5.3). The AeroCom dataset assumes that anthropogenic land cover does not change over time, which is unrealistic (Pongratz et al., 2008), and therefore PI emissions are spatially co-located with observed PD emissions. The SIMFIRE–BLAZE simulation incorporates the Hundred Year Database for Integrated Environmental Assessments (HYDE 3.1) dataset (Klein Goldewijk et al., 2011) within the host LPJ-GUESS vegetation model, which linearly extrapolates historical land cover change based on 1961 land use, and results in increases to anthropogenic land use in western Europe at 1750 (Ellis et al., 2010, 2013; Kaplan et al., 2011). The LMfire simulation incorporates the KK10 dataset (Kaplan et al., 2011) within the host LPJ vegetation model, which assumes a Boserupian view of non-linear land use intensification where low population densities lead to fast anthropogenic land expansion (Ellis et al., 2013; Kaplan et al., 2011). The LMfire simulation therefore features significantly more anthropogenic land use in the early PI period than SIMFIRE–BLAZE, particularly over Eurasia, India, southeast Asia and Africa (Ellis et al., 2013; Kaplan et al., 2011). As LMfire incorporates a dedicated modelling scheme for simulating agricultural fires, the extra impact of agricultural fires on emissions from cropland areas are contributing to the larger emissions in these regions compared to SIMFIRE–BLAZE. Important for climate studies is that incorporation of land cover and land use change significantly increases northern hemisphere fire emissions (Figure 5.3), hence impacting CCN concentrations, and ultimately cloud albedo (Penner et al., 1992), in those regions which also exhibit the highest anthropogenic aerosol-cloud radiative forcing (Carslaw et al., 2013).

Global mean CMIP 1850 fire emissions are double those of AeroCom in 1750. However, they are still lower than emissions from both fire models used here. Depending on the emitted species, global PI fire emissions are estimated to be between three-to-seven times higher than those in AeroCom, suggesting that a large source of aerosol emissions is currently missing from climate models. The modelled fire emissions also lie well outside the perturbations assumed in multi–model studies (Collins et al., 2016), and have a different spatial distribution due to modelled fire emission changes corresponding with changes in the occurrence in fires, rather than a uniform global increase.

5.4.2 Pre-industrial aerosol state

Global mean PI CCN concentrations at 915 hPa (approximately low level warm cloud base) are 180.6 cm^{-3} using AeroCom emissions, and are a factor 1.6 higher with SIMFIRE–BLAZE and a factor 2.7 higher with LMFire (Figure 5.4). Over continental regions CCN increases are higher than the global mean and are a factor of two higher than AeroCom using SIMFIRE–BLAZE emissions and a factor of 3.3 higher using LMfire emissions. A large portion of this difference is due to the substantially increased emissions in the northern hemisphere mid-latitudes (Figure 5.3). Over Africa both LMfire and SIMFIRE–BLAZE fire emissions produce higher CCN concentrations compared to AeroCom, although the spatial pattern of the increase differs. Over Indonesia and northern Australia LMfire emissions lead to higher CCN concentrations than AeroCom while SIMFIRE–BLAZE emissions yield lower CCN concentrations. Over southern Australia both fire model emission datasets lead to higher CCN concentrations than AeroCom. Both the SIMFIRE–BLAZE and LMfire emissions result in marine CCN concentrations that are 1.3-2.1 times higher than AeroCom due to long-range aerosol transport.

These large changes in PI CCN are outside the 2-sigma uncertainty of the modelled CCN caused by uncertainties in the 28 parameters and emissions examined in the previous two chapters (Figure 3.2). This shows that fire emissions constitute the largest single source of uncertainty in PI CCN concentrations in our model.

5.4.3 Changes in aerosol between pre-industrial and present day

Figures 5.5 and 5.6 both show that the PD atmosphere in the AeroCom scenario contains large increases to aerosol concentrations due to anthropogenic activity. Although anthropogenic emissions are matched in all scenarios, much higher levels of PI fire emissions in the two fire modelling scenarios results in many PD continental regions having decreased aerosol concentrations relative to their PI levels. Furthermore, in the LMfire scenario this decrease extends across many SH ocean regions.

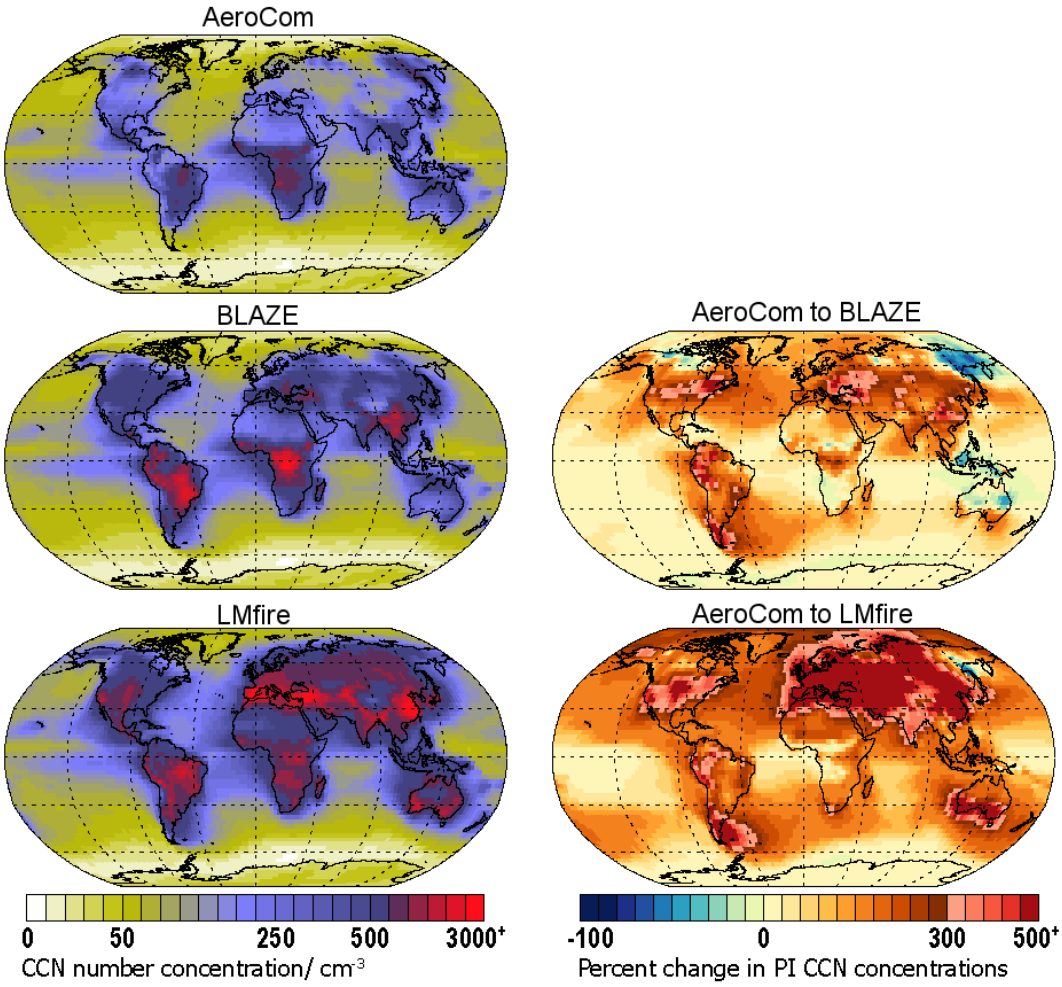

Figure 5.4. Annual mean pre-industrial cloud condensation nuclei (CCN) concentrations (cm^{-3}) and the percent change in the SIMFIRE–BLAZE and LMfire fire emission estimates compared to the AeroCom 1750 dataset. CCN are defined as the aerosol number concentration with a dry diameter above 50 nm at 915 hPa (approximately cloud base for warm shallow, radiatively important clouds).

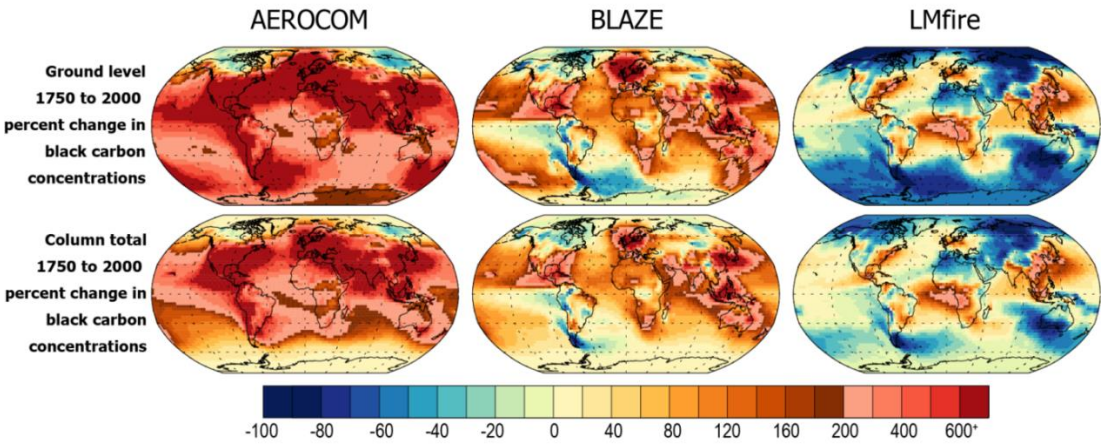

Figure 5.5. Percentage change in modelled surface-level and column black carbon concentrations between the pre-industrial (1750) and present day (2000).

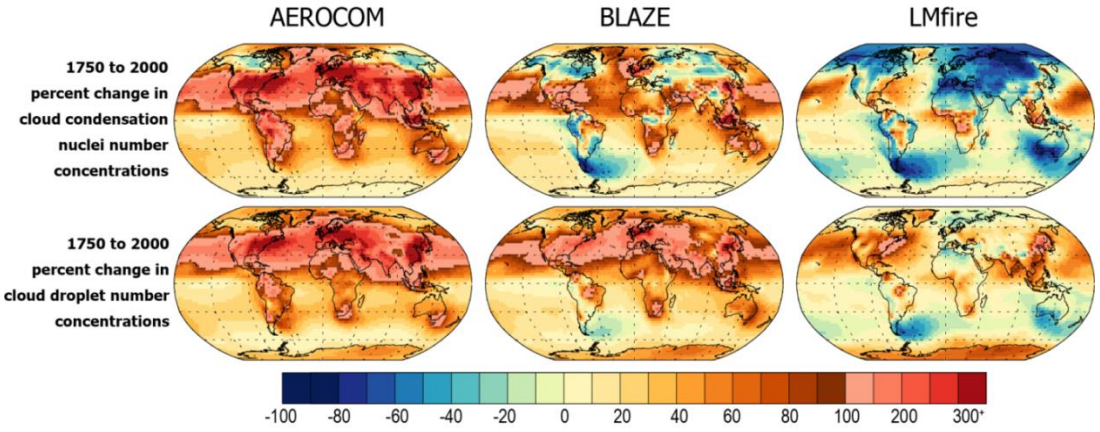

Figure 5.6. Percentage change in modelled surface-level cloud condensation nuclei and cloud droplet concentrations between the pre-industrial (1750) and present day (2000).

5.4.4 Aerosol radiative forcing

Increasing PI CCN concentrations alters both the size and number of cloud drops in the PI, and therefore the magnitude of the cloud radiative perturbation caused by anthropogenic emissions over the historical period. Figure 5.7 shows the resulting PI–to–PD radiative forcing due to changes in cloud albedo for the three PI fire emission simulations. The global annual mean cloud albedo forcing in the simulation with AeroCom emissions is -1.3 W m^{-2} in this model, but this is reduced to -0.17 W m^{-2} in the LMfire simulation and to -0.81 W m^{-2} in the SIMFIRE–BLAZE simulation. All simulations show a similar latitudinal distribution in the forcing (Figure 5.8), driven primarily by anthropogenic industrial emissions. The cloud albedo forcing peaks in the northern hemisphere at around 25°N and in the southern hemisphere close to the equator. We estimate the LMfire cloud albedo forcing to lie between -0.12 and -0.24 W m^{-2}, based on the natural variability in the 150 year PI emissions time series (Figure 5.9), which is smaller than the difference between the two fire models (Figure 5.3). This suggests that it is more important to reduce the structural uncertainty between fire models than to improve our understanding of natural variability in PI fire emissions.

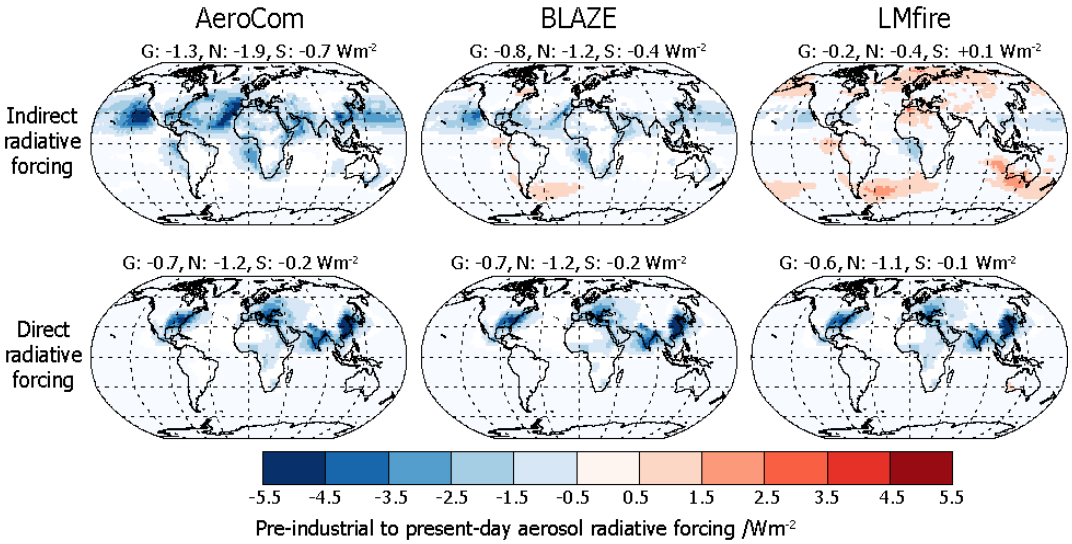

Figure 5.7. Annual mean pre-industrial to present-day aerosol cloud albedo forcing (top row) and direct radiative forcing (bottom row). Annual mean radiative forcing values given above plot for Global (G), Northern Hemisphere (N) and Southern Hemisphere (S) regions.

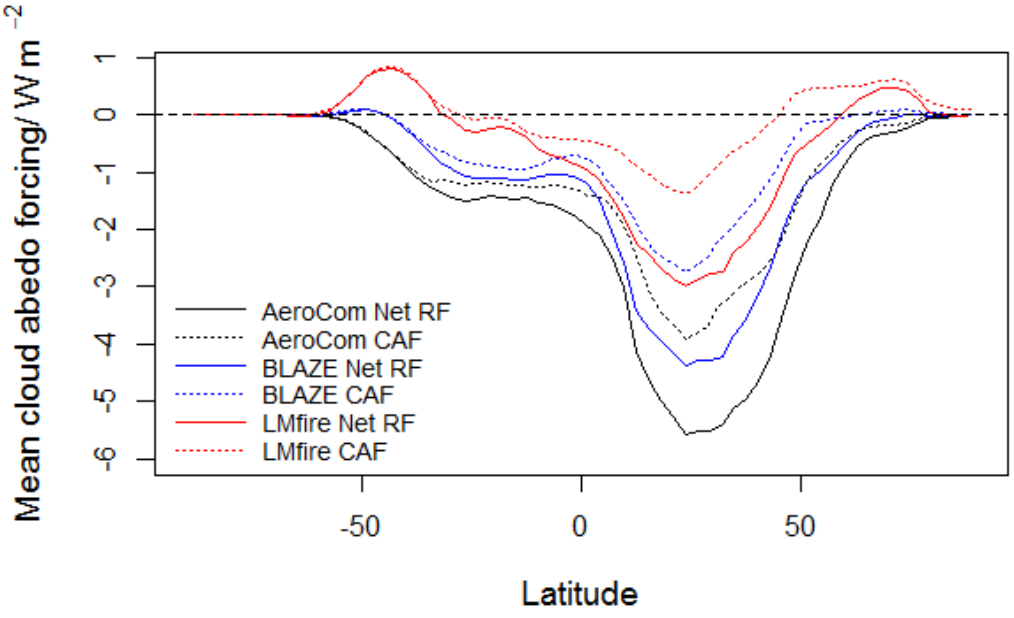

Figure 5.8. Mean cloud albedo forcing (CAF) and net forcing (CAF + direct aerosol forcing) as a function of latitude for the three simulations.

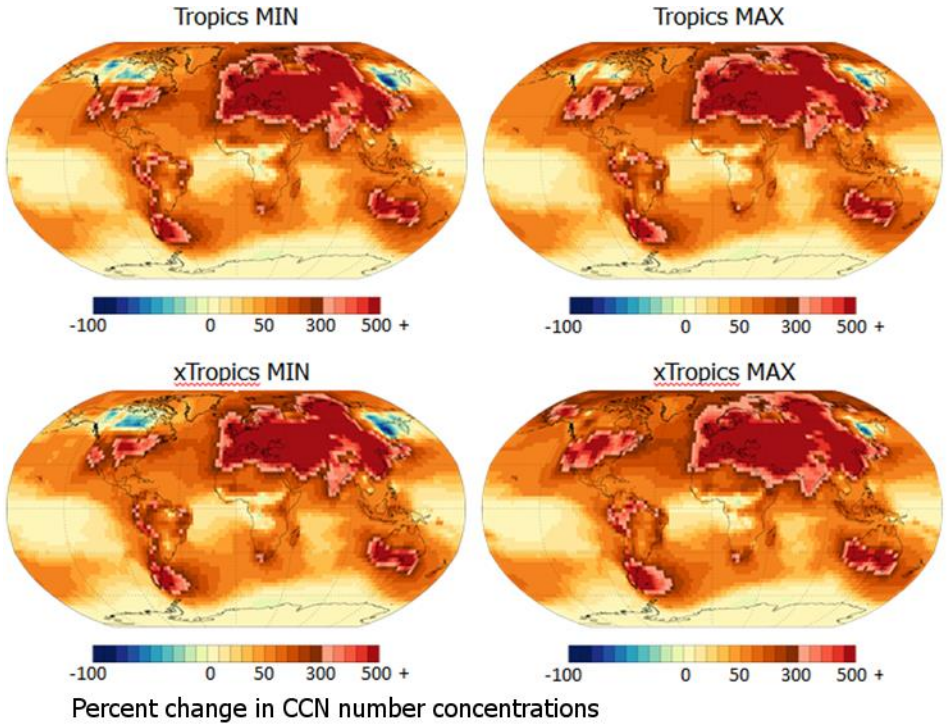

Figure 5.9. Percentage difference between the modelled LMfire emissions and the AeroCom 1750 dataset for four natural variability LMfire scenarios: tropical and extra-tropical maximum and minimum in fire emissions. Each scenario is one of the 15 decadal mean fire climatologies, partitioned from the full 150 year LMfire dataset.

Figure 5.7 also shows the PI-to-PD aerosol direct radiative forcing for each fire emission scenario. Each PI fire emission experiment results in a similar spatial pattern of direct forcing. The global mean differences are much smaller than for the cloud albedo forcing, ranging from -0.71 W m^{-2} for AeroCom PI fire emissions to -0.63 W m^{-2} for LMfire PI fire emissions (Table 5.3). The sensitivity of the direct radiative forcing to the PI aerosol state is weaker than for the cloud albedo forcing because the top-of-atmosphere radiative perturbation to aerosol emissions is more linear than for the cloud albedo effect (Rap et al., 2013).

Table 5.3. Global mean pre–industrial (PI) to present–day (PD) cloud albedo forcing (CAF) and direct radiative forcing (DRF).

	PI-to-PD	
Scenario	**CAF /W m^{-2}**	**DRF/ W m^{-2}**
AeroCom	**-1.34**	**-0.71**
LMfire mean	**-0.17**	**-0.63**
Tropics Max	*-0.21*	*-0.63*
Tropics Min	*-0.23*	*-0.63*
xTropics Max	*-0.13*	*-0.64*
xTropics Min	*-0.25*	*-0.63*
SIMFIRE–BLAZE mean	**-0.81**	**-0.67**

5.5 Model evaluation

Ice core records of BC deposited in the snow can be used to infer some information about the relative change in atmospheric BC concentrations over the industrial period. The D4 Greenland ice core (McConnell et al., 2007) is located at 71.4° N, 44.0°W, the North Greenland Eemian (NEEM) ice cores (Zennaro et al., 2014) at 77.5°N, 51.2°W and the Colle Gnifetti (CG) Swiss-Italian Alps ice core (Thevenon et al., 2009) at 45.6°N, 7.5°E. Each site has BC measurements for different historical periods: D4 starts 1788 and PD stops at 2002; NEEM covers full PI period and PD stops at 1998; CG has a single year PI measurement at 1750 and an average PD measurement between 1950–1980. The wet deposition of BC contains aerosol scavenged from across large areas down wind of the ice core sites. The CG site is located within a heterogeneous alpine environment and BC concentrations in both

time periods are calculated as the average concentrations from the model level matching the ice core site over six grid cells: the grid cell containing the CG site plus the grid cells directly to the east, west, south, southeast and southwest, those adjacent to the north were not included as it is assumed the Alps would provide a barrier to continental air flow. As the Greenland sites are within a more homogenous Arctic environment BC concentrations in both time periods are calculated at the ground level within the closest four grid cells surrounding the site.

While GLOMAP does not directly calculate BC concentrations in snow, as the processes involved are not represented, deposition data was retrieved from the model in a previous study (Jiao et al., 2014) and tested offline within the community land model, which does represent the relevant processes. Results from this study showed that GLOMAP simulates BC deposition data close to the mean for the Arctic region (Jiao et al., 2014). It is therefore expected that the relative modelled BC changes in air and those in the ice are approximately comparable.

Over Greenland most of the BC contained within the ice core in the PI is derived from wood burning (McConnell et al., 2007) transported from boreal North America (Skeie et al., 2011), while in the PD it will also contain large amounts of industrially derived BC, that have been decreasing in strength over the past decades (Bond et al., 2007). Figure 5.10 shows the PD/PI ratio in ice core BC concentrations from two Greenland sites compared to the modelled PD/PI change in ground-level atmospheric BC concentrations (Figure 5.5). Uncertainties in PI natural variability in fire activity and atmospheric circulation, and hence long range transport and aerosol processing, are accounted for by estimating Greenland PI ice core BC concentrations as a 20-year mean (D4: 1788-1807, NEEM-1740-1759). As PD Greenland ice core BC concentrations are heavily influenced by industrial emissions, the PD mean is calculated over a shorter 5-year period (D4: 1998-2002, NEEM-1994-1998). Bars shown in Figure 5.5 bound the estimated uncertainty in the PD/PI ratio of BC ice core measurements calculated from the standard error of the mean. The model with AeroCom emissions simulates a PD/PI ratio that is a factor 1.7-2.4 higher at NEEM and a factor 4.4-6.8 higher at D4, so appears to have PI emissions that are too low. The model with LMfire emissions simulates a PD/PI ratio that is a factor 2.0-2.9 lower at NEEM and between a factor of 1.2 higher and a factor of 1.3 lower at D4, while SIMFIRE-BLAZE simulates a PD/PI ratio that is between a factor of 1.0-1.2 higher at NEEM and a factor of 1.6-2.5 higher at D4.

Modelled BC changes are also compared in Figure 5.10 with ice core records from the CG ice core in the Swiss Alps, which is 4450 m above sea level. At CG, ice core BC concentrations averaged for 1950-to-1980 increased by a factor of 2.9 (Figure 5.5) since 1750. The BC deposited at this site is heavily influenced by European

emissions, which have decreased significantly over the last half century (Turnock et al., 2015). In Figure 5.10 this known increase in BC emissions is accounted by increasing PD modelled concentrations by a factor of 2.9, which is the reduction in BC fossil fuel emissions from 1965 to 2000 in the region as documented in the MACCity emissions inventory (Granier et al., 2011) in the region of the CG glacier ice core. This factor change is then applied to modelled PD BC concentrations at the CG site. AeroCom emissions result in a modelled PD/PI atmospheric BC ratio at the altitude level of the ice core that is a factor 5.8 larger than the increase in the ice core, again consistent with PI emissions that are too low. LMfire emissions result in a PD/PI ratio that is a factor 1.4 lower than the ice core change, while SIMFIRE–BLAZE emissions result in a PD/PI ratio that is 1.3 higher than the change recorded in the ice cores. These comparisons show that the changes in BC recorded in ice cores are inconsistent with the assumption that fire emissions were significantly lower in the PI than in the PD, especially over Europe. The two fire models more closely predict the change in BC, with LMfire underestimating and SIMFIRE–BLAZE slightly overestimating the changes since the PI. Current emissions inventories and models simulate similar errors in carbon monoxide from Antarctic ice cores (Wang et al., 2010), which also suggests PI fire emissions are too high over the southern hemisphere.

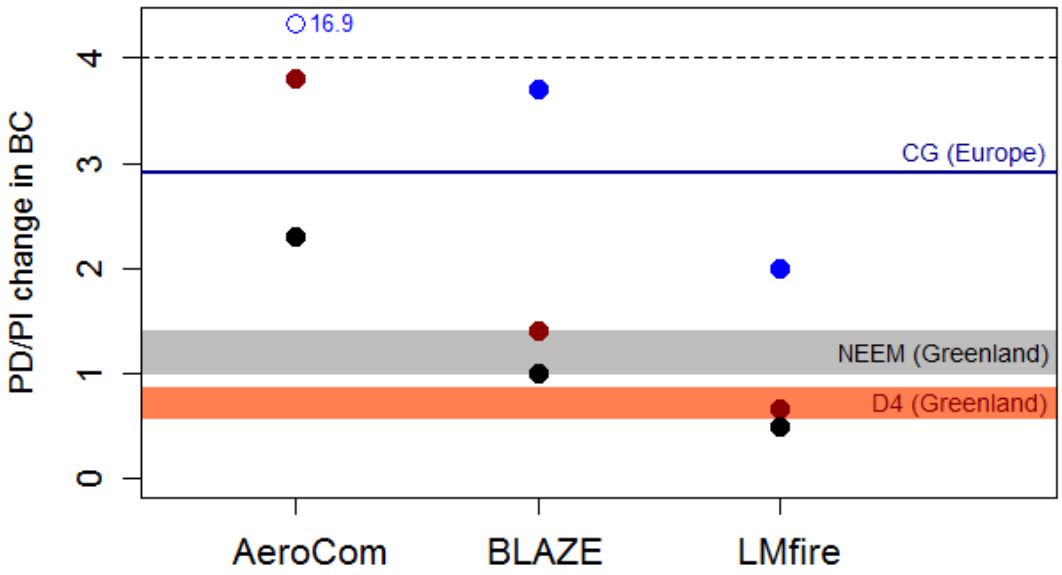

Figure 5.10. Present–day (PD)/pre–industrial (PI) changes in ice core black carbon concentrations at two Greenland sites (D4 and NEEM) and the Colle Gnifetti (CG) site in the Swiss Alps. Standard error of the mean is used as a measure of uncertainty in observations for the Greenland sites. The AeroCom change at the CG site is off the scale and shown as an open circle with its ratio change given.

Further evidence of substantial fire activity in the PI comes from the charcoal sediment record, which can be used to determine local to regional relative changes in fire occurrence over time (Marlon et al., 2008). Across both hemispheres, charcoal records show that fire occurrence in the 1700s was at least similar to, if not higher than, the year 2000 (Marlon et al., 2008, 2016). Observed charcoal sediments do not record information on the emissions from fires, and so direct comparisons with modelled changes in fire emissions are uncertain (Marlon et al., 2016). Nevertheless, the understanding that fire spread was less fragmented by anthropogenic activity in the PI suggests that the charcoal record also supports that fire emissions from both SIMFIRE–BLAZE and LMfire are plausible.

5.6 Conclusions

This Chapter presents a possible upper limit for PI fire emissions, as simulated by the LMfire model. A realistic lower bound for PI fire emissions is currently unknown, but analysis of ice cores and charcoal records suggest it will be closer to SIMFIRE-BLAZE than the AeroCom dataset**.** These revised assumptions about PI fire emissions lead to substantial changes in the regional magnitude and pattern of the net aerosol radiative forcing over the industrial period. Our modelling results imply a substantial change in how the energy balance of the atmosphere has evolved over the industrial period, particularly over the Atlantic, with several possible implications for climate studies. In particular, compared to the AeroCom simulation we estimate that the revised fire emissions reduce the magnitude of the net PI-to-PD aerosol radiative forcing contrast between the northern and southern hemispheres by 0.4 W m^{-2} for the SIMFIRE–BLAZE simulation and by 0.7 W m^{-2} for the LMfire simulation (Figure 5.7). In many coupled atmosphere-ocean climate models, the inter-tropical convergence zone would likely be positioned further southward in the PI than is currently modelled, as tropical precipitation patterns are sensitive to changes in the gradient in the interhemispheric aerosol forcing (Allen et al., 2015). Other dynamical features of the climate system, such as Atlantic and Pacific storm tracks are also sensitive to northern hemisphere aerosol forcing (Booth et al., 2012).

The inclusion of more realistic fire emissions in climate and Earth system models is likely to cause a general reduction in the magnitude of the aerosol radiative forcings that they simulate (Boucher et al., 2013), although limitations to cloud droplet concentrations that are imposed in some models will influence how they respond (Hoose et al., 2009). This change would provide a physical mechanism to bring

some models within the proposed -1.3 W m^{-2} global mean aerosol forcing limit that has been derived from a top-down analysis of the planetary energy budget (Stevens, 2015). Any subsequent adjustment to climate model processes, while still maintaining agreement with historical global mean temperature changes, will affect the climate sensitivity of the models, and hence future climate projections (Andreae et al., 2005).

The results in this chapter highlight the importance of developing a much deeper understanding of how fires evolved over the industrial period, especially since global fire models have mostly been evaluated against PD data. The human population boom over the industrial period has restructured the fire landscape on all inhabited continents and created a permanent change in the energy balance of the atmosphere that is not accounted for in climate models. However, the climate impact of fires will extend beyond changes in aerosol emissions and include many other important processes (Ward et al., 2012) such as changes in CO_2 exchange, surface albedo, ozone and methane concentrations, and diffuse radiation levels. These factors could amplify or dampen the effects we have simulated here. A reduction in the uncertainties in unobservable PI aerosol concentrations will best be achieved through a multi-disciplinary approach, including contributions from: Earth system modelling, palaeontology, geology, anthropology and archaeology.

Chapter 6
Conclusions, implications and future work

The overarching aim of this thesis was to explore the uncertainty in the impact of natural emissions on aerosol concentrations and climate and outline those regions best suited as “natural laboratories” for further study of natural emissions, the processes they undergo and their climate impacts. This was broken down into three components:

1. Where aerosols could be studied in a pristine aerosol state. Pristine regions were defined as those where present-day (PD) cloud condensation nuclei (CCN) number concentrations are within ±20% of pre-industrial (PI) levels and also where the sensitivity of PI and PD CCN to 28 model parameters (including emissions, microphysics and aerosol processes, see Table 3.1) are similar ($r^2 \geq 0.9$).
2. Where and when biomass burning, biogenic volatile organic compound (BVOC), dimethyl sulphide (DMS), sea spray and volcanic emissions dominate aerosol behaviour in the PI and PD atmospheres. Each of these natural emission regimes represents the geographical extent over which the relevant natural emissions control the modelled CCN number concentrations with a minimal interference from other species in the atmosphere.
3. How recent advances in fire modelling alters our understanding of aerosol concentrations in the PI atmosphere and hence the magnitude of the PI-to-PD radiative forcing.

This study, and the related Proceedings of the National Academy of Sciences (Hamilton et al., 2014) and Weather (Hamilton, 2015) articles, presented the first ever analysis of the global spread of pollution in terms of quantities that matter for future studies of both aerosol-cloud forcing and natural aerosol-Earth system interactions and feedbacks. Furthermore, although the behaviour of aerosols in the PI atmosphere has previously been recognised as one of the major weaknesses in the understanding of historical radiative forcing (Carslaw et al., 2013), this thesis has shown that the change in aerosol forcing caused by improved representation of fires in the PI period may exceed the sum of all the uncertainties previously accounted for.

A summary of each chapter's main findings is presented below, and organised in response to the questions posed in Section 1.4.

6.1 Summary of results

1) **Model results using GLOMAP have been used to identify where on Earth we could observe and learn about the properties of aerosol in a "PI-like" aerosol state.**
   a) Annual global mean CCN concentrations at low level warm cloud base (915 hPa) have increased by a factor of 2.2 over the industrial period (1750-to-2000). Figure 3.4 showed that the PI-to-PD change in CCN concentrations is larger in the Northern Hemisphere (NH) than the Southern Hemisphere (SH), due to the difference in hemispheric distributions of anthropogenic pollution. However, modelled increases in biomass burning emissions have also significantly increased CCN number concentrations over tropical continental SH regions. Figure 3.5 showed a clear difference in PI continental and marine CCN concentrations exists, which contradicts an earlier assumption made by Andreae (2007).
   b) Results in Figure 3.6 showed that the aerosol system in many PD environments looks and behaves similarly to the PI era. On a global annual mean, aerosol regions unperturbed by anthropogenic emissions cover 12% of the Earth (16% of the ocean surface and 2% of the land surface). About 90% of pristine regions occur in the SH. In the NH pristine conditions are generally transient and spatially patchy, however NH pristine regions do exist, particularly in the Alaska/Yukon region during boreal summer. There is a strong seasonal variation in the global geographical coverage of pristine regions between 4% in August and 27% in January. The most persistent pristine region occurs over the equatorial Pacific, with New Britain identified as the most pristine location on Earth in terms of the aerosol state.
   c) Regions where the response of CCN to the 28 perturbed parameters is similar in both time periods generally overlaps with those regions where CCN number concentrations are also similar (±20%) for at least half of the month (Figure 3.6). An exception is in tropical biomass burning regions, where the aerosol response is still similar in many months despite the large increases in CCN number concentrations over the same period.
   d) Figure 3.15 showed that aerosol-cloud radiative forcing and pristine regions are, in general, spatially anti-correlated. If the analysis is not restricted to identifying pristine aerosol in regions of non-zero aerosol forcing, but just in

regions with higher than average low cloud fraction (> 0.3), then extensive regions can be found with pristine days of 0 to 31 per month (see maps in Figure 3.15). However, these environments are mostly in the SH, potentially limiting the usefulness in reducing NH forcing uncertainty.

e) A comparison of pristine regions with Global Aerosol Watch baseline stations showed that remote SH island stations (particularly Amsterdam Island and American Samoa) are ideally situated to observe PD aerosol under “PI-like” conditions. Two high Artic stations (Barrow and Alert) are located in NH locations with the potential to observe pristine aerosol conditions for at least part of the year.

2) **Clustering techniques were applied to results from a global model sensitivity analysis of GLOMAP in Chapter 4 to identify where and when natural emissions are controlling CCN number concentrations in the PI and PD atmospheres.**

a) Natural emission regimes were identified in all three examined months (January, April and July) in both the PI and the PD.

i) **Biomass burning (Figure 4.3).** Biomass burning regimes are present in all investigated months. Over tropical continental regions CCN concentrations are controlled solely by the two biomass burning emission parameters (flux and particle size), while over downwind ocean regions CCN is controlled by a combination of biomass burning emissions and dry deposition (Figure 4.4). In July the biomass burning regime covers a large fraction of the boreal region in the PI, which reduces in extent in the PD. This change accounts for the majority of the spatial change in the biomass burning regime since the PI.

ii) **BVOCs (Figure 4.6).** In the PI the BVOC regime is located mainly above 30°N and in North America, with SH coverage located around the tip of South America. A BVOC regime does not occur in any investigated month, likely due to the intermittent transport of pollution from lower latitudes making remote regions appear mildly polluted on the monthly mean time scale used within the analysis.

iii) **DMS (Figure 4.7).** In January the DMS regime covers Antarctica and the majority of the Southern Ocean and SH sub-tropical gyre regions. In April the DMS regime is reduced in both time periods in the SH to cover Antarctica, but increases in the PD NH to cover Greenland and parts of high latitude continental Siberia and Yukon as well as the neighbouring seas

iv) **Sea spray (Figure 4.9).** In PI July the sea spray regime covers the majority of the Southern Ocean region. In the PD, with the exception of a small pure sea spray regime centred around 60°S, a small pervasive anthropogenic component is also present in the location of the sea spray regime.

v) **Volcanic emissions (Figure 4.11).** No single volcanic emission regime occurs in any month in either time period.

b) A seasonal change in geographical coverage can be seen in most natural emission regimes.

i) **Biomass burning.** The biomass burning regime reaches its maximum extent in the NH summertime in both the PI and the PD (~27–28% global coverage), when boreal fire emissions also peak (e.g., Giglio et al., 2010). Over Africa the biomass burning regime migrates from the NH to the SH from January to July. The seasonal pattern in regime occurrence over Africa is related to the dry season in each hemisphere which depends on the position of the inter-tropical convergence zone (ITCZ) position in NH wintertime and the interoceanic confluence in SH wintertime.

ii) **BVOC.** The PI BVOC regime covers ~11% of the globe in January, reducing by ~30% in April and not present in July. One possible reason for the seasonal pattern in regime occurrence running counter to the factors that control BVOC emissions, which are light availability, leaf area index and temperature (Guenther et al., 2012), is that wildfire emissions increasingly dominate aerosol behaviour in boreal regions towards summer when fire emissions peak (Figure 4.3).

iii) **DMS**. The DMS regime reaches its maximum extent in the SH summertime in both the PI and the PD (~19–20% global coverage) and encompasses the main SH subtropical ocean gyre regions as well as the Southern Ocean and Antarctica. In both time periods the DMS regime is reduced in size by April by ~75% and not present in July. The seasonal pattern of the DMS regime follows ocean biological activity and corresponding DMS sea water concentrations (Kettle and Andreae, 2000; Lana et al., 2011).

iv) **Sea spray**. Over SH oceans the pattern of the sea spray regime coverage runs counter to the prior DMS regime, in agreement with previous studies of the contribution of sea salt to total CCN number concentrations in the region (Korhonen et al., 2008; McCoy et al., 2015). Figure 4.10 showed that in SH summertime the sea spray regime is

characterised by the wind speeds reaching a threshold of 9 m s^{-1} in the South Pacific and 10 m s^{-1} in the remainder.

v) **Volcanic emissions**. Although there is no seasonality in volcanic emissions themselves, the only regimes containing a volcanic emission signal occur over marine regions in the PI NH summertime when the marine biological activity and hence DMS concentrations are low (Kettle and Andreae, 2000; Lana et al., 2011).

c) Anthropogenic emissions have increased over the industrial period and altered the way aerosol responds to natural emissions (Spracklen & Rap 2013). A reduction in the global extent of pure natural emission regimes in July from a PI maximum (40.7%) to a PD minimum (28.5%) suggests that the impact of anthropogenic suppression of natural emissions on aerosol currently peaks in the summer.

i) **Biomass burning.** Despite tropical fire activity increasing over the industrial period, the aerosol response to fire emissions has remained relatively similar. Overall, the geographical extent of each month's biomass burning regime is slightly larger in the PD than the PI due to increased anthropogenic activity, except in July in boreal regions where there is a reduction. However, the cause of the spatial change remains the same.

ii) **BVOC.** A BVOC regime does not occur in the PD in any investigated month, likely due to the intermittent transport of pollution from lower latitudes making remote regions appear mildly polluted on the monthly mean time scale used within the analysis.

iii) **DMS**. Each month's DMS regime slightly increases in geographical extent in the PD compared to the PI. In particular the PD DMS regime extends beyond that of the PI to cover Greenland and parts of high latitude continental Siberia and Yukon as well as the neighbouring seas. A suggested explanation for this is that continental anthropogenic emissions are supressing the BVOC regime, which covered these regions in the PI by providing particles to condense upon, thus allowing a marine DMS emission regime close to strong DMS emission sources to occur instead.

iv) **Sea spray**. While both this study and the recent study by McCoy et al. (2015) demonstrate that sea spray is the dominant emission controlling CCN number concentrations in July in the Southern Ocean region, a small pervasive anthropogenic component is also present over the majority of the region.

v) **DMS and sea spray**. The joint sea spray/DMS regime covers much of the SH in April in the PI, but in the PD it disappears leaving only the pure sea spray element of the regime situated across many major global wind flow regions where sea spray emissions peak. Both DMS sea water concentrations and wind speeds are matched in both time periods. Therefore the change in the pattern of DMS and sea spray regimes in April between PI and PD suggests that study into how anthropogenic emissions change aerosol sensitivity to DMS emissions could be observed in austral autumn in this region.

5) Emissions from two fire models were used in GLOMAP in Chapter 5 to investigate how recent advances in fire modelling (e.g., Hantson et al., 2016) changes the PI aerosol state, and hence the PI-to-PD radiative forcing.

a) Compared to the widely used AeroCom dataset (Dentener et al., 2006), global annual mean emissions of black carbon (BC) from fires increase 5.0-fold using the LMfire model and 3.2-fold using the SIMFIRE–BLAZE model, while emissions of particulate organic matter increase 7.1-fold using LMfire and 3.6-fold using SIMFIRE–BLAZE. The different representation of land cover and land use in each fire model results in the largest differences in emissions occurring at mid-latitudes (Figure 5.3).

b) When PI fire emissions from the two models were implemented in GLOMAP, PI global mean CCN number concentrations increased by a factor 1.6–2.7 relative to the widely used AeroCom dataset. This reduced the global mean PI-to-PD change in CCN number concentrations from 2.2-fold using AeroCom emissions to 2.0-fold using SIMFIRE–BLAZE emissions and 1.4-fold using LMfire emissions.

c) Figure 5.10 showed that incorporating fire model emissions brings GLOMAP into better agreement with the relative PI-to-PD changes in BC derived from limited northern hemisphere ice core records. The simulation incorporating LMfire emissions underestimates the change in BC over the industrial period, while the simulation incorporating SIMFIRE–BLAZE emissions slightly overestimates the change over the industrial period.

d) Compared to AeroCom, higher modelled PI aerosol concentrations from SIMFIRE–BLAZE and LMfire emissions cause a substantial reduction in the calculated global mean cloud albedo forcing of 40–88% and a reduction in the direct radiative forcing of 5–10%. For both fire modelling simulations, the majority of the reduction in the negative PI-to-PD RF occurs in the NH, while a positive PI-to-PD RF occurs in the SH between 30 to 60ºS. When

compared to the 28 sources of uncertainty in Chapters 3 and 4, PI fire emissions are by far the single largest source of uncertainty in PI CCN, and hence in our understanding of the magnitude of the historical radiative forcing due to anthropogenic aerosol emissions.

6.2 Research outlooks

6.2.1 Collaborations or projects utilising thesis results

The Biogenic versus Anthropogenic emissions on Clouds and Climate: towards a Holistic UnderStanding (BACCHUS) project http://www.bacchus-env.eu/ aims to quantify key processes and feedbacks controlling aerosol-cloud interactions (ACI) and investigate the importance of biogenic versus anthropogenic emissions for ACI. They have incorporated my Hamilton et al. (2014) results in order to define pristine aerosol regions and included results in their midterm summary for policymakers: http://www.bacchus-env.eu/public/Deliverables/BACCHUS_midterm_summary_policymakers.pdf.

The Global Aerosol Synthesis and Science Project (GASSP) http://gassp.org.uk/ has prioritised the collection of measurements in pristine aerosol environments as defined by Hamilton et al. (2014). Current work includes comparing the locations of aerosol observations with the maps in Figure 3.6 (C. Reddington 2016, University of Leeds, personal communication).

The Southern Ocean Clouds, Radiation, Aerosol, Transport Experimental Study (SOCRATES) http://www.atmos.washington.edu/socrates/SOCRATES_white_paper_Final_Sep29_2014.pdf is interested in understanding how clouds respond to marine emissions over the Southern Ocean. Results similar to those in Figures 3.13 and 3.14 were produced for the Southern Ocean region to help assist in understanding the parameters controlling CCN over the Southern Ocean (R. Wood 2015, University of Washington, personal communication).

Two work packages (3 and 6) within the Coordinated Research in Earth Systems and Climate: Experiments, kNowledge, Dissemination and Outreach (CRESCENDO) project http://crescendoproject.eu/ aim improve and evaluate natural aerosols and trace grasses in earth system models. Part of this will involve assess the ability of models to simulate the pristine (baseline) aerosol and chemistry state under conditions that represent as closely as possible the pre-industrial era. Results from Chapter 5 will also be extended under this project (K. Carslaw 2016, University of Leeds, personal communication).

Currently I am co-authoring review paper which aims to highlight what is currently known and where research opportunities exist about the flux and microphysical, chemical and radiative properties of aerosols in the pre-industrial atmosphere and the processes that control them.

6.2.2 Future work

Despite the importance of characterising the PI atmosphere, very few studies have investigated the uncertainty of natural emissions on PI aerosol properties and the impacts this uncertainty has on the historical radiative forcing. The impact of the uncertainty in PI volcanic emissions on historical radiative forcing was explored by Schmidt et al. (2012) and fires within this thesis. However many open questions still remain, including how advances in our understanding of land use and land cover change (e.g., Ellis et al., 2013 and Figure 5.2) impacts the temporal and spatial distributions of BVOC emissions, as well as how the recent discovery at CERN that nucleation can occur in the absence of sulphate (Kirkby et al., 2016) affects biogenic secondary organic aerosol concentrations the PI atmosphere.

It is common practice in modelling studies of past climate on long timescales to incorporate proxy climate data, particularly from ice cores, such as those within the Paleoclimate Modelling Inter-comparison Project (Braconnot et al., 2012). Studies of the PI atmosphere also have the potential to utilise ice core and other proxy data to help constrain the uncertainty in natural emissions when constructing PI emission datasets. For example, methane sulphonic acid (MSA) is a proxy for DMS emissions (e.g., Figure 1.5) and ice core records show concentrations were regionally up to a factor two higher in the PI (Beaudon et al., 2013; Legrand et al., 1997; Whung et al., 1994) Modelling suggests that changing DMS emissions by 50-100% would substantially alter regional aerosol concentrations and hence the radiative forcing (Carslaw et al., 2013; Korhonen et al., 2008; Woodhouse et al., 2013), but these changes are currently missing in global model datasets (e.g., Dentener et al., 2006; Lamarque et al., 2010).

Although this thesis has focused on aerosol and pre-cursor gas emissions the impacts of changing the PI fire landscape on greenhouse gas emissions, and any impacts these changes have on the magnitude of anthropogenic radiative fording over the industrial period, is another open question. This will partly be addressed in The Copernicus Atmosphere Monitoring Service (CAMS) 74 project https://atmosphere.copernicus.eu/ using updated greenhouse gas emissions I have calculated from the fire models used in Chapter 5.

How fires alter the oxidative capacity of the PI atmosphere was investigated by Murray et al. (2014). This study could be extended to investigate any impacts on the radiative forcing in a coupled chemistry version of GLOMAP, such as was used in Schmidt et al. (2012).

The Artic is currently warming at rate which is faster than the rest of the globe, with the reductions in anthropogenic aerosols due to European clean air acts being suggested to play a significant role (Acosta Navarro et al., 2016). What could be considered further is whether, at similar latitudes over the Holocene, aerosols from wildfire, land clearance and agriculture provided a similar cooling effect as those from the industry which subsequently replaced them. If so, then the Artic could be experiencing an aerosol, and hence RF, low that is unprecedented since the return of forested vegetation to higher latitude temperate and boreal regions after the last glacial maximum.

A limitation of the work presented in this thesis was that no feedbacks of natural emissions with the Earth system and climate could be evaluated due to the aerosol model not being coupled with the ocean, atmospheric chemistry or dynamics. There is therefore a large scope to continue the analysis presented here within Earth System Models. For example, how sensitive are the spatial and temporal distribution of pristine regions and natural emission regimes to feedbacks within the Earth system and climate? Which biogeochemical cycles are sensitive to changes in the PI aerosol state? As tropical precipitation patterns are sensitive to changes in the gradient in interhemispheric aerosol forcing (Allen et al., 2015; Ridley et al., 2015); how does the position and width of the inter tropical convergence zone respond to changes in PI emissions?

No future modelling projections were undertaken in this thesis. The impact of decreasing anthropogenic emissions due to air quality legislation will increase the natural fraction of aerosol in many regions. Furthermore, future changes to vegetation cover distributions and anthropogenic land use will alter both BVOC and fire emissions. The different impacts these changes will have on CCN number concentrations could alter results presented in both Chapters 3 and 4.

Bibliography

Achterberg, E. P., Moore, C. M., Henson, S. A., Steigenberger, S., Stohl, A., Eckhardt, S., Avendano, L. C., Cassidy, M., Hembury, D., Klar, J. K., Lucas, M. I., et al.: Natural iron ferlilisation by the Eyjafjallajokull volcanic eruption, Geophys. Res. Lett., 40, 921–926, doi:10.1002/grl.50221, 2013.

Ackerman, A., Toon, O., Stevens, D., Heymsfield, A., Ramanathan, V. and Welton, E.: Reduction of tropical cloudiness by soot, Science, 288(5468), 1042–7, 2000.

Acosta Navarro, J. C., Varma, V., Riipinen, I., Seland, Ø., Kirkevåg, A., Struthers, H., Iversen, T., Hansson, H.-C. and Ekman, A. M. L.: Amplification of Arctic warming by past air pollution reductions in Europe, Nat. Geosci., 9(4), 277–281, doi:10.1038/ngeo2673, 2016.

Albrecht, B. A.: Aerosols, Cloud Microphysics, and Fractional Cloudiness, Science (80-.)., 245, 1227–1230, doi:10.1126/science.245.4923.1227, 1989.

Allen, R. J., Evan, A. T. and Booth, B. B. B.: Interhemispheric aerosol radiative forcing and tropical precipitation shifts during the late Twentieth Century, J. Clim., 28(20), 8219–8246, doi:10.1175/JCLI-D-15-0148.1, 2015.

Andreae, M. O.: Aerosols before pollution, Science, 315(5808), 50–1, doi:10.1126/science.1136529, 2007.

Andreae, M. O. and Crutzen, P. J.: Atmospheric Aerosols: Biogeochemical Sources and Role in Atmospheric Chemistry, Science, 276(5315), 1052–1058, doi:10.1126/science.276.5315.1052, 1997.

Andreae, M. O., Jones, C. D. and Cox, P. M.: Strong present-day aerosol cooling implies a hot future., Nature, 435, 1187–90, doi:10.1038/nature03671, 2005.

Andreae, M. O. and Merlet, P.: Emissions of trace gases and aerosols from biomass burning, Global Biogeochem. Cycles, 15(4), 955–966, doi:10.1029/2000GB001382, 2001.

Andreae, M. O. and Rosenfeld, D.: Aerosol–cloud–precipitation interactions. Part 1. The nature and sources of cloud-active aerosols, Earth-Science Rev., 89(1–2), 13–41, doi:10.1016/j.earscirev.2008.03.001, 2008.

Andres, R. J. and Kasgnoc, A. D.: A time-averaged inventory of subaerial volcanic, J. Geophys. Res., 103(D19), 25,251-25,261, doi:doi:10.1029/98JD02091, 1998.

Archibald, S., Roy, D. P., van Wilgen, B. W. and Scholes, R. J.: What limits fire? An examination of drivers of burnt area in Southern Africa, Glob. Chang. Biol., 15(3), 613–630, doi:10.1111/j.1365-2486.2008.01754.x, 2009.

Arneth, A., Harrison, S. P., Zaehle, S., Tsigaridis, K., Menon, S., Bartlein, P. J., Feichter, J., Korhola, A., Kulmala, M., O'Donnell, D., Schurgers, G., et al.: Terrestrial biogeochemical feedbacks in the climate system, Nat. Geosci., 3, 525–532, doi:10.1038/ngeo905, 2010.

Arneth, A., Niinemets, U., Pressley, S., Back, J., Hari, P., Karl, T., Noe, S., Prentice, I. C., Serca, D., Hickler, T., Wolf, A., et al.: Process-based estimates of terrestrial ecosystem isoprene emissions: incorporating the effects of a direct CO2-isoprene interaction, Atmos. Chem. Phys., 7, 31–53, doi:10.5194/acpd-6-8011-2006, 2007.

Arnold, S. R., Chipperfield, M. P. and Blitz, M. a.: A three-dimensional model study of the effect of new temperature-dependent quantum yields for acetone photolysis, J. Geophys. Res., 110(D22), 1–14, doi:10.1029/2005JD005998, 2005.

Atkinson, R. and Arey, J.: Atmospheric degradation of volatile organic compounds., Chem. Rev., 103(12), 4605–38, doi:10.1021/cr0206420, 2003.

Atkinson, R., Baulch, D. L., Cox, R. A., Hampson, R. F., Kerr, J. A. and Troe, J.: Evaluated Kinetic and Photochemical Data for Atmospheric Chemistry: Supplement III, J. Phys. Chem. Ref. Data, 21, 881–1097, 1989.

Ayash, T., Gong, S. and Jia, C. Q.: Direct and Indirect Shortwave Radiative Effects of Sea Salt Aerosols, J. Clim., 21(13), 3207–3220, doi:10.1175/2007JCLI2063.1, 2008.

Ayers, G. P. and Gras, J. L.: Seasonal relationship between cloud condensation nuclei and aerosol methanesulphonate in marine air, Nature, 354, 834–835, doi:10.1038/353834a0, 1991.

Bates, T. S.: Preface to special section: First Aerosol Characterization Experiment (ACE 1) Part 2, J. Geophys. Res., 104(D17), 21,645-21,647, doi:doi:10.1029/1999JD900365, 1999.

Bates, T. S., Lamb, B. K., Guenther, A., Dignon, J. and Stoiber, R. E.: Sulfur Emissions to the Atmosphere from Natural Sources, J. Atmos. Chem., 14, 315–337, 1992.

Beaudon, E., Moore, J. C., Martma, T., Pohjola, V. A., Van De Wal, R. S. W., Kohler, J. and Isaksson, E.: Lomonosovfonna and holtedahlfonna ice cores reveal east-west disparities of the Spitsbergen environment since AD 1700, J. Glaciol.,

59(218), 1069–1083, doi:10.3189/2013JoG12J203, 2013.

Bellouin, N., Mann, G. W., Woodhouse, M. T., Johnson, C., Carslaw, K. S. and Dalvi, M.: Impact of the modal aerosol scheme GLOMAP-mode on aerosol forcing in the hadley centre global environmental model, Atmos. Chem. Phys., 13(6), 3027–3044, doi:10.5194/acp-13-3027-2013, 2013.

Berndt, T., Stratmann, F., Bräsel, S., Heintzenberg, J., Laaksonen, A. and Kulmala, M.: SO2 oxidation products other than H2SO4 as a trigger of new particle formation – Part 1: Laboratory investigations, Atmos. Chem. Phys. J1 - ACP, 8(21), 9761–9782, doi:10.5194/acp-8-6365-2008, 2008.

Beven, K.: A manifesto for the equifinality thesis, J. Hydrol., 320(1–2), 18–36, doi:10.1016/j.jhydrol.2005.07.007, 2006.

Bistinas, I., Oom, D., Sá, A. C. L., Harrison, S. P., Prentice, I. C. and Pereira, J. M. C.: Relationships between human population density and burned area at continental and global scales, PLoS One, 8(12), 1–12, doi:10.1371/journal.pone.0081188, 2013.

Blande, J. D., Turunen, K. and Holopainen, J. K.: Pine weevil feeding on Norway spruce bark has a stronger impact on needle VOC emissions than enhanced ultraviolet-B radiation., Environ. Pollut., 157(1), 174–180, 2009.

Bluth, G. J. S., Doiron, S. D., Schnetzler, C. C., Krueger, A. J. and Walter, L. S.: Global tracking of the SO2 clouds from the June, 1991 Mount Pinatubo eruptions, Geophys. Res. Lett., 19(2), 151–154, doi:10.1029/91GL02792, 1992.

Bond, T. C., Bhardwaj, E., Dong, R., Jogani, R., Jung, S., Roden, C., Streets, D. G. and Trautmann, N. M.: Historical emissions of black and organic carbon aerosol from energy-related combustion, 1850-2000, Global Biogeochem. Cycles, 21(2), 1–16, doi:10.1029/2006GB002840, 2007.

Bond, T. C., Doherty, S. J., Fahey, D. W., Forster, P. M., Berntsen, T., Deangelo, B. J., Flanner, M. G., Ghan, S., Kurcher, B., Koch, D., Kinne, S., et al.: Bounding the role of black carbon in the climate system: A scientific assessment, J. Geophys. Res. Atmos., 118(11), 5380–5552, doi:10.1002/jgrd.50171, 2013.

Bond, W. J.: What Limits Trees in C 4 Grasslands and Savannas?, Annu. Rev. Ecol. Evol. Syst., 39(1), 641–659, doi:10.1146/annurev.ecolsys.39.110707.173411, 2008.

Bonsang, B., Polle, C. and Lambert, G.: Evidence for marine production of isoprene, Geophys. Res. Lett., 19(11), 1129–1132, doi:10.1029/92GL00083, 1992.

Booth, B., Dunstone, N. J., Halloran, P. R., Andrews, T. and Bellouin, N.: Aerosols implicated as a prime driver of twentieth-century North Atlantic climate variability., Nature, 484(7393), 228–32, doi:10.1038/nature10946, 2012.

Boucher, O., Randall, D., Artaxo, P., Bretherton, C., Feingold, G., Forster, P., Kerminen, V.-M., Kondo, Y., Liao, H., Lohmann, U., Rasch, P., et al.: Clouds and Aerosols, in Climate Change 2013: The Physical Science Basis. Contribution of Working Group I to the Fifth Assessment Report of the Intergovernmental Panel on Climate Change, edited by T. F. Stocker, D. Qin, G.-K. Plattner, M. Tignor, S. K. Allen, J. Boschung, A. Nauels, Y. Xia, V. Bex, and P. M. Midgley, Cambridge University Press, Cambridge, United Kingdom and New York, NY, USA., 2013.

Boucher, O., Schwartz, S. E., Ackerman, T. P., Anderson, T. L., Bergstrom, B., Bonnel, B., Dahlback, A., Fouquart, Y., Chylek, P., Fu, Q., Halthore, R. N., et al.: Intercomparison of Models Representing Direct Shortwave Radiative Forcing by Sulfate Aerosols, J. Geophys. Res., 103(D14), 16,979-16,998, doi:10.1029/98JD00997, 1998.

Bower, K., Choularton, T., Latham, J., Sahraei, J. and Salter, S.: Computational assessment of a proposed technequie for global warming mitigation via albedo-enhancement of marine stratocumulus clouds, Atmos. Res., 82, 328–336, doi:10.1006/asle.2002.0048, 2006.

Bowman, D. M. J. S., Balch, J., Artaxo, P., Bond, W. J., Cochrane, M. a, D'Antonio, C. M., Defries, R., Johnston, F. H., Keeley, J. E., Krawchuk, M. a, Kull, C. a, et al.: The human dimension of fire regimes on Earth., J. Biogeogr., 38(12), 2223–2236, doi:10.1111/j.1365-2699.2011.02595.x, 2011.

Bowman, D. M. J. S., Balch, J. K., Artaxo, P., Bond, W. J., Carlson, J. M., Cochrane, M. a, D'Antonio, C. M., Defries, R. S., Doyle, J. C., Harrison, S. P., Johnston, F. H., et al.: Fire in the Earth system., Science, 324(5926), 481–4, doi:10.1126/science.1163886, 2009.

Braconnot, P., Harrison, S. P., Kageyama, M., Bartlein, P. J., Masson-Delmotte, V., Abe-Ouchi, A., Otto-Bliesner, B. and Zhao, Y.: Evaluation of climate models using palaeoclimatic data, Nat. Clim. Chang., 2(6), 417–424, doi:10.1038/nclimate1456, 2012.

Brévière, E. H. G., Bakker, D. C. E., Bange, H. W., Bates, T. S., Bell, T. G., Boyd, P. W., Duce, R. A., Garçon, V., Johnson, M. T., Law, C. S., Marandino, C. A., et al.: Surface ocean-lower atmosphere study: Scientific synthesis and contribution to Earth system science, Anthropocene, doi:10.1016/j.ancene.2015.11.001, 2015.

Brito, J., Rizzo, L. V., Morgan, W. T., Coe, H., Johnson, B., Haywood, J., Longo, K., Freitas, S., Andreae, M. O. and Artaxo, P.: Ground based aerosol characterization during the South American Biomass Burning Analysis (SAMBBA) field experiment, Atmos. Chem. Phys., 14, 12069–12083, doi:10.5194/acp-14-12069-2014, 2014.

Browse, J., Carslaw, K. S., Arnold, S. R., Pringle, K. and Boucher, O.: The scavenging processes controlling the seasonal cycle in Arctic sulphate and black carbon aerosol, Atmos. Chem. Phys., 12(15), 6775–6798, doi:10.5194/acp-12-6775-2012, 2012.

Burrows, S. M., Hoose, C., Poschl, U. and Lawrence, M. G.: Ice nuclei in marine air: Biogenic particles or dust?, Atmos. Chem. Phys., 13(1), 245–267, doi:10.5194/acp-13-245-2013, 2013.

Cachier, H. and Ducret, J.: Influence of biomass burning on equatorial African rains, Nature, 352(6332), 228–230, doi:10.1038/352228a0, 1991.

Capaldo, K., Corbett, J., Kasibhatla, P., Fischbeck, P. and Pandis, S. N.: Effects of ship emissions on sulphur cycling and radiative climate forcing over the ocean, Nature, 400, 743–746, 1999.

Carslaw, K. S., Boucher, O., Spracklen, D. V., Mann, G. W., Rae, J. G. L., Woodward, S. and Kulmala, M.: A review of natural aerosol interactions and feedbacks within the Earth system, Atmos. Chem. Phys., 10(4), 1701–1737, doi:10.5194/acp-10-1701-2010, 2010.

Carslaw, K. S., Lee, L. A., Reddington, C. L., Pringle, K. J., Rap, A., Forster, P. M., Mann, G. W., Spracklen, D. V., Woodhouse, M. T., Regayre, L. A. and Pierce, J. R. R.: Large contribution of natural aerosols to uncertainty in indirect forcing, Nature, 503(7474), 67–71, doi:10.1038/nature12674, 2013.

Charlson, R., Lovelock, J., Andreae, M. and Warren, S.: Oceanic phytoplankton, atmospheric sulphur, cloud albedo and climate, Nature, 326, 655–661, doi:doi:10.1038/326655a0, 1987.

Chi, X., Winderlich, J., Mayer, J.-C., Panov, a. V., Heimann, M., Birmili, W., Heintzenberg, J., Cheng, Y. and Andreae, M. O.: Long-term measurements of aerosol and carbon monoxide at the ZOTTO tall tower to characterize polluted and pristine air in the Siberian taiga, Atmos. Chem. Phys., 13(24), 12271–12298, doi:10.5194/acp-13-12271-2013, 2013.

Chipperfield, M. P.: New version of the TOMCAT/SLIMCAT off-line chemical transport model: Intercomparison of stratospheric tracer experiments, Q. J. R. Meteorol. Soc., 132(617), 1179–1203, doi:10.1256/qj.05.51, 2006.

Clarke, A. D., Collins, W. G., Rasch, P. J., Kapustin, V. N., Moore, K., Howell, S. and Fuelberg, H. E.: Dust and pollution transport on global scales: Aerosol measurements and model predictions, J. Geophys. Res., 106(D23), 32555, doi:10.1029/2000JD900842, 2001.

Clarke, A. and Kapustin, V.: Hemispheric aerosol vertical profiles: anthropogenic impacts on optical depth and cloud nuclei., Science, 329(5998), 1488–92, doi:10.1126/science.1188838, 2010.

Cochrane, M. A.: Fire science for rainforests., Nature, 421(6926), 913–919, doi:10.1038/nature01437, 2003.

Cofala, J., Amann, M. and Mechler, R.: Scenarios of world anthropogenic emissions of air pollutants and methane up to 2030., 2005.

Collins, W. J., Lamarque, J.-F., Schulz, M., Boucher, O., Eyring, V., Hegglin, M. I., Maycock, A., Myhre, G., Prather, M., Shindell, D. and Smith, S. J.: AerChemMIP: Quantifying the effects of chemistry and aerosols in CMIP6, Geosci. Model Dev. Discuss., (July), 1–28, doi:10.5194/gmd-2016-139, 2016.

Currin, C., Mitchell, T. J., Morris, M. D. and Ylvisaker, D.: Bayesian prediction of deterministic functions, with applications to the design and analysis of computer experiments, J. Am. Stat. Assoc., 86(416), 953–963, 1991.

Curson, A. R. J., Todd, J. D., Sullivan, M. J. and Johnston, A. W. B.: Catabolism of dimethylsulphoniopropionate: microorganisms, enzymes and genes, Nat. Rev. Microbiol., 9(12), 849–859, doi:10.1038/nrmicro2653, 2011.

von Danckelman, A.: Cloud conditions in South-West Africa, Meteorol. Zeitschrift, 18(3), 341–348, doi:10.1127/0941-2948/2009/355, 2009.

Dentener, F., Kinne, S., Bond, T., Boucher, O., Cofala, J., Generoso, S., Ginoux, P., Gong, S., Hoelzemann, J. J., Ito, A., Marelli, L., et al.: Emissions of primary aerosol and precursor gases in the years 2000 and 1750 prescribed data-sets for AeroCom, Atmos. Chem. Phys., 6, 4321–4344, 2006.

Duggen, S., Croot, P., Schacht, U. and Hoffmann, L.: Subduction zone volcanic ash can fertilize the surface ocean and stimulate phytoplankton growth: Evidence from biogeochemical experiments and satellite data, Geophys. Res. Lett., 34(1), L01612, doi:10.1029/2006GL027522, 2007.

Dunne, E. M., Mikkonen, S., Kokkola, H. and Korhonen, H.: A global process-based study of marine CCN trends and variability, Atmos. Chem. Phys., 14(11), 13631–13642, doi:10.5194/acp-14-13631-2014, 2014.

Dusek, U., Frank, G., Hildebrandt, L., Curtius, J., Schneider, J., Walter, S., Chand, D., Drewnick, F., Hings, S., Jung, D., Borrmann, S., et al.: Size matters more than chemistry for cloud-nucleating ability of aerosol particles., Science, 312(5778), 1375–8, doi:10.1126/science.1125261, 2006.

Edwards, J. and Slingo, A.: Studies with a flexible new radiation code. I: Choosing a configuration for a large scale model, Q. J. R. Meteorol. Soc., 122, 689–719, 1996.

Ellis, E. C.: Anthropogenic transformation of the terrestrial biosphere, Philos. Trans. R. Soc. A Math. Phys. Eng. Sci., 369, 1010–1035, doi:10.1098/rsta.2010.0331, 2011.

Ellis, E. C., Goldewijk, K. K., Siebert, S., Lightman, D. and Ramankutty, N.: Anthropogenic transformation of the biomes, 1700 to 2000, Glob. Ecol. Biogeogr., 19(5), 589–606, doi:10.1111/j.1466-8238.2010.00540.x, 2010.

Ellis, E. C., Kaplan, J. O., Fuller, D. Q., Vavrus, S., Klein Goldewijk, K. and Verburg, P. H.: Used planet: a global history., Proc. Natl. Acad. Sci. U. S. A., 110(20), 7978–85, doi:10.1073/pnas.1217241110, 2013.

Feng, Y., Ramanathan, V. and Kotamarthi, V. R.: Brown carbon: a significant atmospheric absorber of solar radiation?, Atmos. Chem. Phys. Discuss., 13(1), 2795–2833, doi:10.5194/acpd-13-2795-2013, 2013.

Ferretti, D. F., Miller, J. B., White, J. W. C., Etheridge, D. M., Lassey, K. R., Lowe, D. C., Macfarling Meure, C. M., Dreier, M. F., Trudinger, C. M., van Ommen, T. D. and Langenfelds, R. L.: Unexpected changes to the global methane budget over the past 2000 years., Science, 309(5741), 1714–7, doi:10.1126/science.1115193, 2005.

Fiebig, M., Hirdman, D., Lunder, C. R., Ogren, J. a., Solberg, S., Stohl, A. and Thompson, R. L.: Annual cycle of Antarctic baseline aerosol: controlled by photooxidation-limited aerosol formation, Atmos. Chem. Phys., 14(6), 3083–3093, doi:10.5194/acp-14-3083-2014, 2014.

Field, R., van der Werf, G. and Shen, S.: Human amplification of drought-induced biomass burning in Indonesia since 1960, Nat. Geosci., 2(3), 185–188, doi:10.1038/ngeo443, 2009.

Fiore, A. M., Naik, V., Spracklen, D. V, Steiner, A., Unger, N., Prather, M., Bergmann, D., Cameron-Smith, P. J., Cionni, I., Collins, W. J., Dalsøren, S., et al.: Global air quality and climate., Chem. Soc. Rev., 41(19), 6663–83, doi:10.1039/c2cs35095e, 2012.

Fitzgerald, J. W.: Marine Aerosols: A Review, Atmos. Environ., 25A(3/4), 533–545, 1991.

Forster, P., Ramaswamy, V., Artaxo, P., Berntsen, T., Betts, R., Fahey, D. W., Haywood, J., Lean, J., Lowe, D. C., Myhre, G., Nganga, J., et al.: Changes in Atmospheric Constituents and in Radiative Forcing., in Climate Change 2007: The Physical Science Basis. Contribution of Working Group I to the Fourth Assessment Report of the Intergovernmental Panel on Climate Change, edited by S. Solomon, M. M. D. Qin, Z. Chen, M. Marquis, K. B. Averyt, M.Tignor, and H. L. Miller, Cambridge University Press, Cambridge, United Kingdom and New York, NY, USA., 2007.

Fowler, D., Pilegaard, K., Sutton, M. a., Ambus, P., Raivonen, M., Duyzer, J., Simpson, D., Fagerli, H., Fuzzi, S., Schjoerring, J. K., Granier, C., et al.: Atmospheric composition change: Ecosystems–Atmosphere interactions, Atmos. Environ., 43(33), 5193–5267, doi:10.1016/j.atmosenv.2009.07.068, 2009.

Frogner, P., Reynir Gíslason, S. and Óskarsson, N.: Fertilizing potential of volcanic ash in ocean surface water, Geology, 29(6), 487–490, doi:10.1130/0091-7613(2001)029<0487:FPOVAI>2.0.CO;2, 2001.

Fuller, D. O. and Murphy, K.: The ENSO-fire dynamic in insular Southeast Asia, Clim. Change, 74(4), 435–455, doi:10.1007/s10584-006-0432-5, 2006.

Giglio, L., Randerson, J. T., Werf, G. R. Van Der, Kasibhatla, P. S., Collatz, G. J., Morton, D. C. and DeFries, R. S.: Assessing variability and long-term trends in burned area by merging multiple satellite fire products, Biogeochemistry, 7, 1171–1186, 2010.

Ginoux, P., Chin, M., Tegen, I., Prospero, J. M., Holben, B., Dubovik, O. and Lin, S.-J.: Sources and distributions of dust aerosols simulated with the GOCART model, J. Geophys. Res., 106(D17), 20,255-20,273, doi:10.1029/2000JD000053, 2001.

von Glasow, R.: A look at the CLAW hypothesis from an atmospheric chemistry point of view, Environ. Chem., 4(6), 379, doi:10.1071/EN07064, 2007.

von Glasow, R., Bobrowski, N. and Kern, C.: The effects of volcanic eruptions on atmospheric chemistry, Chem. Geol., 263(1–4), 131–142, doi:10.1016/j.chemgeo.2008.08.020, 2009.

von Glasow, R. and Crutzen, P. J.: Model study of multiphase DMS oxidation with a focus on halogens, Atmos. Chem. Phys., 4(3), 589–608, doi:10.5194/acp-4-589-2004, 2004.

Goldstein, A. H. and Galbally, I. E.: Known and unexplored organic constituents in the earth's atmosphere, Environ. Sci. Technol., 41(5), 1514–1521, doi:10.1021/es072476p, 2007.

Gondwe, M.: The contribution of ocean-leaving DMS to the global atmospheric burdens of DMS, MSA, SO 2 , and NSS SO 4 =, Global Biogeochem. Cycles, 17(2), 1056, doi:10.1029/2002GB001937, 2003.

Gong, S. L.: A parameterization of sea-salt aerosol source function for sub- and super-micron particles, Global Biogeochem. Cycles, 17(4), n/a-n/a, doi:10.1029/2003GB002079, 2003.

Graf, H.-F., Langmann, B. and Feichter, J.: The contribution of Earth degassing to the atmospheric sulfur budget, Chem. Geol., 147(1–2), 131–145, doi:10.1016/S0009-2541(97)00177-0, 1998.

Granier, C., Bessagnet, B., Bond, T., D'Angiola, A., van der Gon, H. D., Frost, G. J., Heil, A., Kaiser, J. W., Kinne, S., Klimont, Z., Kloster, S., et al.: Evolution of anthropogenic and biomass burning emissions of air pollutants at global and regional scales during the 1980-2010 period, Clim. Change, 109(1), 163–190, doi:10.1007/s10584-011-0154-1, 2011.

Grythe, H., Ström, J., Krejci, R., Quinn, P. and Stohl, A.: A review of sea-spray aerosol source functions using a large global set of sea salt aerosol concentration measurements, Atmos. Chem. Phys., 14(3), 1277–1297, doi:10.5194/acp-14-1277-2014, 2014.

Guenther, A.: The contribution of reactive carbon emissions from vegetation to the carbon balance of terrestrial ecosystems., Chemosphere, 49(8), 837–44, 2002.

Guenther, A. B., Jiang, X., Heald, C. L., Sakulyanontvittaya, T., Duhl, T., Emmons, L. K. and Wang, X.: The model of emissions of gases and aerosols from nature version 2.1 (MEGAN2.1): An extended and updated framework for modeling biogenic emissions, Geosci. Model Dev., 5(6), 1471–1492, doi:10.5194/gmd-5-1471-2012, 2012.

Guenther, A., Nicholas, C., Fall, R., Klinger, L., Mckay, W. A., Scholes, B., Steinbrecher, R., Tallamraju, R., Taylor, J. and Zimmerman, P.: A global model of natural volatile organic compound emissions, J. Geophys. Res., 100(D5), 8873–8892, 1995.

Guenther, A., Zimmerman, P., Harley, P., Monson, R. and Fall, R.: Isoprene and monoterpene emission rate variability: Model evaluations and sensitivity analyses, J. Geophys. Res., 98(D7), 12609, doi:10.1029/93JD00527, 1993.

Hakola, H., Hellén, H., Hemmilä, M., Rinne, J. and Kulmala, M.: In situ measurements of volatile organic compounds in a boreal forest, Atmos. Chem. Phys., 12(23), 11665–11678, doi:10.5194/acp-12-11665-2012, 2012.

Hallquist, M., Wenger, J. C., Baltensperger, U., Rudich, Y., Simpson, D., Claeys, M., Dommen, J., Donahue, N. M., George, C., Goldstein, A. H., Hamilton, F., et al.: The formation, properties and impact of secondary organic aerosol: current and emerging issues, Atmos. Chem. Phys., 9(November 2008), 5155–5236, 2009.

Hamilton, D. S.: Natural aerosols and climate : Understanding the unpolluted atmosphere to better understand the impacts of pollution, Weather, 70(9), 264–268, 2015.

Hamilton, D. S., Lee, L. A., Pringle, K. J., Reddington, C. L., Spracklen, D. V and Carslaw, K. S.: Occurrence of pristine aerosol environments on a polluted planet., Proc. Natl. Acad. Sci. U. S. A., 111(52), 18466–71, doi:10.1073/pnas.1415440111, 2014.

Hamme, R., Webley, P., Crawford, W., Whitney, F., DeGrandpre, M., Emerson, S., Eriksen, C., Giesbrecht, K., Gower, J., Kavanaugh, M., Peña, M., et al.: Volcanic ash fuels anomalous plankton bloom in subarctic northeast Pacific, Geophys. Res. Lett., 37(L19604), 1–5, doi:10.1029/2010GL044629, 2010.

Hantson, S., Arneth, A., Harrison, S. P., Kelley, D. I., Prentice, I. C., Rabin, S. S., Archibald, S., Mouillot, F., Arnold, S. R., Artaxo, P., Bachelet, D., et al.: The status and challenge of global fire modelling, Biogeosciences, 13, 3359–3375, doi:10.5194/bg-13-3359-2016, 2016.

Heald, C. L., Coe, H., Jimenez, J. L., Weber, R. J., Bahreini, R., Middlebrook, A. M., Russell, L. M., Jolleys, M., Fu, T.-M., Allan, J. D., Bower, K. N., et al.: Exploring the vertical profile of atmospheric organic aerosol: comparing 17 aircraft field campaigns with a global model, Atmos. Chem. Phys., 11(24), 12673–12696, doi:10.5194/acp-11-12673-2011, 2011.

Heald, C. L., Wilkinson, M. J., Monson, R. K., Alo, C. A., Wang, G. and Guenther, A.: Response of isoprene emission to ambient CO2 changes and implications for global budgets, Glob. Chang. Biol., 15(5), 1127–1140, doi:10.1111/j.1365-2486.2008.01802.x, 2009.

Hoffman, M. R. and Jacob, D. J.: Kinetics and mechanisms of the catalytic oxidation of dissolved sulphur dioxide in aqueous solution: An application to night-time fog water chemisty, SO2, NO and NO2 Oxidation, in Acid Precipitation series, Vol. 3, mechanisms, edited by J. G. Calvert, Butterworth Publications., 1984.

Hoose, C., Kristjánsson, J. E., Iversen, T., Kirkevåg, A., Seland and Gettelman, A.: Constraining cloud droplet number concentration in GCMs suppresses the aerosol indirect effect, Geophys. Res. Lett., 36(12), 1–5, doi:10.1029/2009GL038568, 2009.

Houweling, S., van der Werf, G. R., Goldewijk, K. K., Rockmann, T. and Aben, I.: Early anthropogenic CH4 emissions and the variation of CH4 and 13CH4 over the last millennium, Global Biogeochem. Cycles, 22(1), 1–9, doi:10.1029/2007GB002961, 2008.

Huebert, B., Vitousek, P., Sutton, J., Elias, T., Heath, J., Coeppicus, S., Howell, S. and Blomquist, B.: Volcano fixes nitrogen into plant-available forms, Biogeochemistry, 47(1), 111–118, doi:10.1007/BF00993099, 1999.

Jain, A. K., Murty, M. N. and Flynn, P. J.: Data Clustering : A Review, ACM Comput. Surv., 31(3), 265–323, 1999.

Jardine, K., Yañez Serrano, A., Arneth, A., Abrell, L., Jardine, A., Van Haren, J., Artaxo, P., Rizzo, L. V., Ishida, F. Y., Karl, T., Kesselmeier, J., et al.: Within-canopy sesquiterpene ozonolysis in Amazonia, J. Geophys. Res. Atmos., 116(19), 1–10, doi:10.1029/2011JD016243, 2011.

Jiao, C., Flanner, M. G., Balkanski, Y., Bauer, S. E., Bellouin, N., Berntsen, T. K., Bian, H., Carslaw, K. S., Chin, M., De Luca, N., Diehl, T., et al.: An aerocom assessment of black carbon in Arctic snow and sea ice, Atmos. Chem. Phys., 14(5), 2399–2417, doi:10.5194/acp-14-2399-2014, 2014.

Jickells, T. D., An, Z. S., Andersen, K. K., Baker, a R., Bergametti, G., Brooks, N., Cao, J. J., Boyd, P. W., Duce, R. a, Hunter, K. a, Kawahata, H., et al.: Global iron connections between desert dust, ocean biogeochemistry, and climate., Science, 308(5718), 67–71, doi:10.1126/science.1105959, 2005.

Johnson, D. W., Osborne, S., Wood, R., Suhre, K., Johnson, R., Businger, S., Quinn, P. K., Wiedensohler, A., Durkee, P. a., Russell, L. M., Andreae, M. O., et al.: An overview of the Lagrangian experiments undertaken during the North Atlantic regional Aerosol Characterisation Experiment (ACE-2), Tellus, Ser. B Chem. Phys. Meteorol., 52(2), 290–320, doi:10.1034/j.1600-0889.2000.00057.x, 2000.

Johnson, J. S., Cui, Z., Gosling, J. P., Blyth, A. M. and Carslaw, K. S.: Evaluating uncertainty in convective cloud microphysics using statistical emulation, J. Adv. Model. Earth Sytems, 7, 1–21, doi:10.1002/2014MS000314.Received, 2015.

Jolliffe, I. T. and Philipp, A.: Some recent developments in cluster analysis, Phys. Chem. Earth, Parts A/B/C, 35(9–12), 309–315, doi:10.1016/j.pce.2009.07.014, 2010.

Junge, C., Chagnon, C. and Manson, J.: Stratospheric aerosols, J. Meterology, 18, 81–108, 1961.

Kalkstein, L., Tan, G. and Skindlov, J.: An Evaluation of Three Clustering Procedures for Use in Synoptic Climatoloical Classification, J. Clim. Appl. Meterology, 26, 717–730, 1987.

Kaplan, J. O., Krumhardt, K. M., Ellis, E. C., Ruddiman, W. F., Lemmen, C. and Goldewijk, K. K.: Holocene carbon emissions as a result of anthropogenic land cover change, The Holocene, 21(5), 775–791, doi:10.1177/0959683610386983, 2011.

Kaufman, Y. J., Hobbs, P. V, Kirchhoff, V. W. J. H., Artaxo, P., Remer, L. A., Holben, B. N., King, M. D., Ward, D. E., Prins, E. M., Longo, K. M., Mattos, L. F., et al.: Smoke , Clouds , and Radiation-Brazil (SCAR-B) experiment, J. Geophys. Res., 103(D24), 31,783-31,808, 1998.

Kavouras, I. G., Mihalopoulos, N. and Stephanou, E. G.: Formation and gas/particle partitioning of monoterpenes photo-oxidation products over forests, Geophys. Res. Lett., 26(1), 55–58, doi:10.1029/1998GL900251, 1999.

Keene, W. C., Pszenny, A. P., Galloway, N. and Hawley, M. E.: Sea-Salt Corrections and Interpretation of Constituent Ratios in Marine Precipitation, J. Geophys. Res., 91(D6), 6647–6658, 1986.

Keskinen, H., Virtanen, A., Joutsensaari, J., Tsagkogeorgas, G., Duplissy, J., Schobesberger, S., Gysel, M., Riccobono, F., Slowik, J. G., Bianchi, F., Yli-Juuti, T., et al.: Evolution of particle composition in CLOUD nucleation experiments, Atmos. Chem. Phys., 13(11), 5587–5600, doi:10.5194/acp-13-5587-2013, 2013.

Kettle, A. and Andreae, M.: Flux of dimethylsulfide from the oceans: A comparison of updated data sets and flux models, J. Geophys. Res., 105(D22), 26,793-26,808, 2000.

Kirkby, J., Duplissy, J., Sengupta, K., Frege, C., Gordon, H., Williamson, C., Heinritzi, M., Simon, M., Yan, C., Almeida, J., Tröstl, J., et al.: Ion-induced nucleation of pure biogenic particles, Nature, 533(7604), 521–526, doi:10.1038/nature17953, 2016.

Klein Goldewijk, K., Beusen, A., Van Drecht, G. and De Vos, M.: The HYDE 3.1 spatially explicit database of human-induced global land-use change over the past 12,000 years, Glob. Ecol. Biogeogr., 20(1), 73–86, doi:10.1111/j.1466-8238.2010.00587.x, 2011.

Kloster, S., Six, K. D., Feichter, J., Maier-Reimer, E., Roeckner, E., Wetzel, P., Stier, P. and Esch, M.: Response of dimethylsulfide (DMS) in the ocean and atmosphere to global warming, J. Geophys. Res., 112(G3), G03005, doi:10.1029/2006JG000224, 2007.

Knorr, W., Kaminski, T., Arneth, A. and Weber, U.: Impact of human population density on fire frequency at the global scale, Biogeosciences, 11(4), 1085–1102, doi:10.5194/bg-11-1085-2014, 2014.

Koren, I., Dagan, G. and Altaratz, O.: From aerosol-limited to invigoration of warm convective clouds, Science (80-.)., 344(6188), 1143–1146, doi:10.1126/science.1252595, 2014.

Korhonen, H., Carslaw, K. S., Spracklen, D. V., Mann, G. W. and Woodhouse, M. T.: Influence of oceanic dimethyl sulfide emissions on cloud condensation nuclei concentrations and seasonality over the remote Southern Hemisphere oceans: A global model study, J. Geophys. Res., 113(D15), D15204, doi:10.1029/2007JD009718, 2008.

Kulmala, M., Hämeri, K., Aalto, P. P., Mäkelä, J. M., Pirjola, L., Douglas Nilsson, E., Buzorius, G., Rannik, Ü., Dal Maso, M., Seidl, W., Hoffman, T., et al.: Overview of the international project on biogenic aerosol formation in the boreal forest (BIOFOR), Tellus, Ser. B Chem. Phys. Meteorol., 53(4), 324–343, doi:10.1034/j.1600-0889.2001.530402.x, 2001.

Kulmala, M., Laakso, L., Lehtinen, K. E. J., Riipinen, I., Maso, M. D., Anttila, T., Kerminen, V.-M., Horrak, U., Vana, M. and Tammet, H.: Initial steps of aerosol growth, Atmos. Chem. Phys., 4, 2553–2560, 2004a.

Kulmala, M., Lehtinen, K. E. J. and Laaksonen, a.: Cluster activation theory as an explanation of the linear dependence between formation rate of 3nm particles and sulphuric acid concentration, Atmos. Chem. Phys., 6, 787–793, doi:10.5194/acp-6-787-2006, 2006.

Kulmala, M., Suni, T., Lehtinen, K. E. J., Dal Maso, M., Boy, M., Reissell, A., Rannik, Ü., Aalto, P., Keronen, P., Hakola, H., Bäck, J., et al.: A new feedback mechanism linking forests, aerosols, and climate, Atmos. Chem. Phys., 4(2), 557–562, doi:10.5194/acp-4-557-2004, 2004b.

Labonne, M., Bréon, F. M. and Chevallier, F.: Injection height of biomass burning aerosols as seen from a spaceborne lidar, Geophys. Res. Lett., 34(L11806), 1–5, doi:10.1029/2007GL029311, 2007.

Lamarque, J.-F., Bond, T. C., Eyring, V., Granier, C., Heil, A., Klimont, Z., Lee, D.,

Liousse, C., Mieville, A., Owen, B., Schultz, M. G., et al.: Historical (1850–2000) gridded anthropogenic and biomass burning emissions of reactive gases and aerosols: methodology and application, Atmos. Chem. Phys., 10(15), 7017–7039, doi:10.5194/acp-10-7017-2010, 2010.

Lana, A., Bell, T. G., Simó, R., Vallina, S. M., Ballabrera-Poy, J., Kettle, a. J., Dachs, J., Bopp, L., Saltzman, E. S., Stefels, J., Johnson, J. E., et al.: An updated climatology of surface dimethlysulfide concentrations and emission fluxes in the global ocean, Global Biogeochem. Cycles, 25(1), 1–17, doi:10.1029/2010GB003850, 2011.

Laothawornkitkul, J., Taylor, J. E., Paul, N. D. and Hewitt, C. N.: Biogenic volatile organic compounds in the Earth system., New Phytol., 183(1), 27–51, doi:10.1111/j.1469-8137.2009.02859.x, 2009.

Lee, L. A., Carslaw, K. S., Pringle, K. J. and Mann, G. W.: Mapping the uncertainty in global CCN using emulation, Atmos. Chem. Phys., 12(20), 9739–9751, doi:10.5194/acp-12-9739-2012, 2012.

Lee, L. A., Pringle, K. J., Reddington, C. L., Mann, G. W., Stier, P., Spracklen, D. V., Carslaw, K. S., Pierce, J. R. and Carslaw, K. S.: The magnitude and causes of uncertainty in global model simulations of cloud condensation nuclei, Atmos. Chem. Phys., 13(17), 8879–8914, doi:10.5194/acp-13-8879-2013, 2013.

Lee, L. A., Reddington, C. L. and Carslaw, K. S.: On the relationship between aerosol model uncertainty and radiative forcing uncertainty, Proc. Natl. Acad. Sci. U. S. A., 1–8, doi:10.1073/pnas.1507050113, 2016.

Leeuw, G. De, Andreas, E. L., Anguelova, M. D., Fairall, C. W., Ernie, R., Dowd, C. O., Schulz, M. and Schwartz, S. E.: Production Flux of Sea-Spray Aerosol, Rev. Geophys., 49(RG2001), 1–39, doi:10.1029/2010RG000349.1.INTRODUCTION, 2011.

Legrand, M., Hammer, C., De Angelis, M., Savarino, J., Delmas, R., Clausen, H. and Johnsen, S. J.: Sulfur-containing species (methanesulfonate and SO4) over the last climatic cycle in the Greenland Ice Core Project (central Greenland) ice core, J. Geophys. Res. Ocean., 102(C12), 26663–26679, doi:10.1029/97JC01436, 1997.

Lerdau, M.: A positive feedback with negative consequences, Science(Washington), 316, 212–213, 2007.

Li, F., Zeng, X. D. and Levis, S.: A process-based fire parameterization of intermediate complexity in a dynamic global vegetation model, Biogeosciences, 9(7), 2761–2780, doi:10.5194/bg-9-2761-2012, 2012.

Lin, C. T., Baker, A. R., Jickells, T. D., Kelly, S. and Lesworth, T.: An assessment of the significance of sulphate sources over the Atlantic Ocean based on sulphur isotope data, Atmos. Environ., 62, 615–621, doi:10.1016/j.atmosenv.2012.08.052, 2012.

Lovejoy, E. R., Hanson, D. R. and Huey, L. G.: Kinetics and Products of the Gas-Phase Reaction of SO 3 with Water, J. Phys. Chem., 100(51), 19911–19916, doi:10.1021/jp962414d, 1996.

Mahajan, A. S., Fadnavis, S., Thomas, M. A., Pozzoli, L., Gupta, S., Royer, S. J., Saiz-Lopez, A. and Simó, R.: Quantifying the impacts of an updated global dimethyl sulfide climatology on cloud microphysics and aerosol radiative forcing, J. Geophys. Res. D Atmos., 120(6), 2524–2536, doi:10.1002/2014JD022687, 2015.

Mahowald, N.: Aerosol indirect effect on biogeochemical cycles and climate., Science, 334(6057), 794–6, doi:10.1126/science.1207374, 2011.

Mahowald, N., Albani, S., Kok, J. F., Engelstaeder, S., Scanza, R., Ward, D. S. and Flanner, M. G.: The size distribution of desert dust aerosols and its impact on the Earth system, Aeolian Res., doi:10.1016/j.aeolia.2013.09.002, 2013.

Mahowald, N., Ward, D. S., Kloster, S., Flanner, M. G., Heald, C. L., Heavens, N. G., Hess, P. G., Lamarque, J.-F. J.-F. and Chuang, P. Y.: Aerosol impacts on climate and biogeochemistry, Annu. Rev. Environ. Resour., 36(1), 45–74, doi:10.1146/annurev-environ-042009-094507, 2011.

Manktelow, P. T., Carslaw, K. S., Mann, G. W. and Spracklen, D. V.: The impact of dust on sulfate aerosol, CN and CCN during an East Asian dust storm, Atmos. Chem. Phys., 10(2), 365–382, doi:10.5194/acp-10-365-2010, 2010.

Mann, G. W., Carslaw, K. S., Reddington, C. L., Pringle, K. J., Schulz, M., Asmi, A., Spracklen, D. V., Ridley, D. a., Woodhouse, M. T., Lee, L. a., Zhang, K., et al.: Intercomparison and evaluation of global aerosol microphysical properties among AeroCom models of a range of complexity, Atmos. Chem. Phys., 14(9), 4679–4713, doi:10.5194/acp-14-4679-2014, 2014.

Mann, G. W., Carslaw, K. S., Ridley, D. A., Spracklen, D. V., Pringle, K. J., Merikanto, J., Korhonen, H., Schwarz, J. P., Lee, L. a., Manktelow, P. T., Woodhouse, M. T., et al.: Intercomparison of modal and sectional aerosol microphysics representations within the same 3-D global chemical transport model, Atmos. Chem. Phys., 12(1), 4449–4476, doi:10.5194/acpd-12-623-2012, 2012.

Mann, G. W., Carslaw, K. S., Spracklen, D. V., Ridley, D. A., Manktelow, P. T., Chipperfield, M. P., Pickering, S. J. and Johnson, C. E.: Description and evaluation

of GLOMAP-mode: a modal global aerosol microphysics model for the UKCA composition-climate model, Geosci. Model Dev., 3(2), 519–551, doi:10.5194/gmd-3-519-2010, 2010.

Marandino, C. A., Tegtmeier, S., Kruger, K., Zindler, C., Atlas, E. L., Moore, F. and Bange, H. W.: Dimethylsulphide (DMS) emissions from the western Pacific Ocean: A potential marine source for stratospheric sulphur?, Atmos. Chem. Phys., 13(16), 8427–8437, doi:10.5194/acp-13-8427-2013, 2013.

Marlon, J. R., Bartlein, P. J., Carcaillet, C., Gavin, D. G., Harrison, S. P., Higuera, P. E., Joos, F., Power, M. J. and Prentice, I. C.: Climate and human influences on global biomass burning over the past two millennia, Nat. Geosci., 1(10), 697–702, doi:10.1038/ngeo313, 2008.

Marlon, J. R., Kelly, R., Daniau, A.-L., Vannière, B., Power, M. J., Bartlein, P., Higuera, P., Blarquez, O., Brewer, S., Brücher, T., Feurdean, A., et al.: Reconstructions of biomass burning from sediment charcoal records to improve data-model comparisons, Biogeosciences, 13(22), 3225–3244, doi:10.5194/bg-13-3225-2016, 2016.

Martin, S. T., Andreae, M. O., Althausen, D., Artaxo, P., Baars, H., Borrmann, S., Chen, Q., Farmer, D. K., Guenther, a., Gunthe, S. S., Jimenez, J. L., et al.: An overview of the Amazonian Aerosol Characterization Experiment 2008 (AMAZE-08), Atmos. Chem. Phys., 10(23), 11415–11438, doi:10.5194/acp-10-11415-2010, 2010.

McConnell, J. R., Edwards, R., Kok, G. L., Flanner, M. G., Zender, C. S., Saltzman, E. S., Banta, J. R., Pasteris, D. R., Carter, M. M. and Kahl, J. D. W.: 20th-century industrial black carbon emissions altered Arctic climate forcing., Science, 317(5843), 1381–4, doi:10.1126/science.1144856, 2007.

McCoy, D. T., Burrows, S. M., Wood, R., Grosvenor, D. P., Elliott, S. M., Ma, P.-L., Rasch, P. J. and Hartmann, D. L.: Natural aerosols explain seasonal and spatial patterns of Southern Ocean cloud albedo, Sci. Adv., 1(6), 1–12, doi:10.1126/sciadv.1500157, 2015.

McFiggans, G., Artaxo, P., Baltensperger, U., Coe, H., Facchini, M. C., Feingold, G., Fuzzi, S., Gysel, M., Laaksonen, A., Lohmann, U., Mentel, T. F., et al.: The effect of physical and chemical aerosol properties on warm cloud droplet activation, Atmos. Chem. Phys., 6, 2593–2649, 2006.

McNeal, R. J., Mugler, J. P., Harriss, R. C. and Hoell, J. M.: NASA global tropospheric experiment, Eos, Trans. Am. Geophys. Union, 64(38), 561–562,

doi:10.1029/EO064i038p00561-01, 1983.

Mechoso, C. R., Wood, R., Weller, R., Bretherton, C. S., Clarke, A. D., Coe, H., Fairall, C., Farrar, J. T., Feingold, G., Garreaud, R., Grados, C., et al.: Ocean–Cloud–Atmosphere–Land Interactions in the Southeastern Pacific: The VOCALS Program, Bull. Am. Meteorol. Soc., 95(3), 357–375, doi:10.1175/BAMS-D-11-00246.1, 2014.

Mercado, L. M., Bellouin, N., Sitch, S., Boucher, O., Huntingford, C., Wild, M. and Cox, P.: Impact of changes in diffuse radiation on the global land carbon sink., Nature, 458(7241), 1014–7, doi:10.1038/nature07949, 2009.

Merikanto, J., Spracklen, D. V, Mann, G. W., Pickering, S. J. and Carslaw, K. S.: Impact of nucleation on global CCN, Atmos. Chem. Phys., 9, 8601–8616, 2009.

Metzger, A., Verheggen, B., Dommen, J., Duplissy, J., Prevot, A. S. H., Weingartner, E., Riipinen, I., Kulmala, M., Spracklen, D. V., Carslaw, K. S. and Baltensperger, U.: Evidence for the role of organics in aerosol particle formation under atmospheric conditions, Proc. Natl. Acad. Sci., 107(15), 6646–6651, doi:10.1073/pnas.0911330107, 2010.

Muhlbauer, A., McCoy, I. L. and Wood, R.: Climatology of stratocumulus cloud morphologies: microphysical properties and radiative effects, Atmos. Chem. Phys., 14(13), 6695–6716, doi:10.5194/acp-14-6695-2014, 2014.

Murphy, D. M., Anderson, J. R., Quinn, P. K., McInnes, L. M., Brechtel, F. J., Kreidenweis, S. M., Middlebrook, A. M., Posfai, M., Thomson, D. S. and Buseck, P. R.: Influence of sea-salt on aerosol radiative properties in the Southern Ocean marine boundary layer, Nature, 392, 62–65, 1998.

Murray, L. T., Mickley, L. J., Kaplan, J. O., Sofen, E. D., Pfeiffer, M. and Alexander, B.: Factors controlling variability in the oxidative capacity of the troposphere since the Last Glacial Maximum, Atmos. Chem. Phys., 14(7), 3589–3622, doi:10.5194/acp-14-3589-2014, 2014.

Myhre, G., Shindell, D., Breon, F.-M., Collins, W., Fuglestvedt, J., Huang, J., Koch, D., Lamarque, J.-F., Lee, D., Mendoza, B., Nakajima, T., et al.: Anthropogenic and Natural Radiative Forcing, in Anthropogenic and Natural Radiative Forcing. In: Climate Change 2013: The Physical Science Basis. Contribution of Working Group I to the Fifth Assessment Report of the Intergovernmental Panel on Climate Change, edited by T. F. Stocker, D. Qin, G.-K. Plattner, M. Tignor, S. K. Allen, J. Boschung, A. Nauels, Y. Xia, V. Bex, and P. M. Midgley, pp. 659–740, Cambridge University Press, Cambridge, United Kingdom and New York, NY, USA., 2013.

Nepstad, D., Lefebvre, P., Lopes da Silva, U., Tomasella, J., Schlesinger, P., Solorzano, L., Moutinho, P., Ray, D. and Guerreira Benito, J.: Amazon drought and its implications for forest flammability and tree growth: a basin-wide analysis, Glob. Chang. Biol., 10(5), 704–717, doi:10.1111/j.1529-8817.2003.00772.x, 2004.

Nightingale, P. D., Liss, P. S. and Schlosser, P.: Measurements of air-sea gas transfer during an open ocean algal bloom, Geophys. Res. Lett., 27(14), 2117–2120, doi:10.1029/2000GL011541, 2000.

O'Dowd, C., Ceburnis, D., Ovadnevaite, J., Vaishya, A., Rinaldi, M. and Facchini, M. C.: Do anthropogenic, continental or coastal aerosol sources impact on a marine aerosol signature at Mace Head?, Atmos. Chem. Phys., 14(19), 10687–10704, doi:10.5194/acp-14-10687-2014, 2014.

O'Dowd, C. D., Facchini, M. C., Cavalli, F., Ceburnis, D., Mircea, M., Decesari, S., Fuzzi, S., Yoon, Y. J. and Putaud, J.: Biogenically driven organic contribution to marine aerosol, Nature, 431, 676–680, doi:10.1038/nature02970.1., 2004.

Okin, G. S., Bullard, J. E., Reynolds, R. L., Ballantine, J. A. C., Schepanski, K., Todd, M. C., Belnap, J., Baddock, M. C., Gill, T. E. and Miller, M. E.: Dust : Small-Scale Processes With Global Consequences, Eos (Washington. DC)., 92(29), 241–248, 2011.

Olgun, N., Duggen, S., Croot, P. L., Delmelle, P., Dietze, H., Schacht, U., Óskarsson, N., Siebe, C., Auer, A. and Garbe-Schönberg, D.: Surface ocean iron fertilization: The role of airborne volcanic ash from subduction zone and hot spot volcanoes and related iron fluxes into the Pacific Ocean, Global Biogeochem. Cycles, 25(GB4001), 1–15, doi:10.1029/2009GB003761, 2011.

Ovadnevaite, J., Manders, a., De Leeuw, G., Ceburnis, D., Monahan, C., Partanen, a. I., Korhonen, H. and O'Dowd, C. D.: A sea spray aerosol flux parameterization encapsulating wave state, Atmos. Chem. Phys., 14(4), 1837–1852, doi:10.5194/acp-14-1837-2014, 2014.

Pacifico, F., Folberth, G. a., Sitch, S., Haywood, J. M., Artaxo, P. and Rizzo, L. V.: Biomass burning related ozone damage on vegetation over the Amazon forest, Atmos. Chem. Phys., 15, 2791–2804, doi:10.5194/acp-15-2791-2015, 2015.

Pechony, O. and Shindell, D. T.: Driving forces of global wildfires over the past millennium and the forthcoming century, Proc. Natl. Acad. Sci., 107(45), 19167–19170, doi:10.1073/pnas.1003669107, 2010.

Penner, J.E. and Andreae, M. and Annegarn, H. and Barrie, L. and Feichter, J. and Hegg, D. and Jayaraman, A. and Leaitsch, R. and Murphy, D. and Nganga, J. and

Pitari, G.: Aerosols, their Direct and Indirect Effects, Clim. Chang. 2001 Sci. c Basis. Contrib. Work. Gr. I to Third Assess. Rep. Intergov. Panel Clim. Chang. [Houghton, J.T., al. (eds.)]., 289– 348, 2001.

Penner, J. E., Dickinson, R. E. and O´Neill, C. A.: Effects of Aerosols from biomass burning on the Global Radiation Budget., Science, 256(5062), 1432–1433, 1992.

Penner, J. E., Zhou, C. and Xu, L.: Consistent estimates from satellites and models for the first aerosol indirect forcing, Geophys. Res. Lett., 39(L13810), 1–5, doi:10.1029/2012GL051870, 2012.

Penner, J., Xu, L. and Wang, M.: Satellite methods underestimate indirect climate forcing by aerosols., Proc. Natl. Acad. Sci. U. S. A., 108(33), 13404–8, doi:10.1073/pnas.1018526108, 2011.

Peñuelas, J., Filella, I., Stefanescu, C. and Llusià, J.: Caterpillars of Euphydryas aurinia (Lepidoptera: Nymphalidae) feeding on Succisa pratensis leaves induce large foliar emissions of methanol., New Phytol., 167(3), 851–7, doi:10.1111/j.1469-8137.2005.01459.x, 2005.

Peñuelas, J. and Llusià, J.: BVOCs: plant defense against climate warming?, Trends Plant Sci., 8(3), 105–9, doi:10.1016/S1360-1385(03)00008-6, 2003.

Peñuelas, J. and Staudt, M.: BVOCs and global change., Trends Plant Sci., 15(3), 133–44, doi:10.1016/j.tplants.2009.12.005, 2010.

Petters, M. D. and Kreidenweis, S. M.: A single parameter representation of hygroscopic growth and cloud condensation nucleus activity, Atmos. Chem. Phys., 7(8), 1961–1971, doi:10.5194/acp-7-1961-2007, 2007.

Pfeiffer, M., Spessa, A. and Kaplan, J. O.: A model for global biomass burning in preindustrial time: LPJ-LMfire (v1.0), Geosci. Model Dev., 6(3), 643–685, doi:10.5194/gmd-6-643-2013, 2013.

Pham, M., Müller, J.-F., Brasseur, G. P., Granier, C. and Megie, G.: A three-dimensional study of the tropospheric sulfur cycle, J. Geophys. Res., 100(D12), 26061–26092, doi:10.1029/95JD02095, 1995.

Pierce, J. R., Leaitch, W. R., Liggio, J., Westervelt, D. M., Wainwright, C. D., Abbatt, J. P. D., Ahlm, L., Al-Basheer, W., Cziczo, D. J., Hayden, K. L., Lee, a. K. Y., et al.: Nucleation and condensational growth to CCN sizes during a sustained pristine biogenic SOA event in a forested mountain valley, Atmos. Chem. Phys., 12(7), 3147–3163, doi:10.5194/acp-12-3147-2012, 2012.

Pollack, J., Toon, O., Danielsen, E., Hofmann, D. and Rosen, J.: The El Chichon

volcanic cloud: an introduction, Geophys. Res. Lett., 10, 989–992, 1983.

Pongratz, J., Reick, C., Raddatz, T. and Claussen, M.: A reconstruction of global agricultural areas and land cover for the last millennium, Global Biogeochem. Cycles, 22(3), doi:10.1029/2007GB003153, 2008.

Pöschl, U., Martin, S. T., Sinha, B., Chen, Q., Gunthe, S. S., Huffman, J. a, Borrmann, S., Farmer, D. K., Garland, R. M., Helas, G., Jimenez, J. L., et al.: Rainforest aerosols as biogenic nuclei of clouds and precipitation in the Amazon., Science, 329(5998), 1513–6, doi:10.1126/science.1191056, 2010.

Prather, K. A., Bertram, T. H., Grassian, V. H., Deane, G. B., Stokes, M. D., Demott, P. J., Aluwihare, L. I., Palenik, B. P., Azam, F., Seinfeld, J. H., Moffet, R. C., et al.: Bringing the ocean into the laboratory to probe the chemical complexity of sea spray aerosol., Proc. Natl. Acad. Sci. U. S. A., 110(19), 7550–5, doi:10.1073/pnas.1300262110, 2013.

Prestel, M. A. F.: Meteorologische Untersuchungen betreffend die Verbreitung des Moorrauchs in den Tagen von 20. bis 26. Mai 1860, die isobarometrischen Linien am 22. Mai und die Gewitter am 20. und 26. Mai 1860, Hahn., 1861.

Pringle, K. J., Carslaw, K. S., Fan, T., Mann, G. W., Hill, A., Stier, P., Zhang, K. and Tost, H.: A multi-model assessment of the impact of sea spray geoengineering on cloud droplet number, Atmos. Chem. Phys., 12(23), 11647–11663, doi:10.5194/acp-12-11647-2012, 2012.

Pringle, K. J., Carslaw, K. S., Spracklen, D. V., Mann, G. M. and Chipperfield, M. P.: The relationship between aerosol and cloud drop number concentrations in a global aerosol microphysics model, Atmos. Chem. Phys., 9, 4131–4144, 2009.

Quinn, P. K. and Bates, T. S.: The case against climate regulation via oceanic phytoplankton sulphur emissions., Nature, 480(7375), 51–6, doi:10.1038/nature10580, 2011.

Quinn, P. K., Bates, T. S., Baum, E., Doubleday, N., Fiore, a. M., Flanner, M., Fridlind, A., Garrett, T. J., Koch, D., Menon, S., Shindell, D., et al.: Short-lived pollutants in the Arctic: their climate impact and possible mitigation strategies, Atmos. Chem. Phys., 8(6), 1723–1735, doi:10.5194/acp-8-1723-2008, 2008.

Raes, F., Dingenen, R. Van, Vignati, E., Wilson, J., Putaud, J.-P., Seinfeld, J. H. and Adams, P.: Formation and cycling of aerosols in the global troposphere, Atmos. Environ., 34(25), 4215–4240, doi:10.1016/S1352-2310(00)00239-9, 2000.

Rap, A., Scott, C. E., Spracklen, D. V., Bellouin, N., Forster, P. M., Carslaw, K. S.,

Schmidt, A. and Mann, G.: Natural aerosol direct and indirect radiative effects, Geophys. Res. Lett., 40(12), 3297–3301, doi:10.1002/grl.50441, 2013.

Rap, A., Spracklen, D. V, Mercado, L., Reddington, C. L., Haywood, J. M., Ellis, R. J., Phillips, O. L., Artaxo, P., Bonal, D., Coupe, N. R. and Butt, N.: Fires increase Amazon forest productivity through increases in diffuse radiation, Geophys. Res. Lett., 1–9, doi:10.1002/2015GL063719.Received, 2015.

Read, K. A., Lewis, A. C., Bauguitte, S., Rankin, A. M., Salmon, R. A., Wolff, E. W., Saiz-Lopez, A., Bloss, W. J., Heard, D. E., Lee, J. D. and Plane, J. M. C.: DMS and MSA measurements in the Antarctic boundary layer: impact of BrO on MSA production, Atmos. Chem. Phys., 8(1), 2985–2997, doi:10.5194/acp-8-2985-2008, 2008.

Reade, L., Jennings, S. G. and McSweeney, G.: Cloud condensation nuclei measurements at Mace Head, Ireland, over the period 1994–2002, Atmos. Res., 82, 610–621, doi:10.1016/j.atmosres.2006.02.017, 2006.

Reddington, C. L., Butt, E. W., Ridley, D. A., Artaxo, P., Morgan, W. T., Coe, H. and Spracklen, D. V: Air quality and human health improvements from reductions in deforestation-related fire in Brazil, Nat. Geosci., 8, 768–771, doi:10.1038/NGEO2535, 2015.

Reddington, C. L., Yoshioka, M., Balasubramanian, R., Ridley, D., Toh, Y. Y., Arnold, S. R. and Spracklen, D. V: Contribution of vegetation and peat fires to particulate air pollution in Southeast Asia, Environ. Res. Lett., 9(9), 94006, doi:10.1088/1748-9326/9/9/094006, 2014.

Regayre, L. A., Pringle, K. J., Booth, B. B. B., Lee, L. A., Mann, G. W., Browse, J., Woodhouse, M. T., Rap, A., Reddington, C. L. and Carslaw, K. S.: Uncertainty in the magnitude of aerosol-cloud radiative forcing over recent decades, Geophys. Res. Lett., 41, 1–10, doi:10.1002/2014GL062029.Received, 2014.

Regayre, L. A., Pringle, K. J., Lee, L. A., Rap, A., Browse, J., Mann, G. W., Reddington, C. L., Carslaw, K. S., Booth, B. B. B. and Woodhouse, M. T.: The Climatic Importance of Uncertainties in Regional Aerosol–Cloud Radiative Forcings over Recent Decades, J. Clim., 28(17), 6589–6607, doi:10.1175/JCLI-D-15-0127.1, 2015.

Riccobono, F., Schobesberger, S., Scott, C. E., Dommen, J., Ortega, I. K., Rondo, L., Almeida, J., Amorim, A., Bianchi, F., Breitenlechner, M., David, A., et al.: Oxidation products of biogenic emissions contribute to nucleation of atmospheric particles., Science, 344(6185), 717–21, doi:10.1126/science.1243527, 2014.

Ridley, H. E., Asmerom, Y., Baldini, J. U. L., Breitenbach, S. F. M., Aquino, V. V., Prufer, K. M., Culleton, B. J., Polyak, V., Lechleitner, F. a., Kennett, D. J., Zhang, M., et al.: Aerosol forcing of the position of the intertropical convergence zone since ad 1550, Nat. Geosci., 8(February), 195–200, doi:10.1038/ngeo2353, 2015.

Robock, A.: The Mount St. Helens volcanic eruption of 18 May 1980: minimal climatic effect, Science (80-.)., 212, 1383–1384, 1981.

Robock, A.: Volcanic eruptions and climate, Rev. Geophys., 38(2000), 191–219, 2000.

Roesler, E. L. and Penner, J. E.: Can global models ignore the chemical composition of aerosols?, Geophys. Res. Lett., 37(24), 1–5, doi:10.1029/2010GL044282, 2010.

Rose, V. I., Chnan, R. L., Giggenbach, W. F., Kyle, P. R. and Symonds, R. B.: Rates of sulfur dioxide and particle emissions from White Island volcano, New Zealand, and an estimate of the total flux of major gaseous species, Bull. Volcanol., 48, 181–188, 1986.

Rosenfeld, D.: TRMM observed first direct evidence of smoke from forest fires inhibiting rainfall, Geophys. Res. Lett., 26(20), 3105–3108, doi:10.1029/1999GL006066, 1999.

Rosenfeld, D., Sherwood, S., Wood, R. and Donner, L.: Atmospheric science. Climate effects of aerosol-cloud interactions., Science, 343(6169), 379–80, doi:10.1126/science.1247490, 2014.

Rossow, W. B. and Schiffer, R. A.: International Satellite Cloud Climatology Project (ISCCP) cloud data projects, , 72(1), 2–20, 1991.

Rossow, W. B. and Schiffer, R. A.: Advances in Understanding Clouds from ISCCP, Bull. Am. Meteorol. Soc., 80(11), 2261–2287, doi:10.1175/1520-0477(1999)080<2261:AIUCFI>2.0.CO;2, 1999.

Satheesh, S. and Krishnamoorthy, K.: Radiative effects of natural aerosols: A review, Atmos. Environ., 39(11), 2089–2110, doi:10.1016/j.atmosenv.2004.12.029, 2005.

Savoie, D. L., Prospero, J. M., Merrill, J. T. and Uematsu, M.: Nitrate in the atmospheric boundary layer of the tropical South Pacific: Implications regarding sources and transport, J. Atmos. Chem., 8, 391–415, 1989.

Schmidt, A., Carslaw, K. S., Mann, G. W., Rap, A., Pringle, K. J., Spracklen, D. V., Wilson, M. and Forster, P. M.: Importance of tropospheric volcanic aerosol for

indirect radiative forcing of climate, Atmos. Chem. Phys., 12(16), 7321–7339, doi:10.5194/acp-12-7321-2012, 2012.

Schmidt, A., Carslaw, K. S., Mann, G. W., Wilson, M., Breider, T. J., Pickering, S. J. and Thordarson, T.: The impact of the 1783–1784 AD Laki eruption on global aerosol formation processes and cloud condensation nuclei, Atmos. Chem. Phys., 10(13), 6025–6041, doi:10.5194/acp-10-6025-2010, 2010.

Schulz, M., Textor, C., Kinne, S., Balkanski, Y., Bauer, S., Berntsen, T., Berglen, T., Boucher, O., Dentener, F., Guibert, S., Isaksen, I. S. a., et al.: Radiative forcing by aerosols as derived from the AeroCom present-day and pre-industrial simulations, Atmos. Chem. Phys., 6, 5225–5246, doi:10.5194/acpd-6-5095-2006, 2006.

Schwartz, S. E.: The whitehouse effect- short wave radiative forcing of climate by anthrop ogenic aerosols: an overview, J. Aerosol Sci., 27(3), 359–382, doi:10.1016/0021-8502(95)00533-1, 1996.

Sciare, J., Mihalopoulos, N. and Dentener, F. J.: Interannual variability of atmospheric dimethylsulfide in the southern Indian Ocean, J. Geophys. Res., 105(D21), 26369–26377, doi:10.1029/2000JD900236, 2000.

Scott, C. E., Rap, A., Spracklen, D. V., Forster, P. M., Carslaw, K. S., Mann, G. W., Pringle, K. J., Kivekäs, N., Kulmala, M., Lihavainen, H. and Tunved, P.: The direct and indirect radiative effects of biogenic secondary organic aerosol, Atmos. Chem. Phys., 14(1), 447–470, doi:10.5194/acp-14-447-2014, 2014.

Sena, E. T., Artaxo, P. and Correia, A. L.: Spatial variability of the direct radiative forcing of biomass burning aerosols and the effects of land use change in Amazonia, Atmos. Chem. Phys., 13(3), 1261–1275, doi:10.5194/acp-13-1261-2013, 2013.

Silver, G. and Fall, R.: Charecterization of Aspen Isoprene Synthase, an Enzyme Responsible for Leaf Isoprene Emission to the Atmosphere, J. Biol. Chem., 270(22), 1310–13016, 1995.

Sitch, S., Cox, P. M., Collins, W. J. and Huntingford, C.: Indirect radiative forcing of climate change through ozone effects on the land-carbon sink., Nature, 448(7155), 791–4, doi:10.1038/nature06059, 2007.

Sitch, S., Smith, B., Prentice, I. C., Arneth, A., Bondeau, A., Cramer, W., Kaplan, J. O., Levis, S., Lucht, W., Sykes, M. and Others: Evaluation of ecosystem dynamics, plant geography and terrestrial carbon cycling in the LPJ dynamic global vegetation model, Glob. Chang. Biol., 9(2), 161–185, doi:10.1046/j.1365-2486.2003.00569.x, 2003.

Skeie, R. B., Berntsen, T., Myhre, G., Pedersen, C. a., Ström, J., Gerland, S. and Ogren, J. a.: Black carbon in the atmosphere and snow, from pre-industrial times until present, Atmos. Chem. Phys., 11(14), 6809–6836, doi:10.5194/acp-11-6809-2011, 2011.

Smith, B., Prentice, I. C. and Sykes, M. T.: Representation of vegetation dynamics in modelling of European ecosystems: comparison of two contrasting approaches, Glob. Ecol. Biogeogr., 10, 621–637, doi:10.1046/j.1466-822X.2001.t01-1-00256.x, 2001.

Spielmeyer, A., Gebser, B. and Pohnert, G.: Dimethylsulfide sources from microalgae: Improvement and application of a derivatization-based method for the determination of dimethylsulfoniopropionate and other zwitterionic osmolytes in phytoplankton, Mar. Chem., 124(1–4), 48–56, doi:10.1016/j.marchem.2010.12.001, 2011.

Spracklen, D. V.: Development and Application of a Global Model of Aerosol Processes, Universty of Leeds., 2005.

Spracklen, D. V., Carslaw, K. S., Kulmala, M., Kerminen, V.-M., Mann, G. W. and Sihto, S.-L.: The contribution of boundary layer nucleation events to total particle concentrations on regional and global scales, Atmos. Chem. Phys., 6, 5631–5648, doi:10.5194/acp-6-5631-2006, 2006.

Spracklen, D. V., Carslaw, K. S., Kulmala, M., Kerminen, V.-M., Sihto, S.-L., Riipinen, I., Merikanto, J., Mann, G. W., Chipperfield, M. P., Wiedensohler, A., Birmili, W., et al.: Contribution of particle formation to global cloud condensation nuclei concentrations, Geophys. Res. Lett., 35(6), L06808, doi:10.1029/2007GL033038, 2008a.

Spracklen, D. V., Carslaw, K. S., Pöschl, U., Rap, A. and Forster, P. M.: Global cloud condensation nuclei influenced by carbonaceous combustion aerosol, Atmos. Chem. Phys., 11(17), 9067–9087, doi:10.5194/acp-11-9067-2011, 2011a.

Spracklen, D. V., Jimenez, J. L., Carslaw, K. S., Worsnop, D. R., Evans, M. J., Mann, G. W., Zhang, Q., Canagaratna, M. R., Allan, J., Coe, H., McFiggans, G., et al.: Aerosol mass spectrometer constraint on the global secondary organic aerosol budget, Atmos. Chem. Phys., 11(23), 12109–12136, doi:10.5194/acp-11-12109-2011, 2011b.

Spracklen, D. V., Pringle, K. J., Carslaw, K. S., Chipperfield, M. P. and Mann, G. W.: A global off-line model of size-resolved aerosol microphysics: I. Model development and prediction of aerosol properties, Atmos. Chem. Phys. Discuss.,

5(1), 179–215, doi:10.5194/acpd-5-179-2005, 2005a.

Spracklen, D. V., Pringle, K. J., Carslaw, K. S., Chipperfield, M. P. and Mann, G. W.: A global off-line model of size-resolved aerosol microphysics: II. Identification of key uncertainties, Atmos. Chem. Phys. Discuss., 5(3), 3437–3489, doi:10.5194/acpd-5-3437-2005, 2005b.

Spracklen, D. V. and Rap, A.: Natural aerosol-climate feedbacks suppressed by anthropogenic aerosol, Geophys. Res. Lett., 40, 1–4, doi:10.1002/2013GL057966, 2013.

Spracklen, D. V, Bonn, B. and Carslaw, K. S.: Boreal forests, aerosols and the impacts on clouds and climate., Philos. Trans. A. Math. Phys. Eng. Sci., 366(1885), 4613–26, doi:10.1098/rsta.2008.0201, 2008b.

Stark, H., Brown, S. S., Goldan, P. D., Aldener, M., Kuster, W. C., Jakoubek, R., Fehsenfeld, F. C., Meagher, J., Bates, T. S. and Ravishankara, A. R.: Influence of nitrate radical on the oxidation of dimethyl sulfide in a polluted marine environment, J. Geophys. Res. Atmos., 112(10), 1–11, doi:10.1029/2006JD007669, 2007.

Stephens, G. L. and L'Ecuyer, T.: The Earth's energy balance, Atmos. Res., 166, 195–203, doi:10.1016/j.atmosres.2015.06.024, 2015.

Stevens, B.: Rethinking the lower bound on aerosol radiative forcing, J. Clim., 28(12), 4794–4819, doi:10.1175/JCLI-D-14-00656.1, 2015.

Stevens, B. and Feingold, G.: Untangling aerosol effects on clouds and precipitation in a buffered system., Nature, 461(7264), 607–13, doi:10.1038/nature08281, 2009.

Stevenson, D. S., Johnson, C. E., Collins, W. J. and Derwent, R. G.: The tropospheric sulphur cycle and the role of volcanic SO2, Geol. Soc. London, Spec. Publ., 213(1), 295–305, doi:10.1144/GSL.SP.2003.213.01.18, 2003.

Stier, P., Feichter, J., Kinne, S., Kloster, S., Vignati, E., Wilson, J., Ganzeveld, L., Tegen, I., Werner, M., Balkanski, Y., Schulz, M., et al.: The aerosol-climate model ECHAM5-HAM, Atmos. Chem. Phys., 5, 1125–1156, doi:10.5194/acpd-4-5551-2004, 2005.

Stocker, T., Qin, D., Plattner, G., Tignor, M., Allen, S., Boschung, J., Nauels, A., Xia, Y., Bex, V. and Midgley, P.: IPCC 2013: Summary for Policy Makers, in Climate Change 2013: The Physical Science Basis. Contribution of Working Group I to the Fifth Assessment Report of the Intergovernmental Panel on Climate Change, edited by T. Stocker, D. Qin, G. Plattner, M. Tignor, S. Allen, J. Boschung, A. Nauels, Y. Xia, V. Bex, and P. Midgley, pp. 1–27, Cambridge University Press,

Cambridge, United Kingdom and New York, NY, USA., 2013.

Stockwell, W. R. and Calvert, J. G.: The mechanism of the HO-SO2 reaction, Atmos. Environ., 17(11), 2231–2235, doi:10.1016/0004-6981(83)90220-2, 1983.

Suni, T., Guenther, A., Hansson, H. C., Kulmala, M., Andreae, M. O., Arneth, A., Artaxo, P., Blyth, E., Brus, M., Ganzeveld, L., Kabat, P., et al.: The significance of land–atmosphere interactions in the Earth system—iLEAPS achievements and perspectives., Anthropocene, doi:10.1016/j.ancene.2015.12.001, 2015.

Textor, C., Graf, H.-F., Timmreck, C. and Robock, A.: Emissions from volcanoes, in Emissions of atmospheric trace compounds, edited by C. Granier, C. Reeves, and P. Artaxo, pp. 269–303, Kluwer, Dordrecht., 2004.

Textor, C., Schulz, M., Guibert, S., Kinne, S., Balkanski, Y., Bauer, S., Berntsen, T., Berglen, T., Boucher, O., Chin, M., Dentener, F., et al.: Analysis and quantification of the diversities of aerosol life cycles within AeroCom, Atmos. Chem. Phys., 6, 1777–1813, doi:10.5194/acpd-5-8331-2005, 2006.

Thevenon, F., Anselmetti, F. S., Bernasconi, S. M. and Schwikowski, M.: Mineral dust and elemental black carbon records from an Alpine ice core (Colle Gnifetti glacier) over the last millennium, J. Geophys. Res. Atmos., 114(17), 1–11, doi:10.1029/2008JD011490, 2009.

Thonicke, K., Spessa, a., Prentice, I. C., Harrison, S. P., Dong, L. and Carmona-Moreno, C.: The influence of vegetation, fire spread and fire behaviour on biomass burning and trace gas emissions: Results from a process-based model, Biogeosciences, 7(6), 1991–2011, doi:10.5194/bg-7-1991-2010, 2010.

Torgerson, W. S.: Multidimentional Scaling: I. Theory and Method, Psychometrika, 17(4), 401–419, 1952.

Tosca, M. G., Randerson, J. T. and Zender, C. S.: Global impact of smoke aerosols from landscape fires on climate and the Hadley circulation, Atmos. Chem. Phys., 13(10), 5227–5241, doi:10.5194/acp-13-5227-2013, 2013.

Trenberth, K. E. and Fasullo, J. T.: Simulation of Present-Day and Twenty-First-Century Energy Budgets of the Southern Oceans, J. Clim., 23(2), 440–454, doi:10.1175/2009JCLI3152.1, 2010.

Tsigaridis, K. and Kanakidou, M.: Global modelling of secondary organic aerosol in the troposphere: A sensitivity analysis, Atmos. Chem. Phys. Discuss., 3(3), 2879–2929, doi:10.5194/acpd-3-2879-2003, 2003.

Tsigaridis, K., Lathière, J., Kanakidou, M. and Hauglustaine, D. a.: Naturally driven

variability in the global secondary organic aerosol over a decade, Atmos. Chem. Phys., 5(2), 1891–1904, 2005.

Tunved, P., Hansson, H.-C., Kerminen, V.-M., Ström, J., Maso, M. D., Lihavainen, H., Viisanen, Y., Aalto, P. P., Komppula, M. and Kulmala, M.: High natural aerosol loading over boreal forests., Science, 312(5771), 261–3, doi:10.1126/science.1123052, 2006.

Tunved, P., Strm, J., Kulmala, M., Kerminen, V.-M., Dal Maso, M., Svenningson, B., Lunder, C. and Hansson, H.-C.: The natural aerosol over Northern Europe and its relation to anthropogenic emissionsimplications of important climate feedbacks, Tellus B, 60B, 473–484, doi:10.1111/j.1600-0889.2008.00363.x, 2008.

Turnock, S. T., Spracklen, D. V., Carslaw, K. S., Mann, G. W., Woodhouse, M. T., Forster, P. M., Haywood, J., Johnson, C. E., Dalvi, M., Bellouin, N. and Sanchez-Lorenzo, A.: Modelled and observed changes in aerosols and surface solar radiation over Europe between 1960 and 2009, Atmos. Chem. Phys., 15(16), 9477–9500, doi:10.5194/acp-15-9477-2015, 2015.

Twomey, S.: Pollution and the planetary albedo, Atmos. Environ., 8, 1251–1256, 1974.

Twomey, S.: The Influence of Pollution on the Shortwave Albedo of Clouds, J. Atmos. Sci., 34(7), 1149–1152, doi:10.1175/1520-0469(1977)034<1149:TIOPOT>2.0.CO;2, 1977.

Twomey, S.: Aerosols, clouds and radiation, Atmos. Environ. Part A. Gen. Top., 25(11), 2435–2442, doi:10.1016/0960-1686(91)90159-5, 1991.

Uematsu, M., Toratani, M., Kajino, M., Narita, Y., Senga, Y. and Kimoto, T.: Enhancement of primary productivity in the western North Pacific caused by the eruption of the Miyake-jima Volcano, Geophys. Res. Lett., 31(L06106), 1–4, doi:10.1029/2003GL018790, 2004.

Vehkamäki, H., Kulmala, M., Napari, I., Lehtinen, K. E. J., Timmreck, C., Noppel, M. and Laaksonen, A.: An improved parameterization for sulfuric acid–water nucleation rates for tropospheric and stratospheric conditions, J. Geophys. Res., 107(D22), 1–10, doi:10.1029/2002JD002184, 2002.

Wang, Z., Chappellaz, J., Park, K. and Mak, J. E.: Large variations in Southern Hemisphere biomass burning during the last 650 years., Science, 330(6011), 1663–1666, doi:10.1126/science.1197257, 2010.

Ward, D. S., Kloster, S., Mahowald, N. M., Rogers, B. M., Randerson, J. T. and

Hess, P. G.: The changing radiative forcing of fires: Global model estimates for past, present and future, Atmos. Chem. Phys., 12(22), 10857–10886, doi:10.5194/acp-12-10857-2012, 2012.

Ward, D. S., Mahowald, N. M. and Kloster, S.: Potential climate forcing of land use and land cover change, Atmos. Chem. Phys., 14(8), 12701–12724, doi:10.5194/acpd-14-12167-2014, 2014.

Wardell, L. J., Kyle, P. R., Dunbar, N. and Christenson, B.: White Island volcano, New Zealand: carbon dioxide and sulfur dioxide emission rates and melt inclusion studies, Chem. Geol., 177, 187–200, doi:10.1016/S0009-2541(00)00391-0, 2001.

Weber, R. J., Sullivan, A. P., Peltier, R. E., Russell, A., Yan, B., Zheng, M., de Grouw, J., Warneke, C., Brock, C., Holloway, J. S., Atlas, E. L., et al.: A study of secondary organic aerosol formation in the anthropogenic-influenced southeastern United States, J. Geophys. Res. Atmos., 112(13), 1–13, doi:10.1029/2007JD008408, 2007.

Went, F. W.: Blue hazes in the atmosphere, Nature, 187, 641–643, 1960.

van der Werf, G. R., Dempewolf, J., Trigg, S. N., Randerson, J. T., Kasibhatla, P. S., Giglio, L., Murdiyarso, D., Peters, W., Morton, D. C., Collatz, G. J., Dolman, a J., et al.: Climate regulation of fire emissions and deforestation in equatorial Asia., Proc. Natl. Acad. Sci. U. S. A., 105(51), 20350–5, doi:10.1073/pnas.0803375105, 2008a.

van der Werf, G. R., Peters, W., van Leeuwen, T. T. and Giglio, L.: What could have caused pre-industrial biomass burning emissions to exceed current rates?, Clim. Past, 9(1), 289–306, doi:10.5194/cp-9-289-2013, 2013.

van Der Werf, G. R., Randerson, J. T., Collatz, G. J. and Giglio, L.: Carbon emissions from fires in tropical and subtropical ecosystems, Glob. Chang. Biol., 9(4), 547–562, doi:10.1046/j.1365-2486.2003.00604.x, 2003.

van der Werf, G. R., Randerson, J. T., Giglio, L., Collatz, G. J., Mu, M., Kasibhatla, P. S., Morton, D. C., DeFries, R. S., Jin, Y. and van Leeuwen, T. T.: Global fire emissions and the contribution of deforestation, savanna, forest, agricultural, and peat fires (1997–2009), Atmos. Chem. Phys., 10(23), 11707–11735, doi:10.5194/acp-10-11707-2010, 2010.

van der Werf, G. R., Randerson, J. T., Giglio, L., Gobron, N. and Dolman, a. J.: Climate controls on the variability of fires in the tropics and subtropics, Global Biogeochem. Cycles, 22(3), n/a-n/a, doi:10.1029/2007GB003122, 2008b.

Whung, P. Y., Saltzman, E. S., Spencer, M. J., Mayewski, P. A. and Gundestrup, N.: Two-hundred-year record of biogenic sulfur in a south Greenland ice core (20D), J. Geophys. Res., 99(D1), 1147–1156, doi:10.1029/93JD02732, 1994.

Wilcox, E. M.: Stratocumulus cloud thickening beneath layers of absorbing smoke aerosol, Atmos. Chem. Phys., 10(23), 11769–11777, doi:10.5194/acp-10-11769-2010, 2010.

Wilcox, L. J., Highwood, E. J., Booth, B. B. B. and Carslaw, K. S.: Quantifying sources of inter-model diversity in the cloud albedo effect, Geophys. Res. Lett., 42, 1568–1575, doi:10.1002/2015GL063301.Received, 2015.

Wilson, T. W., Ladino, L. A., Alpert, P. A., Breckels, M. N., Brooks, I. M., Browse, J., Burrows, S. M., Carslaw, K. S., Huffman, J. A., Judd, C., Kilthau, W. P., et al.: A marine biogenic source of atmospheric ice-nucleating particles, Nature, 525(7568), 234–238, doi:10.1038/nature14986, 2015.

Wood, R., Comstock, K. K., Bretherton, C. S., Cornish, C., Tomlinson, J., Collins, D. R. and Fairall, C.: Open cellular structure in marine stratocumulus sheets, J. Geophys. Res., 113(D12), D12207, doi:10.1029/2007JD009371, 2008.

Woodhouse, M. T., Carslaw, K. S., Mann, G. W., Vallina, S. M., Vogt, M., Halloran, P. R. and Boucher, O.: Low sensitivity of cloud condensation nuclei to changes in the sea-air flux of dimethyl-sulphide, Atmos. Chem. Phys., 10(16), 7545–7559, doi:10.5194/acp-10-7545-2010, 2010.

Woodhouse, M. T., Mann, G. W., Carslaw, K. S. and Boucher, O.: Sensitivity of cloud condensation nuclei to regional changes in dimethyl-sulphide emissions, Atmos. Chem. Phys., 13(5), 2723–2733, doi:10.5194/acp-13-2723-2013, 2013.

Yang, G.-P., Levasseur, M., Michaud, S., Merzouk, A., Lizotte, M. and Scarratt, M.: Distribution of dimethylsulfide and dimethylsulfoniopropionate and its relation with phytoneuston in the surface microlayer of the western North Atlantic during summer, Biogeochemistry, 94(3), 243–254, doi:10.1007/s10533-009-9323-y, 2009.

Yassaa, N., Peeken, I., Zöllner, E., Bluhm, K., Arnold, S., Spracklen, D. and Williams, J.: Evidence for marine production of monoterpenes, Environ. Chem., 5(6), 391, doi:10.1071/EN08047, 2008.

Young, P. J., Arneth, A., Schurgers, G., Zeng, G. and Pyle, J. A.: The CO2 inhibition of terrestrial isoprene emission significantly affects future ozone projections, Atmos. Chem. Phys., 9, 2793–2803, doi:10.5194/acp-9-2793-2009, 2009.

Yu, H., Remer, L. a, Chin, M., Bian, H., Tan, Q., Yuan, T. and Zhang, Y.: Aerosols from overseas rival domestic emissions over North America., Science, 337(6094), 566–9, doi:10.1126/science.1217576, 2012.

Zennaro, P., Kehrwald, N., McConnell, J. R., Schupbach, S., Maselli, O. J., Marlon, J., Vallelonga, P., Leuenberger, D., Zangrando, R., Spolaor, A., Borrotti, M., et al.: Fire in ice: Two millennia of boreal forest fire history from the Greenland NEEM ice core, Clim. Past, 10(5), 1905–1924, doi:10.5194/cp-10-1905-2014, 2014.

Zhang, L., Gong, S., Padro, J. and Barrie, L.: A size-segregated particle dry deposition scheme for an atmospheric aerosol module, Atmos. Environ., 35(3), 549–560, doi:10.1016/S1352-2310(00)00326-5, 2001.